Charge Transfer and Support Effects in Heterogeneous Catalysis

by

Antoine Hervier

A dissertation submitted in partial satisfaction of the

requirements for the degree of

Doctor of Philosophy

in

Chemistry

in the

Graduate Division

of the

University of California, Berkeley

Committee in Charge:

Professor Gabor A. Somorjai, Chair
Professor Peidong Yang
Professor Martin Head-Gordon
Professor Kyriakos Komvopoulos

Fall 2011

DISCLAIMER

Abstract

Charge transfer and Support Effects in Heterogeneous Catalysis

by

Antoine Hervier

Doctor of Philosophy in Chemistry

University of California, Berkeley

Professor Gabor A. Somorjai, Chair

The kinetic, electronic and spectroscopic properties of two-dimensional oxide-supported catalysts were investigated in order to understand the role of charge transfer in catalysis.

Pt/TiO_2 nanodiodes were fabricated and used as catalysts for hydrogen oxidation. During the reaction, the current through the diode, as well as its I-V curve, were monitored, while gas chromatography was used to measure the reaction rate. The current and the turnover rate were found to have the same temperature dependence, indicating that hydrogen oxidation leads to the non-adiabatic excitation of electrons in Pt. A fraction of these electrons have enough energy to ballistically transport through Pt and overcome the Schottky barrier at the interface with TiO_2. The yield for this phenomenon is on the order of 10^{-4} electrons per product molecule formed, similar to what has been observed for CO oxidation and for the adsorption of many different molecules.

The same Pt/TiO_2 system was used to compare currents in hydrogen oxidation and deuterium oxidation. The current through the diode under deuterium oxidation was found to be greater than under hydrogen oxidation by a factor of three. Weighted by the difference in turnover frequencies for the two isotopes, this would imply a chemicurrent yield 5 times greater for D_2 compared to H_2, contrary to what is expected given the higher mass of D_2. Reversible changes in the rectification factor of the diode are observed when switching between D_2 and H_2. These changes are a likely cause for the differences in current between the two isotopes.

In the nanodiode experiments, surface chemistry leads to charge flow, suggesting the possibility of creating charge flow to tune surface chemistry. This was done first by exposing a Pt/Si diode to visible light while using it as a catalyst for H_2 oxidation. Absorption of the light in the Si, combined with the band bending at the interface, gives rise to a steady-state flow of hot holes to the surface. This leads to a decrease in turnover on the surface, an effect which is enhanced when a reverse bias is applied to the diode.

Similar experiments were carried out for CO oxidation. On Pt/Si diodes, the reaction rate was found to increase when a forward bias was applied. When the diode was exposed to visible light and a reverse bias was applied, the rate was instead decreased. This implies that a flow of negative charges to the surface increases turnover, while positive charges decrease it.

Charge flow in an oxide supported metal catalyst can be modified even without designing the catalyst as a solid state electronic device. This was done by doping stoichiometric and non-stoichiometric TiO_2 films with F, and using the resulting oxides as supports for Pt films. In the case of stoichiometric TiO_2, F was found to act as an *n*-type dopant, creating a population of filled electronic states just below the conduction band, and dramatically increasing the conductivity of the oxide film. The electrons in those states can transfer to surface O, activating it for reaction with CO, and leading to increased turnover for CO oxidation. This reinforces the hypothesis that CO oxidation is activated by a flow of negative charges to the surface.

The same set of catalysts was used for methanol oxidation. The electronic properties of the TiO_2 films again correlated with the turnover rates, but also with selectivity. With stoichiometric TiO_2 as the support, F-doping caused an increase in selectivity toward the formation of partial oxidation products, formaldehyde and methyl formate, versus the total oxidation product, CO_2. With non-stoichiometric TiO_2, F-doping had the reverse effect.

Ambient Pressure X-Ray Photoelectron Spectroscopy was used to investigate this F-doping effect in reaction conditions. In O_2 alone, and in CO oxidation conditions, the O1s spectrum showed a high binding energy peak that correlated in intensity with the activity of the different films: for stoichiometric films, the peak decreased in intensity with F-doping, while for non-stoichiometric films, the opposite was observed. No such changes were visible in the C1s spectrum, confirming the role of O activation in the reaction.

This thesis adds to the body of knowledge on the importance of charge transfer at the metal-oxide interface in shaping the reactivity of heterogeneous catalysts, and provides examples of how this can be the basis for new methods to tune reactivity.

Table of Contents

Acknowledgements

This dissertation is the result of four years of work within the Surface Science and Catalysis laboratory at University of California, Berkeley and Lawrence Berkeley National Laboratory, under the supervision of Gabor Somorjai. Research was supported by the U.S. Department of Energy, Office of Basic Energy Sciences, under Contract No. DE-AC02-05CH11231. There were many challenges and difficulties along the way, but my time here was exciting, instructive, and fun. For this I have many people to thank.

I thank of course Professor Somorjai, for giving me the opportunity to work in such a unique environment, with access to the brightest minds and the latest instruments, at the "frontiers of surface science". I am grateful for his scientific guidance, which is provided not just to obtain results, but also because he takes it as his personal responsibility that his students must accomplish valuable work and learn along the way those things that are important for being a researcher. Finally, I thank him for his warmth and kindness, which are a great relief in graduate school, where the pressure can be sometimes overwhelming.

I also thank for Kyriakos Komvopoulos, for the advice he provided me during my work here, for the financial help which helped make this work possible, and for including me as a part of his research group. This experience exposed me to research I would never have known of if I had not ventured from the chemistry department.

I am grateful to the many people who worked in the group during my stay here. The sad part of working in research is that there is barely enough time to appreciate the company of colleagues before they move on to the next step in their careers. The group was a great resource for scientific advice, learning how laboratory work is done, and discovering the field. They were also great company. Jeong Park and Russ Renzas taught me everything one needs to know to study catalytic reactions, and took me under their wing to continue the hot electron project. Hyungtak Seo was of great help in understanding semiconductor electronics. Griffin Kennedy and Matthijs van Spronsen provided considerable help in running reactions. Anthony Contreras (along with Elad Gross, Vladimir Pushkarev, and Will Michalak), was invaluable in helping me put back together a UHV system that is now used in a student laboratory class, and I have fond memories of driving to the local 7-11 for snacks in the middle of the night, to take breaks from working out the details of equipment that was nearly forty years old.

Most of all, I am grateful for Robert Baker, who was a source of great insight and motivation. Very little of this work would have been possible without his expertise and wisdom. I am inspired by how much he has accomplished, while at the same time raising a family. And I am sure he will someday be renowned enough that I will boast having worked with him.

The best part about Berkeley is the enormous size of the chemistry department, which meant I had many fellow students in my year. This was a great help in settling into a new area. They made the experience extremely enjoyable, and I will miss them dearly. I think in particular of Dan Lucas, who was a warm, caring person, and who showed such promise, but whose life was cut short before he could become the great researcher he was going to be.

I had the good fortune of living with great roommates while I was here, Cyrus Maher, Alex Kintzer, Lindsay Miller, Ida-Marie Høyvik, Michael Aviles, Andrew Ignacio and Robert Marks. They were great company and I will miss them. I wish Michael could have stayed in Berkeley longer.

I am grateful to the students of the Berkeley Masters of Public Health class of 2011, who awarded me a very unofficial honorary degree in public health and who were a great group of friends. I thank the Strawberry Canyon Aquatic Masters for their warm welcome and the opportunity to swim throughout graduate school, an important contribution to my well-being.

I was lucky to have many friends make the very long trip from France to come and visit me during my stay here, namely Nicolas Bonneau, Martin Labrune, Marie-Claire Ong, Linna Bun, Emmanuel Charbit, Arnaud Luong, Théodora Gennuso, Daphné Barthelet, Guillaume Claire, and Wendy Blanchet, who made it to Berkeley just in time before I left.

Finally, and most importantly, I thank my family for supporting me throughout graduate school. My aunt, uncle and cousins in the Bay Area made me feel right away like I had a home here. I can never thank them enough for including me in their lives and supporting me like they did. I feel very lucky to have been here for the birth of Shaan.

My father had the good sense to push me to work hard, and his patience and determination with me were crucial. My mother not only showed me unwavering support, she also suggested that I apply to graduate school, a rather ingenious idea. I thank them and my brother and sister for calling me and coming to visit me so often, I could not have done this without them. I hope they will forgive me for being away so long.

Introduction

The science of heterogeneous catalysis has already led to several dramatic, transformative discoveries. The world's population, for example, would likely be half what it is today were it not for the synthesis of ammonia, developed by Haber and Bosch.[1] Another famous example is the catalytic converter which led to a 60% drop in carbon monoxide levels between 1990 and 2005.[2] More broadly, as many as 90% of all chemicals produced rely on heterogeneous catalysts, as does all of our fuel derived from crude oil.[3] This success, and the economic development it has allowed, come with a price however, in the form of an energy crisis and increasing atmospheric levels of greenhouse gases.

Catalysis will be critical in finding solutions to these problems, whether by providing fuels from biomass, or through the development of fuel cells or batteries to replace the traditional combustion engine, or by finding energy efficient ways to split carbon dioxide (CO_2) and water.

These breakthroughs can only be achieved by first understanding the mechanisms behind catalytic reactions. Industrially, catalysis is still very much an empirical undertaking.[4] A more fundamental approach is needed, one that will eventually lead to the rational design of catalysts.

This requires the study of charge dynamics, which are central to surface chemistry. Although heterogeneous catalysis begins and ends with neutral atoms and molecules, most reactions are governed by charge transfers involving adsorbates, catalysts and their support. Furthermore, understanding these charge transfers allows us to work at the interface with the field of semiconductor electronics, fabricating catalysts that are also diodes, transistors, or photovoltaic devices.

Such catalysts can be used in two ways: first, if chemical reactions lead to charge flow, then the device could be used to measure, or even harvest the resulting electrical current. This is covered in chapters 2 through 4. Second, if charge flow plays a role in a reaction mechanism, then modifying the conditions for charge flow, by applying a field or a current to the device, or by doping it to modify its electronic structure, can lead to changes in reactivity. This is covered in chapters 5 through 11.

Chapters 3 and 4 fall into the first category, describing hydrogen oxidation on catalytic nanodiodes. These diodes consist of a metal film, a few nanometers in thickness, deposited onto a semiconductor. Both the metal and the semiconductor are connected to an external circuit. The Fermi level mismatch between the two materials gives rise to transient charge transfer from one to the other, resulting in the formation of an energy barrier at the interface. This barrier serves as high-pass energy filter for the electrons in the metal, and is the basis for showing that hydrogen oxidation turnover on a platinum / titanium dioxide (Pt/TiO_2) catalyst

results in the non-adiabatic excitation of electrons within the metal. As the reaction proceeds on the surface, chemical energy is converted into an electrical current in proportion with turnover.

Chapters 5 through 11 fall into the second category. In chapter 5, a photocurrent is generated by shining light on a platinum / silicon (Pt/Si) photodiode. When this is done in hydrogen oxidation reaction conditions, we show that turnover is reduced. This effect is due to a steady state flow of hot holes to the surface resulting from electron-hole pair generation in the Si. The magnitude of this effect can be enhanced by applying a reverse bias to the Pt/Si diode.

In chapter 6, Pt/Si nanodiodes are used as catalysts for carbon monoxide (CO) oxidation. We show that turnover for the reaction can be increased by applying a reverse bias to the diode, which corresponds to the formation of a negative charge on the platinum film. Turnover can also be decreased by exposing the diode to visible light under reverse bias, which leads to a flow of positive charge from the semiconductor to the platinum.

In chapters 8 through 11, we describe a novel method for doping TiO_2 with fluorine (F), which modifies the electronic structure of the semiconductor. We show how this opens up new, electronically activated reaction pathways for CO oxidation on stoichiometric TiO_2, increasing turnover frequency. Kinetic and electronic measurements indicate that electronic activation of surface O is responsible for this change in activity. On methanol oxidation, which is a multi-path reaction, this also affects selectivity, favoring the formation of partially oxidized products, formaldehyde and methyl formate, over CO_2, the totally oxidized product.

Chapter 11 shows *in situ* XPS data which confirms the role of surface oxygen in the change in reactivity for CO oxidation.

References

(1) Smil, V. Enriching the Earth: Fritz Haber, Carl Bosch, and the Transformation of World Food Production; MIT Press, 2004.

(2) Committee on the Review of the Basic Energy Sciences, Catalysis Science Program, National Research Council Catalysis for Energy: Fundamental Science and Long-Term Impacts of the U.S. Department of Energy Basic Energy Science Catalysis Science Program; The National Academies Press: Washington, D.C., 2009.

(3) Masel, R. I. Principles of adsorption and reaction on solid surfaces; Wiley-IEEE, 1996.

(4) Ertl, G. Reactions at solid surfaces; John Wiley and Sons, 2009.

Chapter 1

Experimental Considerations

The bulk of this work was achieved by carrying out gas phase reactions on two dimensional catalysts, in three similar batch reactors, and measuring the reaction kinetics by gas chromatography. The reactors were used in batch mode because the surface area of two dimensional catalysts is too small to achieve measurable conversion rates in flow reactors. The catalysts were two dimensional because this allows for better control of catalyst design: it makes it possible to give the catalyst a Schottky diode structure, or to easily anneal or dope the oxide support before adding the metal catalyst.

1. Batch reactor

All three reactors share the same basic design, shown in Figure 1: a chamber of volume roughly 1 L is equipped with a manifold for introducing gases, and connected to a turbomolecular pump backed by a mechanical pump to evacuate the chamber down to a pressure of 5 x 10^{-6} Torr. In the center of the chamber sits a ceramic heater (HTR1001 - Momentive), connected to a temperature controller (built around a Watlow series 96 controller) outside the chamber by a feedthrough that also serves as a cooling line. Flowing water through these lines ensures that the heater leads stay close to room temperature, to prevent them from contributing to the catalysis.

A metal bellows pump (Senior Flexonics) recirculates the gases through a line to an injection valve to the gas chromatograph (5890 – Hewlett-Packard). Periodically, the valve allows a pressurized helium gas line to force an aliquot of the chamber gas into the GC column, where the different components of the mixture are separated, before going through a thermal conductivity detector or a flame ionization detector. The column is chosen so as to obtain good separation and low retention times for the different reactants and products involved in the reaction.

The reactions are run at temperatures low enough that conversion of the reactants stays below 10 % over several hours. This ensures that the catalyst is subjected to the same pressure conditions throughout the experiment, so that a steady-state measurement can be made.

The batch reactors are also equipped with two electrical feedthroughs. Gold wires, which are catalytically inert, are used to connect the terminals of diodes inside the chamber to the feedthroughs. The wires are pressed down on the diode using custom-made MACOR parts. This makes it possible to measure current or to apply a bias to the catalyst in reaction conditions.

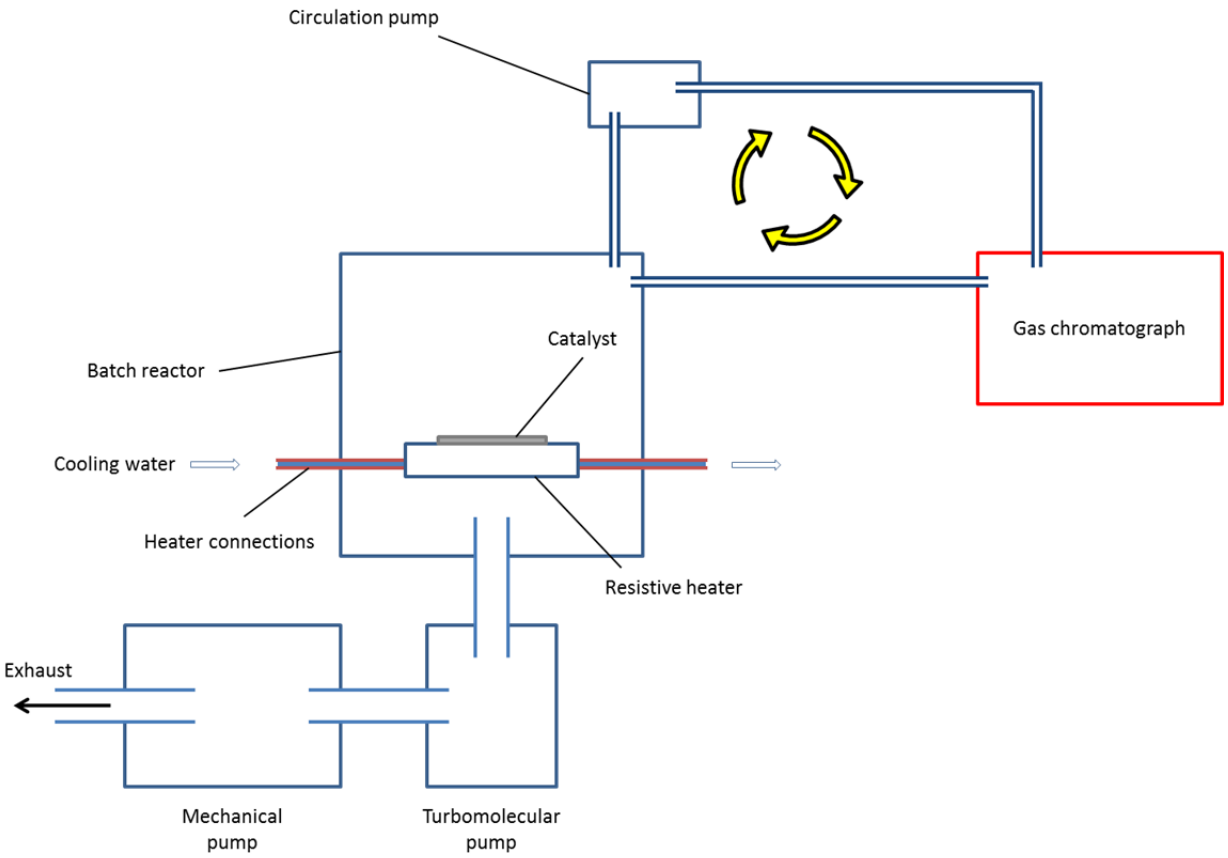

Figure 1 – *Schematic of the batch reactors*

2. Thin film fabrication

The catalysts are fabricated by depositing thin films of oxides and metals onto polished (100) silicon wafers. Two deposition techniques are used: electron beam evaporation and sputtering.

2.1. Electron beam evaporation

The silicon substrate is suspended from the top of a vacuum chamber with base pressure 4 x 10^{-6} Torr. The electron beam evaporator (eVap Mighty Source – MDC) consists of a crucible that can hold liners filled with target metals. A filament is built into the crucible assembly but electrically insulated from it. High voltage feedthroughs connect a power supply to the filament, so that a bias of 4.5 kV can be applied between the filament and chamber ground. Current is run through the filament, which heats up and emits electrons. The high voltage bias, along with a magnetic field created by magnets lining the crucible assembly, steer the electrons towards the target metal, causing intense local heating. With enough emission current, vapor is generated by the target and a film begins to grow on the substrate.

Deposition in an electron beam evaporator is directional: by placing the substrate behind a mask, the film can be patterned onto the silicon.

2.2. Sputtering

Sputtering also takes place with the substrate suspended over a metal target inside a vacuum chamber, with base pressure 7 x 10^{-6} Torr (Auto 306 DC and RF Sputter Coater – Edwards). Once at vacuum, a mass flow controller is opened to flow in 2-20 sccm of Argon and / or some other gas. An RF or DC current can be applied to strike a plasma inside the chamber. This generates ions which are accelerated towards the target, ejecting atoms into the gas phase as they impinge on the surface. As these atoms coat the surface of the substrate, a film grows.

This technique is also directional.

2.3. Quartz Crystal Microbalance (QCM)

For both of these deposition techniques, thickness is monitored during the deposition using a quartz crystal microbalance (SQM160 – MDC). This consists of a thin quartz crystal disc covered on both sides with gold electrodes. An AC current is applied to the crystal, causing it to oscillate due to its piezoelectric properties. Periodically, this current is stopped, letting the crystal oscillation dissipate, which in turn generates a damping current. The speed at which this damping occurs is closely related to the weight of the crystal. If a material with a known density is deposited onto the QCM, the deposition rate and the amount of material deposited can be measured. This makes it possible to deposit a film of a known thickness.

3. Rapid thermal annealing

When using electron beam evaporation and sputtering, films are grown a few atoms at a time. Since no heat is provided during the deposition, the resulting material is highly amorphous. To improve the crystallinity of the oxides, they were annealed at high temperatures (623 – 773 K) in a Rapid Thermal Annealer (Heatpulse 210T RTA – AG associates). Rapid, controlled heating is achieved using an array of halogen lamps. By annealing in different gas environments, it is possible to vary the degree of oxidation of the film.

This process is not possible with metal films, since they usually have a higher surface energy than oxides, and tend to agglomerate into large particles when heated past 200-300°C.

4. Scanning Electron Microscope

At thicknesses below 20 nm, metal films are rarely continuous, and instead form islands. The morphology of the films is of crucial importance, since it determines the active area exposed to the gas phase, as well as the number of sites located at the interface between the metal and the support. Under the high temperatures and strongly reducing or oxidizing conditions of catalytic reactions, this morphology can change, and with it the activity and selectivity.

Film morphology was observed by SEM (Ultra 55 – Zeiss). The sample is placed in a vacuum chamber with base pressure 10^{-7} Torr, connected by an aperture to a separate, differentially pumped chamber with bas pressure 10^{-10} Torr, containing an electron gun. The electron beam is accelerated to several keV, and can be focused down to the nanometer scale using electron

optics. The beam is raster scanned across the sample, and as the high energy electrons thermalize, secondary electrons are emitted and collected, producing an image with resolution 1-2 nm.

5. Plasma-Thermal Parallel Plate Plasma Etcher

Some of the oxides were fluorine-doped after annealing. This was achieved by exposing them to a nitrogen plasma with traces of SF_6. The plasma is produced inside a vacuum chamber with a base pressure of 3 mTorr (PK-12 RIE – Plasma Therm). A mass flow controller introduces gas into the chamber at 5 – 100 sccm, and a radiofrequency (RF) power supply generates a field that partially ionizes the gas, leading to ion bombardment of the substrate.

This can be used to either etch samples, or to implant ions into the material, in this case, fluorine.

6. Semiconductor curve tracer

A Schottky diode is characterized mainly by its intensity vs. voltage (I-V) curve, which is obtained by applying a voltage across the terminals of the diode and measuring the resulting current. I-V curves for the diodes studied here were measured using the Keithley 2400 Sourcemeter.

7. X-Ray Photoelectron Spectroscopy (XPS)

In XPS, the sample to be characterized is exposed to monochromated X-Ray radiation from a Mg or Al source with energy on the order of 1 keV (5400 ESCA XPS – Physical Electronics). This ionizes core electrons in the sample, some of which are ejected in the direction of a hemispherical mass analyzer. There, an electric field is used to curve their trajectories so that only electrons with a specific kinetic energy reach the detector. Since the photon energy is known, the energies of the ionized core levels can be calculated. These energies are element specific, and are shifted by the electron's chemical environment, providing some information about what elements are present on the surface, and what they are bound to.

The ionized electrons have an energy on the order of 100 – 1000 eV, giving them a mean free path in the metal of a few nanometers at most. This means that only electrons from the first few layers of the sample have a chance of reaching the detector, making this technique surface specific.

Chapter 2

An Introduction to Hot Electron Chemistry

1. The Born-Oppenheimer approximation

The study of chemical dynamics often relies on the Born-Oppenheimer approximation. The approximation relies on the fact that electrons move on a much shorter time scale than nuclei, because of the considerable difference in mass.[1] As the nuclei positions change, the electrons have ample time to sample the space available to them and find the energy minimum, preventing nuclear motion from causing electronic excitations.[2] This makes it considerably easier to describe the potential energy landscape of polyatomic systems: each electronic level has its own distinct potential surface, with the nuclear coordinates as the only variables. A system that behaves this way is described as adiabatic.

This situation does not always hold. Along a given reaction coordinate, two potential energy surfaces, corresponding to two different electronic states A and B, may cross, as shown in figure 1. At the crossing point, an electronic transition requires no change in energy. The superposition of both states A and B implies a non-zero probability that the transition will occur.

Let us assume we start in the lower energy state A at an infinite distance, and decrease the reaction coordinate. At short distances, state B is lower in energy. In the adiabatic situation, the motion along the reaction coordinate is slow enough that the system will transition to B, the lower energy state, when it reaches the crossing point: crossing is “avoided”, and the Born-Oppenheimer approximation holds. This is no longer true if the nuclei move too fast for the electrons to respond. Landau, Zener, Stückelberg and Majorana all independently derived the expression for the probability p_{LZ} of transitioning at the cross-over region in the case of the one-dimensional system:[3–7]

$$p_{LZ} = \exp\left(-\frac{4\pi V_{AB}^2}{hv|s_A - s_B|}\right)$$

where v is the velocity along the reaction coordinate at the crossing point, s_A and s_B are the slopes of the potential energy curves for A and B at the crossing point, and V_{AB} is half the difference in energy between the two curves at the crossing point. In the adiabatic approximation, v approaches 0, and the transition probability approaches 1.

The transition may also occur with some delay, after the system has gone beyond the cross-over region (see figure 1). The system would then be in an excited electronic state, and if relaxation were to occur, an amount of energy ΔE would have to be dissipated.

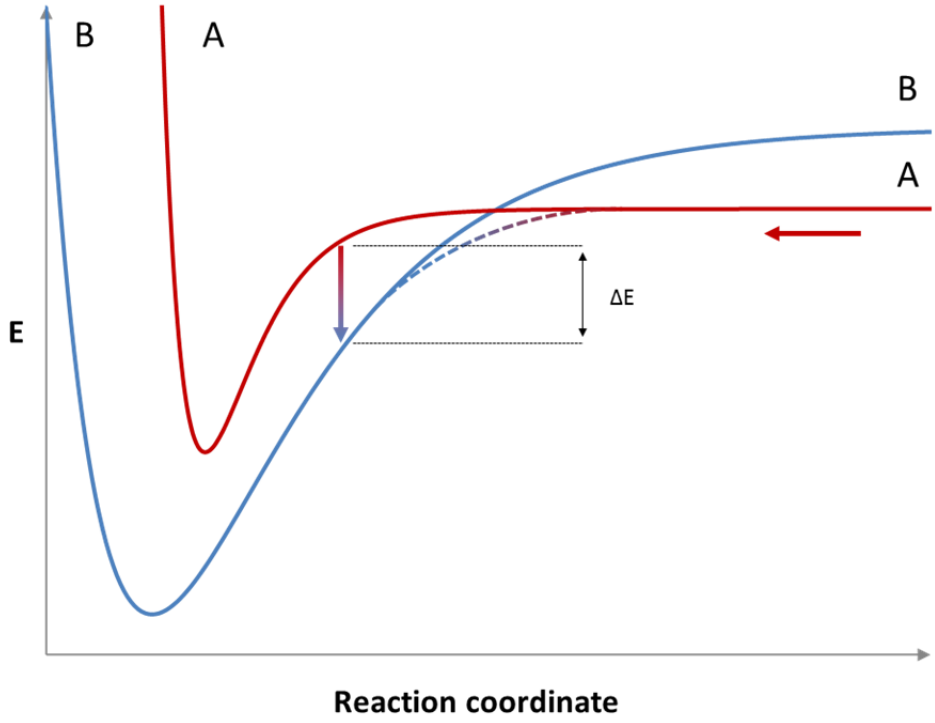

Figure 1 – *One-dimensional potential energy curves for a system that can exist in two electronic states A and B. If the system starts in state A and moves toward the left, the system approaches a crossing point, where the system has some probability of existing in either state A or B. In the Born-Oppenheimer case, the motion along the nuclear coordinates is slow enough that the electron has enough time to transition to state B (dashed line), which is the lower energy state past the crossing point; crossing is "avoided". In a non-adiabatic situation, nuclear motion is fast enough that the system is still in state A past the crossing point, and no longer in the electronic ground state. If relaxation occurs then, an amount of energy ΔE is released by the system.*

If A is a solid surface and B a molecule imping on it, creation of an electron-hole pair within the solid is one possible channel for dissipating this excess energy. A non-adiabatic process is especially likely for an atom or molecule reacting with a solid surface. The energy levels of the solid form a continuous band, as shown in Figure 2, which implies a continuum of crossing points. In the region where the energy of the impinging molecule overlaps with one of these bands, the V_{AB} term in P_{LZ} approaches zero, and the probability of transition approaches 1.

2. Experimental evidence of non-adiabatic phenomena

The energy dissipation after the reaction event can be used to show that a non-adiabatic mechanism has taken place. Kasemo observed photon emission upon adsorption of O_2 on Al and Mg, with a probability on the order of 10^{-7} and an intensity proportional to the rate of adsorption.[8] Böttcher *et al.* showed that oxidation of Cs by O_2 led to the ejection of an electron

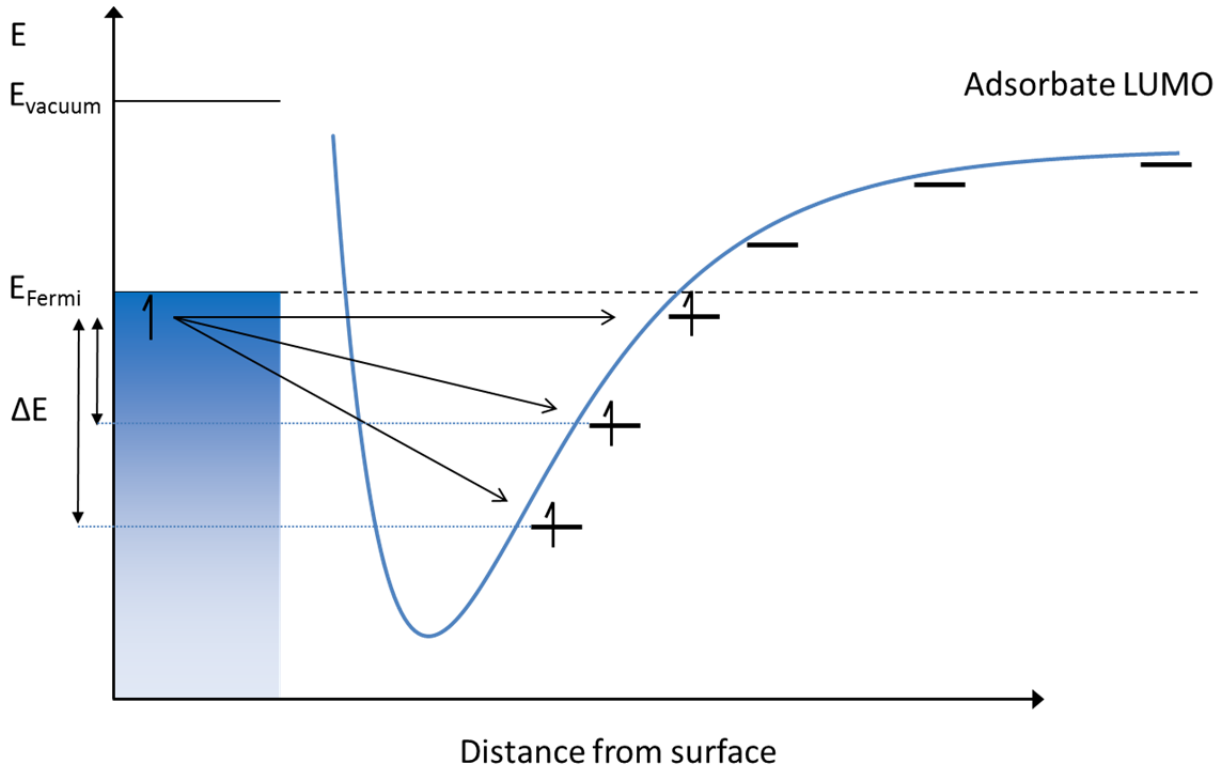

Figure 2 – *One dimensional potential energy curve for a molecule approaching a metal surface. Physisorption and chemisorption imply the existence of an energy minimum close to the surface. As the energy of the adsorbing molecule's lowest unoccupied orbital drops below the Fermi level of the metal, an electron transfer may occur, along with the release of energy ΔE, which may lead to the excitation of another electron within the metal.*

from the surface by an Auger process.[9] Cesium lends itself particularly well to demonstrating this effect, since its low work function allows electron with even modest excitation energies to be ejected.

Showing that nuclear motion couples to electronic excitation is more difficult if the excitation is too small to cause emission. Relaxation of these hot electrons happens on the femtosecond to picosecond timescale, and their mean free path is on the order of 10 nm.[10] This implies two detection strategies: the first is to obtain sufficient time resolution to observe these excitations. The second consists of instead reducing the size of the setup to below the mean free path.

2.1. High Time-Resolution Experiments

Morin *et al.* measured the vibrational lifetime of CO molecules adsorbed on a Cu(100) surface and found it to be 2.0 ± 1.0 ps, in agreement with theory.[11,12] For CO on NaCl(100), Chang *et al.* had found a lifetime of 4.3 ms, over 9 orders of magnitude greater.[13] The lifetime is comparably long for a CO molecule in the gas phase.[12] This enormous difference is explained by the possibility on Cu for the vibrational motion of the CO molecule to couple to electronic

excitations. In the gas phase, or on an insulating surface like NaCl with a large bandgap, there are no states for CO to couple with, and the CO molecule is left to stretch and compress on average 10^6 times before finally relaxing.

Electronic coupling of surface electrons to adsorbate vibrations holds great promise for catalysis, since it offers a key parameter to tune in the rational design of catalysts. This is made clear by Bonn *et al*, in a study of CO oxidation on Ru(0001).[14]

If CO and O are co-adsorbed on a Ru(0001) single crystal and the crystal is heated, CO and O desorb before any CO_2 is produced. Instead of conventional heating, the authors used an infrared femtosecond laser to increase the surface temperature. Two pulses were fired at the surface, separated by a variable delay on the picosecond scale. The laser pulses initially raise the electronic temperature, up to several thousand Kelvins, since the heat capacity of electrons is quite low, while the lattice temperature remains almost unaffected. The electrons eventually equilibrate with the phonons in the lattice, with a characteristic time of 300 fs, and after several picoseconds, the surface is at thermal equilibrium. Figure 3 shows the electronic and lattice temperatures, calculated based on a previously published model.[15,16]

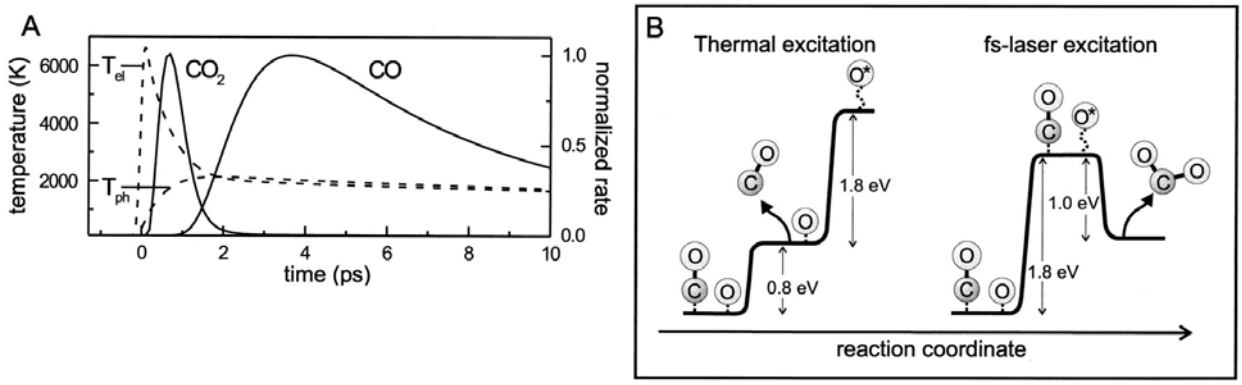

Figure 3 – *A.* *Calculated electron and phonon temperatures (dashed lines) of Rh metal after excitation by a femtosecond laser pulse, along with calculated reaction rates for CO oxidation and CO desorption.* ***B.*** *Schematic mechanism for desorption of CO_2 and CO. The activation energy for desorption is much lower than for oxygen activation for CO oxidation, and no CO_2 is formed from heating. The laser pulse makes it possible to activate the oxygen while the lattice temperature is low enough to prevent CO desorption, and CO_2 is formed. Reproduced from [14]*

A single laser pulse produces no CO_2. Two laser pulses separated by more than 10 ps are also unable to lead to turnover, since in that time the lattice has equilibrated with the electrons (see Figure 3). But if the second laser pulse occurs before this equilibration takes place, CO_2 is observed desorbing from the surface. With a short delay, the surface electrons reach a temperature high enough that a previously inaccessible, non-thermal reaction pathway is opened.

DFT calculations show an anti-bonding orbital for O adsorbed on Ru, 1.7 eV above the Fermi level. The electronic heating caused by the laser pulse creates a population of electrons at that

energy in the metal surface, which may populate the anti-bonding orbital, activating the O atom for reaction with CO.

2.2. The nanodiode

A non-adiabatic event on a surface produces an electron that is out of thermal equilibrium with the other metal electrons. If this hot electron has an energy greater than the work function of the metal, it can be ejected into the vacuum and detected. At lower energies, the electron stays confined within the metal, and quickly thermalizes. A hot electron detector must therefore be able to do two things: its size must be small enough that hot electrons are collected before they thermalize; and it must be able to distinguish high energy electrons excited by the non-adiabatic event from other electrons in the crystal.

A thin film Schottky diode fulfills these requirements. A Schottky diode is a type of metal-semiconductor contact. When two different solids are brought into contact, electrons in the higher chemical potential solid tend to flow into the solid with the lower chemical potential, until the potentials equilibrate. A negative charge forms where the electrons have migrated, and a positive charge forms where the nuclei were left behind.

This gives rise to an electric field in the semiconductor that can be represented by a bending of the energy bands. If electrons are the majority carrier in the semiconductor (an *n*-type semiconductor), and if the metal's chemical potential was higher than that of the metal, the bands bend downward, leaving no barrier to electron flow. This is referred to as an Ohmic contact, since current through this interface is proportional to voltage as shown in Figure 4.

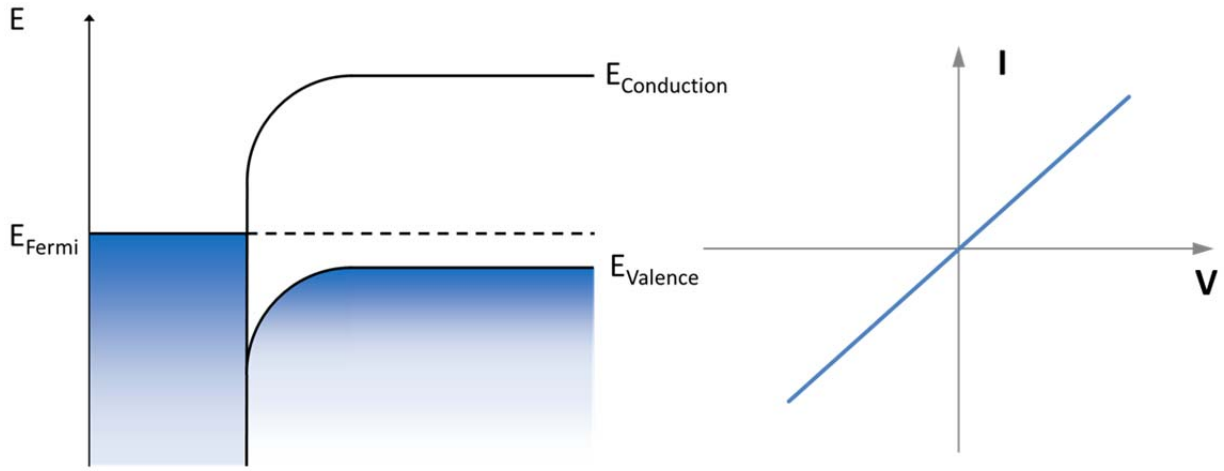

Figure 4 – *Energy diagram and I-V curve of an Ohmic contact*

If the semiconductor's chemical potential was higher, the bands now bend upwards, forming at the interface a barrier to electron flow from the metal to the semiconductor, referred to as a Schottky barrier, ϕ_B. The barrier height, as well as other properties of the diode, can be obtained by measuring its current through the diode as a function of voltage. The

resulting graph is known as the I-V curve, shown in figure 5 for a Schottky diode. A diode that acts as a Schottky contact for electrons is Ohmic for holes, and vice versa.

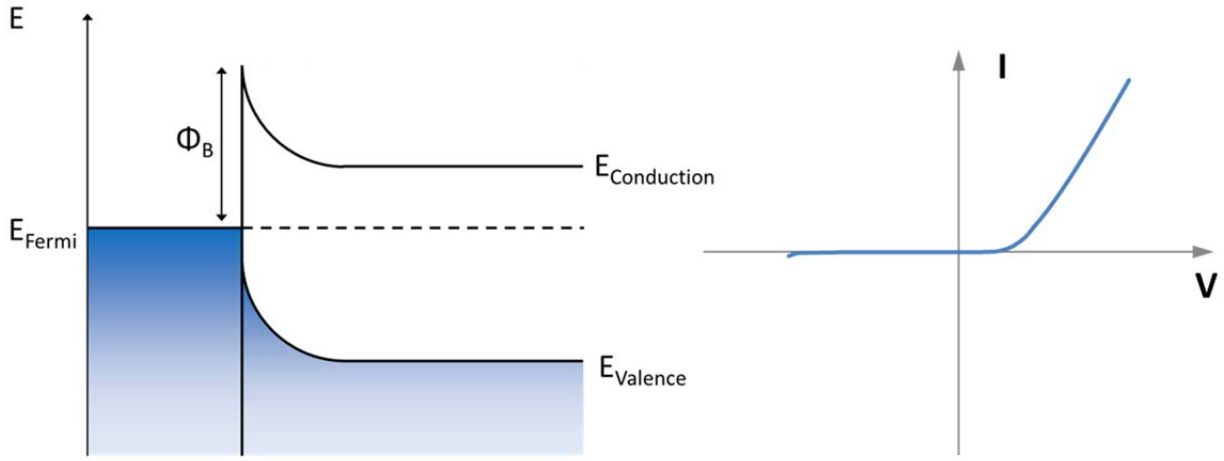

Figure 5 – *Energy diagram and I-V curve of a Schottky contact*

A non-adiabatic reaction event on a metal surface may generate hot electrons in the metal. If the electron's mean free path is greater than the thickness of the metal film, the electron may reach the Schottky barrier and transfer to the semiconductor, if it has a high enough energy. Finally, if the metal and semiconductor are connected into a closed circuit, this flow of electrons can be collected as a current.

Nienhaus *et al.* were the first to successfully measure such a current on a nanodiode.[17] Their devices consisted of Ag and Cu thin films deposited onto *n*- and *p*-doped Si wafers, with ohmic contacts on both sides of the wafer. When these diodes were exposed to a beam of H atoms, a current on the order of 0.01-1 nA was observed. This *chemicurrent* decayed exponentially to a steady-state value, in agreement with the kinetics of impinging particles competing for surface sites. Chemicurrent also showed an exponential decrease with film thickness, as predicted for hot charge carriers thermalizing in a solid. The chemicurrent yield, which is defined as the number of hot electrons collected for each adsorption event, was compared for atomic deuterium and hydrogen adsorption on Ag/*n*-Si. Deuterium produced 6 times less current than hydrogen, in agreement with a first-principles model of chemicurrent from hydrogen and deuterium on Cu.[18]

The same scheme was used for different types of diode and adsorbates: H on Ag/*n*-Si and Fe/*n*-Si, O_2 on Ag/*n*-Si,[19] NO and O_2 on Ag/*n*-Si,[20] or Mg on Mg/*p*-Si. [21] The chemicurrent yields vary from 10^{-6} to $5x10^{-3}$, depending on the diode and the adsorbate. The yield was found to closely correlate with the adsorption energy of many different species on Ag/*n*-Si, as did the chemicurrent kinetics.[22]

2.3. The catalytic nanodiode

In the previous experiments, chemicurrent was generated solely from adsorption events. However, nothing prevents any reaction occurring on a surface from behaving non-adiabatically and generating hot charge carriers. This includes desorption, as well as any step of a catalytic reaction that involves the motion of adsorbate nuclei and releases an amount of energy greater than the Schottky barrier used, if hot charge carriers are to be collected.

In an adsorption experiment, atoms or molecules impinge on the surface, adsorb or not, and desorb once the energy available from the thermal bath is high enough. Since the species desorbing is the same as the one that adsorbed, there is no net change in energy, and therefore no driving force to the process. This limits the amount of generated chemicurrent.

If instead the surface is the stage for an exothermic catalytic reaction, preferably that produces a species that quickly desorbs, the exothermicity will drive the reaction forward if the temperature is high enough for the molecules to overcome the activation barriers of the reaction. This would produce larger currents through the device.

This was done in our group for two reactions, CO oxidation and H_2 oxidation. For CO oxidation, Pt/TiO_2, Pd/TiO_2 and Pt/GaN diodes were used.[23–25] The device architectures are shown in figure 6, along with the detection scheme for the Pt/TiO_2 diode. The H_2 oxidation experiment is described in Chapter 3.[26]

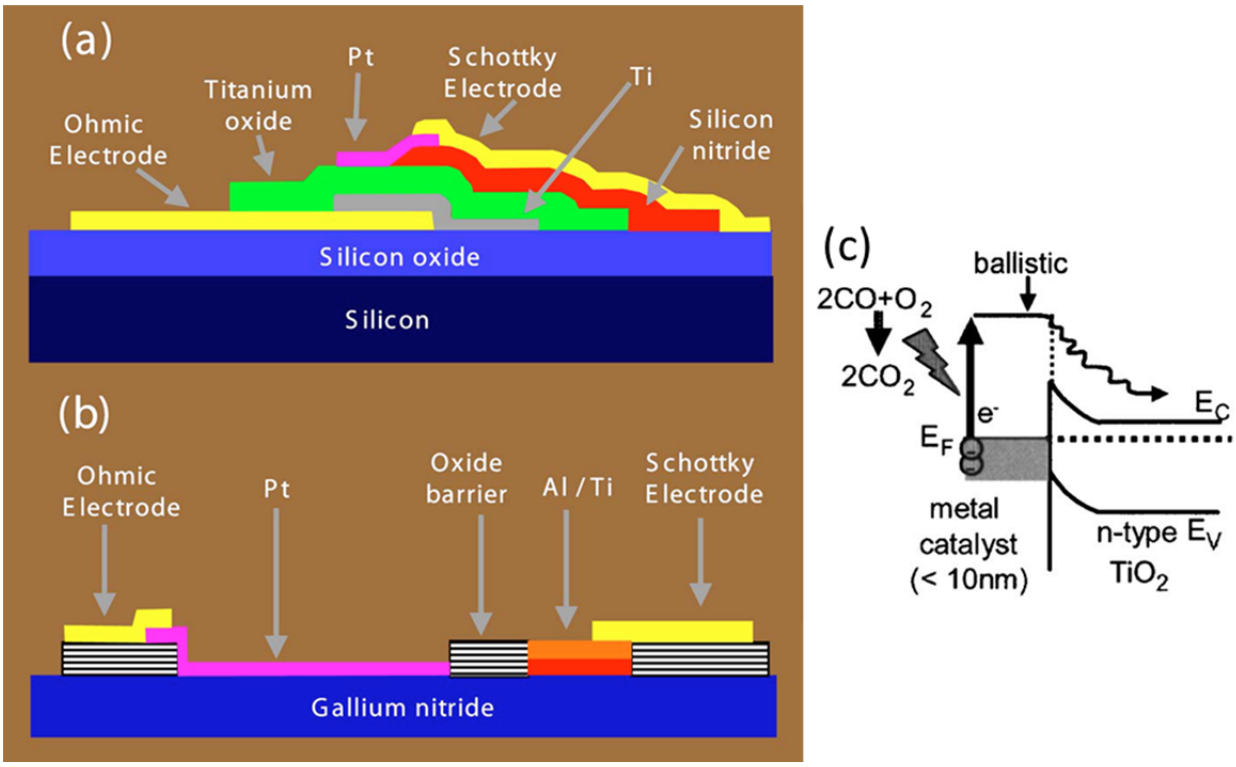

Figure 6 – ***(a) and (b)*** *Schematic cross sections of a Pt/TiO2 diode and a Pt/GaN diode, respectively.* ***(c)*** *Detection scheme for a hot electron collecting nanodiode. Reproduced from* [23]

The principle of the experiment is the same as for the experiments described in the previous section, but the currents measured are considerably greater, on the order of 10-100 nA. This is not due to higher efficiency: the number of hot electrons collected per reaction event varies from 10^{-4} to 10^{-3} on the catalytic nanodiodes, values comparable to those found by Nienhaus. This comes as no surprise, since the mechanism for generating chemicurrent is essentially the same. The increase in current is instead due to the higher turnover, which itself is the result of the higher temperature and the exothermic nature of the reaction.

3. Future possibilities

Catalytic nanodiodes can be thought of as a novel type of fuel cell, converting chemical energy into electricity. Without a dramatic enhancement in yield, however, their use as such remains limited. Their excellent sensitivity to chemistry suggests their use as sensors. Semiconductor electronic devices have long been used as gas detectors. In a typical configuration, a semiconductor is exposed to a gas. As gas molecules adsorb onto the semiconductor, a change in its conductivity occurs, which can be transduced into a measure of gas concentration in the air.[27]

A nanodiode could be made to work in a similar fashion, but is sensitive to turnover events in addition to gas concentration. A well-designed, stable nanodiode, calibrated for a particular reaction, would allow us to quantify the turnover reaction with a much higher time resolution than a gas chromatograph, for example.

The other, more exciting possibility is to operate in the opposite configuration. A bias applied to the diode results in either a charge flow to the surface or the presence of an electric field at the interface, which may influence the reactivity. The study by Bonn *et al*, discussed in section 2.1., of hot electron induced CO oxidation on Ru(0001), suggests as much.

Another study, by Maksymovych *et al.* leads to the same conclusions.[28] The authors prepared a surface of dimethyldisulfide (CH_3SSCH_3) molecules adsorbed on Au(111) and Au(100). Injecting hot electrons into the gold surface using the tip of a scanning tunneling microscope caused neighboring CH_3SSCH_3 molecules to split their S-S bond, and form a new one with their nearest neighbor. This led to conformation changes along chains up to 15 molecules in length.

Rather than induce charge flow to the surface, Mikheeva studied the effect of electric fields on reactivity.[29] The author designed reactors where the catalyst is placed in between macroscopic electrodes. Very high voltages, on the order of 10^8 $V.m^{-1}$ were applied, but with only small effects on surface chemistry. The use of large scale electrodes limits the magnitude of the field felt by molecules. Even at 10^8 $V.m^{-1}$, the voltage change over 1 nm is only 0.1 V.

While these experimental schemes are much too elaborate to have practical applications, they show that surface chemistry can be controlled to some extent by changing the electronic environment of adsorbates, and there are examples of this with nano-scaled electronic devices.

Wolf *et al* measured the vibrational frequency of CO adsorbed on a Pt/TiO_2 nanodiode using FTIR. They showed that when applying a bias to the diode, the vibrational frequency of the CO bond varies, in one direction or the other depending on the direction of bias. The change is reversible, and varies depending on where the adsorbates are located relative to the metal oxide interface. This is evidence that charge transfer occurs between a catalyst and its adsorbate, and that this charge transfer can be controlled to affect chemistry by changing bond strength.

Zhang *et al.* fabricated a field effect transistor with a SnO_2 nanowire acting as the gate oxide.[30] By varying the gate bias, the conductivity of the nanowire changes along with its electron density. The conductivity of the nanowire is also affected by adsorption of gas onto its surface, and measurements made while exposing the nanowire to different gas conditions seem to indicate that the rates of adsorption, desorption and CO oxidation could be changed by varying the gate bias.

The active area of a device built around a single nanowire is much too small to measure turnover rates. A nanodiode is two- rather than one-dimensional, and allows us to externally control turnover frequency using bias, as shown in Chapters 5 and 6.

References

(1) Born, M.; Oppenheimer, R. *Annalen der Physik* **1927**, *389*, 457-484.
(2) Levine, R. D. *Molecular reaction dynamics*; Cambridge University Press, 2005.
(3) Landau, L. D. *Phys. Z. Sowjetunion* **1932**, *2*.
(4) Zener, C. *Proceedings of the Royal Society of London. Series A* **1932**, *137*, 696 -702.
(5) Stückelberg, E. C. G. *Helvetica Physica Acta* **1932**, *5*, 369-423.
(6) Majorana, E. *Il Nuovo Cimento* **1932**, *9*, 43-50.
(7) Steinfeld, J. I.; Francisco, J. S.; Hase, W. L. *Chemical kinetics and dynamics*; Prentice Hall, 1999.
(8) Kasemo, B. *Phys. Rev. Lett.* **1974**, *32*, 1114.
(9) Böttcher, A.; Imbeck, R.; Morgante, A.; Ertl, G. *Phys. Rev. Lett.* **1990**, *65*, 2035.
(10) Martin, W. *Surface Science* **1997**, *377-379*, 343-349.
(11) Morin, M.; Levinos, N. J.; Harris, A. L. *The Journal of Chemical Physics* **1992**, *96*, 3950.
(12) Head-Gordon, M.; Tully, J. C. *The Journal of Chemical Physics* **1992**, *96*, 3939.
(13) Chang, H.-C.; Ewing, G. E. *Phys. Rev. Lett.* **1990**, *65*, 2125.
(14) Bonn, M.; Funk, S.; Hess, C.; Denzler, D. N.; Stampfl, C.; Scheffler, M.; Wolf, M.; Ertl, G. *Science* **1999**, *285*, 1042 -1045.
(15) Anisimov, S. I.; Kapeliovich, T. L.; Perelman, T. L. *Zhurnal Eksperimentalnoi I Teoreticheskoi Fiziki* **1974**, *66*, 776-781.
(16) Anisimov, S. I.; Rethfeld, B. In *Proceedings of the SPIE - The International Society for Optical Engineering*; SPIE-Int. Soc. Opt. Eng: USA, 1997; pp. 192-203.
(17) Nienhaus, H.; Bergh, H. S.; Gergen, B.; Majumdar, A.; Weinberg, W. H.; McFarland, E. W. *Phys. Rev. Lett.* **1999**, *82*, 446.
(18) Trail, J. R.; Graham, M. C.; Bird, D. M.; Persson, M.; Holloway, S. *Phys. Rev. Lett.* **2002**, *88*, 166802.

(19) Nienhaus, H.; Bergh, H. S.; Gergen, B.; Majumdar, A.; Weinberg, W. H.; McFarland, E. W. *Surface Science* **2000**, *445*, 335-342.
(20) Gergen, B.; Weyers, S. J.; Nienhaus, H.; Weinberg, W. H.; McFarland, E. W. *Surface Science* **2001**, *488*, 123-132.
(21) Hagemann, U.; Krix, D.; Nienhaus, H. *Phys. Rev. Lett.* **2010**, *104*, 028301.
(22) Gergen, B.; Nienhaus, H.; Weinberg, W. H.; McFarland, E. W. *Science* **2001**, *294*, 2521 - 2523.
(23) Park, J. Y.; Somorjai, G. A. *Journal of Vacuum Science & Technology B: Microelectronics and Nanometer Structures* **2006**, *24*, 1967.
(24) Park, J. Y.; Renzas, J. R.; Hsu, B. B.; Somorjai, G. A. *J. Phys. Chem. C* **2007**, *111*, 15331-15336.
(25) Park, J. Y.; Lee, H.; Renzas, J. R.; Zhang, Y.; Somorjai, G. A. *Nano Lett.* **2008**, *8*, 2388-2392.
(26) Hervier, A.; Renzas, J. R.; Park, J. Y.; Somorjai, G. A. *Nano Lett.* **2009**, *9*, 3930-3933.
(27) Seiyama, T.; Kato, A.; Fujiishi, K.; Nagatani, M. *Anal. Chem.* **1962**, *34*, 1502-1503.
(28) Maksymovych, P.; Sorescu, D. C.; Jordan, K. D.; Yates, J. T. *Science* **2008**, *322*, 1664 -1667.
(29) Mikheeva, E. P. *Russian Chemical Reviews* **1989**, *58*, 517-533.
(30) Zhang, Y.; Kolmakov, A.; Chretien, S.; Metiu, H.; Moskovits, M. *Nano Lett.* **2004**, *4*, 403-407.

Chapter 3

Hydrogen Oxidation-Driven Hot Electron Flow Detected by Catalytic Nanodiodes

Hydrogen oxidation on platinum is shown to be a surface catalytic chemical reaction that generates a steady state flux of hot (> 1 eV above the Fermi level) conduction electrons. These hot electrons are detected as a steady-state chemicurrent across Pt/TiO_2 Schottky diodes whose Pt surface is exposed to hydrogen and oxygen. Kinetic studies establish that the chemicurrent is proportional to turnover frequency for temperatures ranging from 298 K to 373 K, for P_{H2} between 1 and 8 Torr and P_{O2} at 760 Torr. Both chemicurrent and turnover frequency exhibit a first order dependence on P_{H2}.

Introduction

Any exothermic adsorption process or chemical reaction at a metal surface produces electron-hole pairs since no gap exists between occupied and unoccupied electronic energy levels in metals. Usually only a small fraction of the reaction heat is transferred to an electron-hole pair. A few chemical processes on high work-function metal surfaces have been recently discovered that transfer a substantial fraction of the reaction heat to the kinetic energy of individual metal electrons.[1–12] There is growing evidence which indicates that these energetic electrons, often called hot electrons, influence surface reactivity.[13,14] These energetic subsurface electrons have been directly detected in metal/semiconductor Schottky diodes whose metal surface is subject to a chemical process.[15–17] These diodes are made by depositing a thin-metal film onto a semiconductor in such a way that a Schottky barrier between the two is created, as shown in figure 1. If the fraction of the reaction heat that is transferred to a metal electron exceeds the Schottky barrier, the electron will travel ballistically through the metal conduction band, and possibly reach the semiconductor, where it would contribute to the observed electric current, referred to as chemicurrent as shown in Fig. 1a. Non-catalytic metal-semiconductor diodes have been used to prove that hot electrons are generated in adsorption reactions in ultrahigh vacuum (UHV) at temperatures below 150 K.[18–20] By using catalytic metal-semiconductor diodes such as Pt/TiO_2 or Pt/GaN, it has also been possible to detect steady chemicurrent from catalytic CO oxidation at atmospheric pressure, between 400 K and 550 K.[16,21] A family of models assuming that the non-adiabatic energy transfer during a surface chemical process is dominated by electron-hole pair excitations has been suggested.[4,22–24] Nonetheless, the question of whether surface catalytic reactions other than CO oxidation can generate chemicurrent has not been confirmed. This question is of importance because it can indicate that hot electron generation during an exothermic catalytic reaction is a general phenomenon.

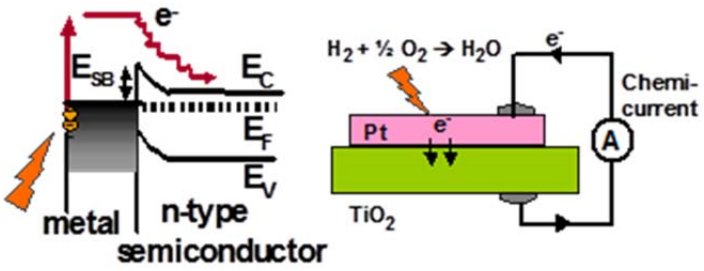

Figure 1 – *Energy diagram of a catalytic metal-semiconductor diode, along with a cross-section of the Pt/TiO₂ diode. The metal-semiconductor interface creates a Schottky barrier (E_{SB}), equal to the difference between the metal's work function and the semiconductor's electron affinity. In order to be collected, electrons need to have an excess energy higher than the Schottky barrier.*

We describe here the detection of steady state chemicurrent in catalytic hydrogen oxidation on Pt. Hydrogen oxidation has a reaction heat of $\Delta h_{H_2O} = -2.5$ eV per water molecule,[25] which is well below platinum's work function of 5–6 eV, and below the thresholds for Pt surface or bulk electronic collective modes.[11] Distinct reaction pathways may be followed in different conditions.[25–28] Hydrogen oxidation well above water desorption temperature proceeds mainly via a Langmuir-Hinshelwood rate-limiting step $O_{(a)}+H_{(a)} \rightarrow OH_{(a)}$.[27,29] The reactive desorption of H_2O may involve $H_{(a)} + OH_{(a)} \rightarrow H_2O_{(a)}$ [26,28] or $2OH_{(a)} \rightarrow H_2O_{(a)} + O_{(a)}$; with reported low coverage activation energies of 16 kcal/mol and 18 kcal/mol respectively.[30] The activation energy is substantially lowered below the water desorption temperature, as surface water catalyzes hydroxyl formation.[28] On oxygen-covered Pt(111), another channel, $H_2O_{(a)} + O_{(a)} \rightarrow 2OH_{(a)}$, is open above 150K, and reactive desorption, $2OH_{(a)} \rightarrow H_2O_{(a)} + O_{(a)}$ begins above 215K and continues beyond 300K.[31] Most of these studies are conducted in UHV; much less is known at atmospheric pressure.

In this chapter, we present the experimental detection of a continuous flux of energetic (hot) electrons during catalytic hydrogen oxidation using Pt/TiO_2 catalytic nanodiodes at atmospheric pressures. The hydrogen oxidation reaction reported to produce hot electrons is the second catalytic reaction under atmospheric pressures following the CO oxidation reaction that was reported elsewhere earlier.[15,21] We establish the dependence of the hot electron flow, referred to as chemicurrent, and reaction turnover rate on hydrogen partial pressure.

Experimental section

The design of nanodiodes tested in this work is described elsewhere.[32] Briefly, p-type (100) silicon wafers with a 500 nm thermally grown silicon oxide film were subjected to a standard piranha clean prior to further processing. The first step consists of depositing a 4×4 mm^2, 150 nm thick film of titanium oxide onto the silicon oxide through an aluminum shadow mask, by reactive direct current (DC) magnetron sputtering. The wafer is then annealed in O_2, using rapid thermal annealing at 648 K for 5 minutes. A 10 nm film of titanium is then deposited through a second mask using electron beam evaporation. A 50 nm gold film, which constitutes the

nanodiode's two ohmic electrodes, is then deposited through the same mask. The titanium serves as an adhesive between the gold and the titanium oxide. Finally, a 5 nm platinum catalyst film is deposited through a third mask, for a total active area of 3 mm^2 per diode. Barrier heights and ideality factors for the nanodiode are obtained by fitting the current-voltage (I-V) curves of diodes to the thermionic emission equation.[32] Typical barrier height and ideality factors for the Pt/TiO_2 nanodiodes are 1.1–1.2 eV, and 1.5–2.0, respectively.

The nanodiode is placed on a ceramic heater, and the temperature is monitored by a thermocouple, fluctuating by less than 0.5 K. The turnover of water molecules was obtained by monitoring the amount of H_2 during the reaction, using a gas chromatograph connected to the chamber by a sample loop equipped with a circulation pump. The nanodiode's electrodes are connected to an electrical circuit with gold wires, making it possible to characterize the device by measuring its I-V curve with a sourcemeter. The same sourcemeter is used to measure chemicurrent passing through the diode while the chemical reaction is taking place. No voltage bias is applied to the diode.

Since TiO_2 is quickly (within seconds) reduced by atomic hydrogen, which diffuses through the platinum film,[33] and since the hydrogen/oxygen mixture is explosive in certain conditions, oxygen is used in large excess (>99%). The reaction is conducted in a batch reactor with a volume of about 1 liter, pumped down to 10^{-6} Torr in between runs. The rectifying performance of the diodes degrades with hydrogen exposure because of the spill-over effect as. Under our hydrogen oxidation conditions, however, where we have a large excess of oxygen, the diodes sustain their rectifying behavior. This suggests that the oxygen keeps the semi-conductor part of the diode oxidized, or prevents the hydrogen from diffusing through the platinum. With spill-over largely absent, the Schottky barrier remains constant on the time scale of the experiments.

Results and Discussion

Figure 2a shows the current measured with a Pt/TiO_2 diode under reaction conditions, as a function of time, during a temperature ramp from 298 K to 373 K, in 6 Torr of H_2 and 760 Torr of O_2. The current increases with temperature and is stable at fixed temperatures. The thermoelectric current was separately measured under 1 atmosphere of He, and is found to be lower than 0.3 nA at 373 K. Because the current detected under hydrogen oxidation at 373 K (17±1 nA) is much higher than the thermoelectric current, most of the current signal can be attributed to the chemicurrent. The reaction is concurrently monitored using a gas chromatograph in order to determine chemicurrent yield (number of electrons detected per reaction event). Figure 2b shows the number of water molecules per platinum site produced on the Pt/TiO_2 diode under 6 Torr of H_2 and 760 Torr of O_2, as a function of time; it is assumed that the surface Pt site density is equivalent to that of Pt(111). The turnover frequency at different temperatures is obtained by taking the slope of the plots, and increases with temperature, as shown in figure 2b.

The activation energy is determined using the turnover rate and chemicurrent measured as a function of temperature. Figure 3 shows the resulting Arrhenius plots on the same graph. The error bars in the plot correspond to the standard deviations of the measurements. The two

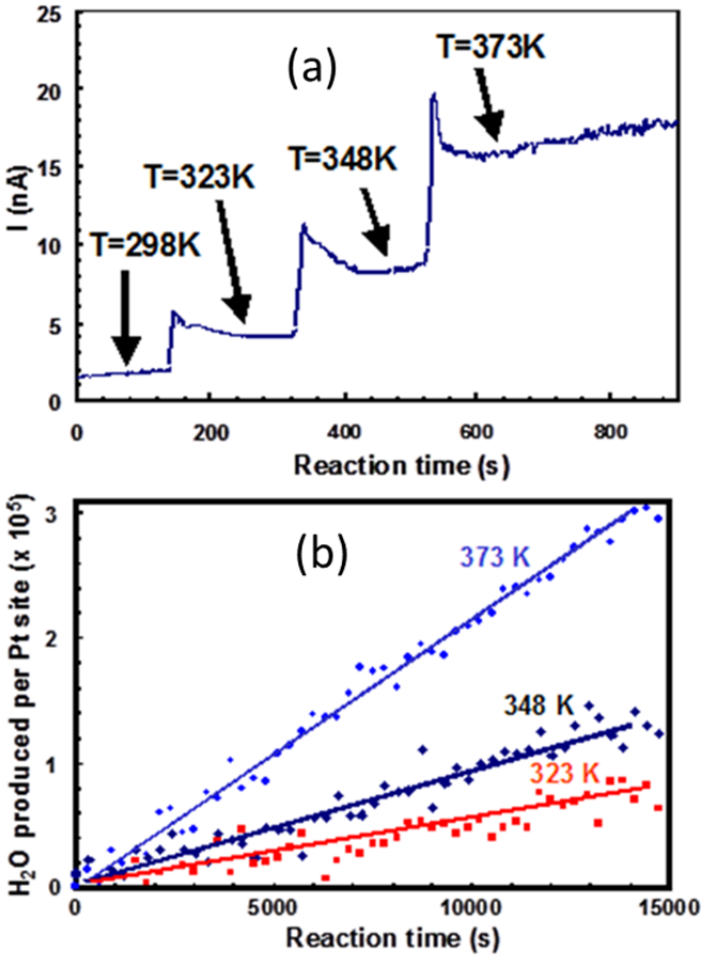

Figure 2 – *(a) Chemicurrent measured at different temperatures on a Pt/TiO_2 diode, in 6 Torr of H_2 and 760 Torr O_2. (b) Plot of water molecules produced in hydrogen oxidation reaction per platinum site as a function time. Turnover at different temperatures can be obtained by taking the slope of the plots.*

resulting activation energies match (7.4 ± 0.3 kcal/mol for chemicurrent and 7.6 ± 0.6 kcal/mol for turnover rate), which implies that the chemicurrent originates from the catalytic reaction. Again, thermoelectric current is negligible (<0.3 nA) in the range of temperatures (298–373 K) used here. The effect of an increase in the sample temperature due to the heat of reaction has been shown to be negligible in previous work [21]. The activation energy for hydrogen oxidation under identical conditions (6 Torr of H_2 and 760 Torr of O_2) measured on a Pt foil separately is 8.3 (± 0.6) kcal/mol, which is comparable to that on Pt/TiO_2 nanodiodes within the experimental error.

The dependence of chemicurrent and turnover rate on the partial pressure of H_2 is also investigated. Figure 4a shows the measurement of turnover rate at five different partial pressures of H_2 from 1 to 8 Torr, and indicates a linear relationship between water formation

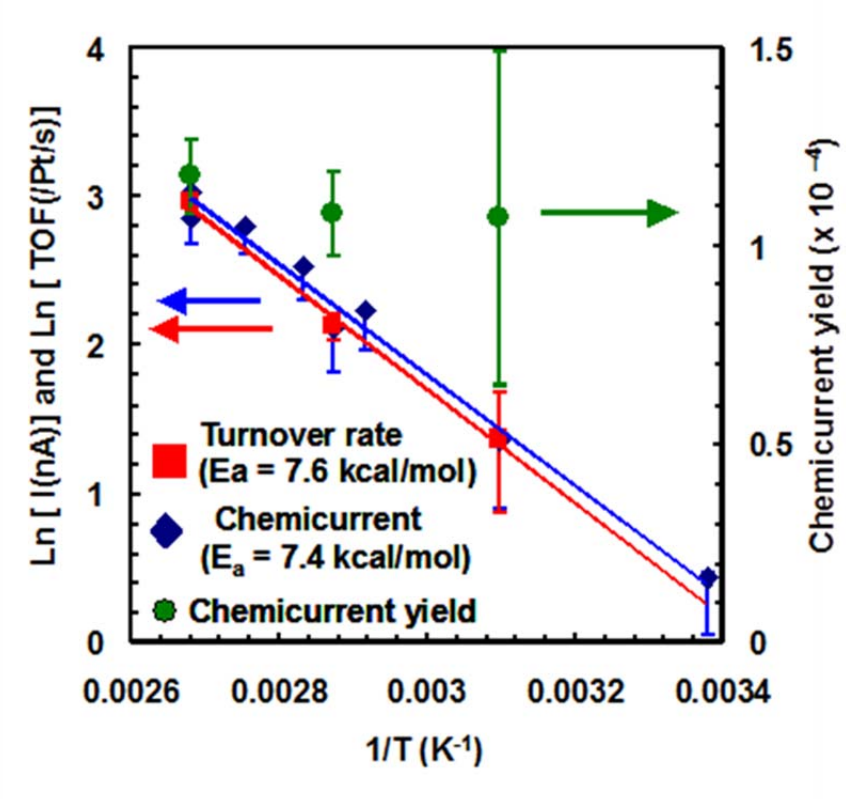

Figure 3 – *Arrhenius plots obtained from chemicurrent and turnover measurements on a Pt/TiO_2 diode with pressure of 6 Torr of H_2 and 760 Torr O_2. Both give similar activation energies, which implies that hot electron generation under hydrogen oxidation is proportional to the catalytic turnover rate. The error is associated with multiple measurements of chemicurrent and turnover rates.*

and H_2 partial pressure, consistent with a Langmuir-Hinshelwood mechanism. Figure 4b shows the plot of chemicurrent as a function of partial pressure of H_2 measured at four different temperatures, with again a linear dependence between chemicurrent and partial pressure of H_2.

The apparent chemicurrent yield can be obtained by dividing chemicurrent (number of electron per second) by turnover rate (number of product molecules per platinum site per second). Therefore, the chemicurrent yield represents the hot electrons collected per product molecule formed on a single metal site. Its value in hydrogen oxidation, based on measurements at several different temperatures, is $(1.1 \pm 0.1) \times 10^{-4}$. The apparent yield in CO oxidation on the same 5 nm Pt/TiO_2 diode[32] is $2.3 \pm 0.5 \times 10^{-4}$. The lower chemicurrent yield of H_2 oxidation compared to CO oxidation may be associated with the lower reaction heat of H_2 oxidation (2.5 eV per product molecule, H_2O[34,35]) compared to that of CO oxidation (2.9 eV per product molecule, CO_2[36]). These apparent chemicurrent yields are comparable in order of magnitude to those seen in chemisorption of hydrogen on Ag/n-Si(111) and Cu/n-Si(111) diodes

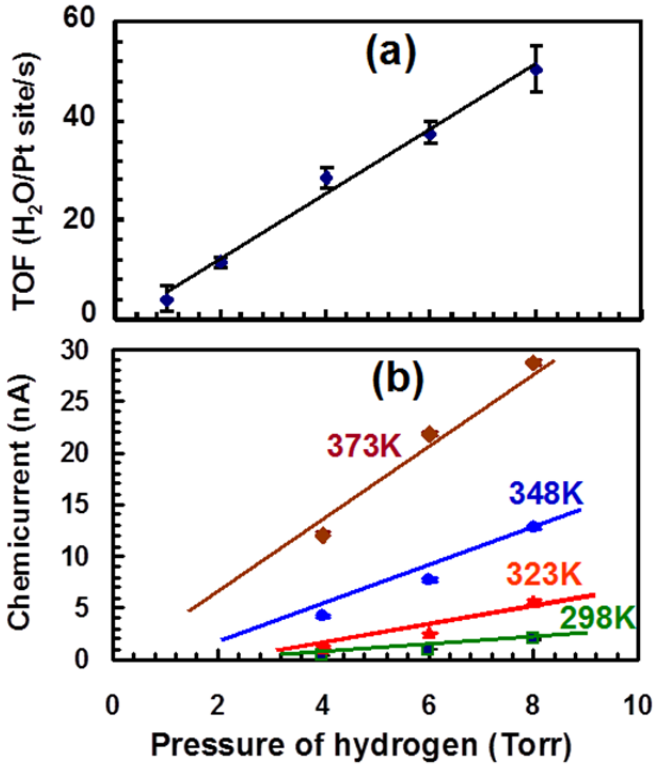

Figure 4 – *(a) Turnover frequency for different pressures of H_2 in 760 Torr of O_2, at 353K, measured with gas chromatography. (b) A plot of chemicurrent as a function of different pressures of H_2 in 760 Torr of O_2. Both series of measurements exhibit a linear increase as the pressure of hydrogen rises.*

with 7.5 nm metal films (chemicurrent yields of 4.5×10^{-3} and 1.5×10^{-4} electrons per adsorption event, respectively).[20]

Figure 5 shows the I-V curve of a 5 nm Pt/TiO_2 device after exposure to 2 Torr of hydrogen in 760 Torr of helium. The hydrogen diffuses through the platinum, a phenomenon referred to as spill-over[37] , and quickly reduces the TiO_2,[33,38,39], changing the diode into a resistor. In addition to damaging the device, hydrogen spillover shifts the baseline current by the order of 100 nA at room temperature, making it difficult to reliably measure chemicurrent. Pumping down the chamber does nothing to reduce the current through the diode. This current disappears after oxidizing conditions such as moderate heating (350 K) in 760 Torr of oxygen for several minutes, presumably because it allows the oxygen to re-oxidize the titanium oxide.

However, under hydrogen oxidation conditions where the pressure of oxygen is larger than that of hydrogen, we found that the spill-over effect is ignorable. Figure 5 shows the I-V plot of diodes measured under hydrogen oxidation conditions (6 Torr of hydrogen in 760 Torr of oxygen) providing evidence of good rectifying behaviors. The Schottky barrier of the diode obtained by fitting I-V curve to thermionic emission is 1.1 eV, which is maintained throughout the hydrogen oxidation reaction. Furthermore, this current disappears immediately when the chamber is pumped down, contrary to what occurs without oxygen. It is likely that in a large

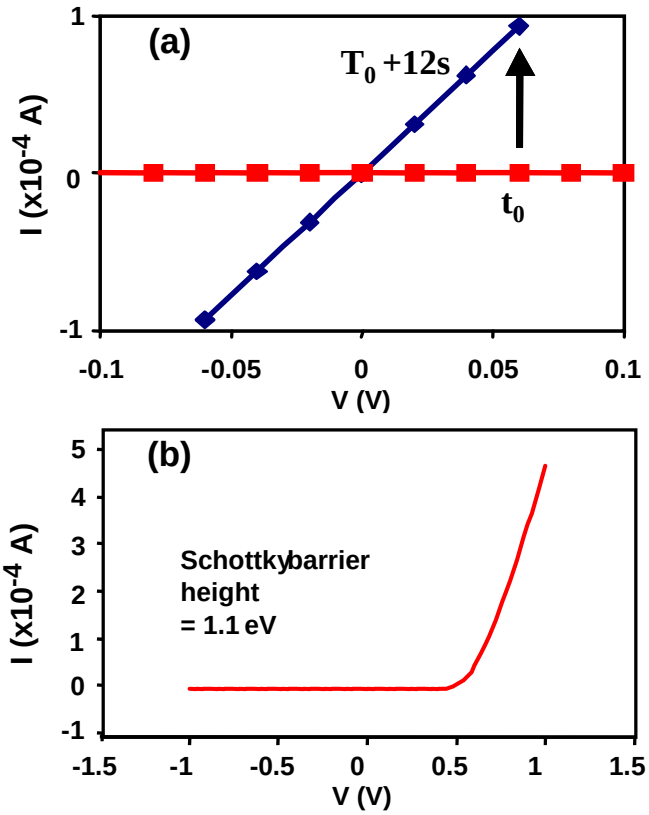

Figure 5 – *(a) I-V curve of a 5 nm Pt/TiO2 device after exposure to 2 Torr of hydrogen in 760 Torr of helium. After 12 seconds of exposure to hydrogen, the diode turns into the resistor because of hydrogen spillover effect. (b) I-V plot of diodes measured under hydrogen oxidation condition (6 Torr of hydrogen in 760 Torr of oxygen) showing the absence of a hydrogen spillover effect under excess oxygen. The Schottky barrier height obtained from the I-V curve is 1.1 eV*

excess of oxygen, the hydrogen is oxidized before it has a chance to diffuse through the platinum, and that the current measured is the result of the hydrogen oxidation, not of hydrogen spill-over.

Conclusion

These H_2 oxidation results, together with earlier results for CO oxidation, can be seen as model reactions for hot electron generation in the complete combustion of hydrogen and oxygen containing species: hydrocarbons, alcohols, ethers, aldehydes, ketones, and carboxylic acids, etc. This points to potential applications of nanodiodes as chemical sensors that could perform across a wide pressure range from the ultrahigh vacuum to the high pressures relevant in industrial catalysis.

In conclusion, the catalytic oxidation of hydrogen on a Pt/TiO_2 nanodiode yields a steady state chemicurrent, which is proportional to turnover frequency. In contrast to the earlier studies of CO oxidation, stronger evidence for the intimate correlation between the surface

chemistry and hot electron flow is presented here as the thermoelectric effect is negligible due to the low temperature of reaction (below 120^{o}C) compared to the earlier studies of CO oxidation. The fact that both H_2/O_2 and CO oxidation are exothermic catalytic reactions yielding experimentally measured hot electron flow suggests that the chemical phenomenon of hot electron production during catalytic reactions on transition metal surfaces may be widespread.

References

(1) Denzler, D. N.; Frischkorn, C.; Hess, C.; Wolf, M.; Ertl, G. *Phys. Rev. Lett.* **2003**, *91*, 226102.
(2) Gadzuk, J. W. *J. Phys. Chem. B* **2002**, *106*, 8265-8270.
(3) Masel, R. I. *Principles of adsorption and reaction on solid surfaces*; Wiley: New York, 1996.
(4) Mizielinski, M. S.; Bird, D. M.; Persson, M.; Holloway, S. *The Journal of Chemical Physics* **2005**, *122*, 084710.
(5) Somorjai, G. A.; Park, J. Y. *Catalysis Letters* **2007**, *115*, 87-98.
(6) Hasselbrink, E. *Current Opinion in Solid State and Materials Science* **2006**, *10*, 192-204.
(7) Wodtke, A. M.; Matsiev, D.; Auerbach, D. J. *Progress in Surface Science* **2008**, *83*, 167-214.
(8) Huang, Y.; Wodtke, A. M.; Hou, H.; Rettner, C. T.; Auerbach, D. J. *Phys. Rev. Lett.* **2000**, *84*, 2985.
(9) Kasemo, B.; Törnqvist, E.; Nørskov, J. K.; Lundqvist, B. I. *Surface Science* **1979**, *89*, 554-565.
(10) Hermann, N. *Surface Science Reports* **2002**, *45*, 1-78.
(11) Liebsch, A. *Electronic excitations at metal surfaces*; Plenum Press: New York, 1997.
(12) Shenvi, N.; Cheng, H.; Tully, J. C. *Phys. Rev. A* **2006**, *74*, 062902.
(13) Komeda, T.; Kim, Y.; Fujita, Y.; Sainoo, Y.; Kawai, M. *The Journal of Chemical Physics* **2004**, *120*, 5347.
(14) Maksymovych, P.; Sorescu, D. C.; Jordan, K. D.; Yates, J. T. *Science* **2008**, *322*, 1664 -1667.
(15) Ji, X.; Zuppero, A.; Gidwani, J. M.; Somorjai, G. A. *Nano Lett.* **2005**, *5*, 753-756.
(16) Park, J. Y.; Somorjai, G. A. *Journal of Vacuum Science & Technology B: Microelectronics and Nanometer Structures* **2006**, *24*, 1967.
(17) Park, J. Y.; Lee, H.; Renzas, J. R.; Zhang, Y.; Somorjai, G. A. *Nano Lett.* **2008**, *8*, 2388-2392.
(18) Gergen, B.; Nienhaus, H.; Weinberg, W. H.; McFarland, E. W. *Science* **2001**, *294*, 2521 - 2523.
(19) Krix, D.; Nünthel, R.; Nienhaus, H. *Journal of Vacuum Science & Technology A: Vacuum, Surfaces, and Films* **2007**, *25*, 1156.
(20) Nienhaus, H.; Bergh, H. S.; Gergen, B.; Majumdar, A.; Weinberg, W. H.; McFarland, E. W. *Phys. Rev. Lett.* **1999**, *82*, 446.
(21) Park, J. Y.; Somorjai, G. A. *ChemPhysChem* **2006**, *7*, 1409-1413.
(22) Maximoff, S. N.; Head-Gordon, M. P. *Proceedings of the National Academy of Sciences* **2009**, *106*, 11460 -11465.
(23) Persson, M.; Hellsing, B. *Phys. Rev. Lett.* **1982**, *49*, 662.
(24) Trail, J. R.; Graham, M. C.; Bird, D. M.; Persson, M.; Holloway, S. *Phys. Rev. Lett.* **2002**, *88*, 166802.
(25) Williams, W. R.; Marks, C. M.; Schmidt, L. D. *J. Phys. Chem.* **1992**, *96*, 5922-5931.

(26) Michaelides, A.; Hu, P. *J. Am. Chem. Soc.* **2001**, *123*, 4235-4242.
(27) Smith, J.; Palmer, R. *Journal of Chemical Physics* **1972**, *56*, 13-&.
(28) Völkening, S.; Bedürftig, K.; Jacobi, K.; Wintterlin, J.; Ertl, G. *Phys. Rev. Lett.* **1999**, *83*, 2672-2675.
(29) Verheij, L. K.; Hugenschmidt, M. B.; Cölln, L.; Poelsema, B.; Comsa, G. *Chemical Physics Letters* **1990**, *166*, 523-530.
(30) Anton, A. B.; Cadogan, D. C. *Surface Science* **1990**, *239*, L548-L560.
(31) Fisher, G. B.; Sexton, B. A. *Phys. Rev. Lett.* **1980**, *44*, 683.
(32) Park, J. Y.; Renzas, J. R.; Hsu, B. B.; Somorjai, G. A. *J. Phys. Chem. C* **2007**, *111*, 15331-15336.
(33) Roland, U.; Braunschweig, T.; Roessner, F. *Journal of Molecular Catalysis A: Chemical* **1997**, *127*, 61-84.
(34) Hanson, F. V.; Boudart, M. *Journal of Catalysis* **1978**, *53*, 56-67.
(35) Hellsing, B.; Kasemo, B.; Zhdanov, V. P. *Journal of Catalysis* **1991**, *132*, 210-228.
(36) Kwong, D. W. J.; De Leon, N.; Haller, G. L. *Chemical Physics Letters* **1988**, *144*, 533-540.
(37) Conner, W. C.; Falconer, J. L. *Chem. Rev.* **2011**, *95*, 759-788.
(38) Walton, R. M.; Dwyer, D. J.; Schwank, J. W.; Gland, J. L. *Applied Surface Science* **1998**, *125*, 187-198.
(39) Beck, D. D.; White, J. M. *J. Phys. Chem.* **1984**, *88*, 174-175.

Chapter 4

Isotope Effects in Hydrogen and Deuterium Oxidation on Catalytic Nanodiodes

Previous experiments have shown that reactions occurring on the surface of a metal / semiconductor nanodiode can generate a current proportional to the turnover frequency of the reaction. Isotope studies have been performed to elucidate the mechanism for the generation of these chemicurrents, in the case of hydrogen adsorption. We report here that current produced under hydrogen oxidation on a Pt/TiO_2 diode is 3 to 4 times smaller than under deuterium oxidation. Turnover frequencies are measured for both reactions to show that this would imply that the chemicurrent yield for deuterium is almost 5 times higher than for hydrogen, contrary to what would be expected from the slower speed of deuterium at a given temperatue, and contrary to what has been reported for adsorption experiments. The different rates of spillover from Pt to TiO_2 for the two isotopes may also explain the differences in current.

Introduction

The Born-Oppenheimer approximation states that nuclear motion does not couple with electronic excitations.[1] The electrons, which are many orders of magnitude lighter than nuclei and therefore much faster, ordinarily have enough time to adapt to nuclear motion to stay in a relaxed state. There are examples however, where motion along the nuclear coordinates is fast enough, and where the energy for electronic excitation is small enough, that the Born-Oppenheimer approximation breaks down, a situation referred to as non-adiabatic.[2–4] This situation is likely to occur on metal surfaces, where there exists a continuum of energy states available to the electrons.[5]

The detection of such electronic excitations is difficult however, since in most cases, the excited electron still has an energy lower than the work function, and remains confined to the metal, where it thermalizes within femtoseconds.[6] Nanodiodes have proven a useful tool in quantifying these hot electrons: they consist of a thin metal film deposited onto a semiconductor chosen such that an energy barrier, known as the Schottky barrier, forms at the interface. By making the metal film thinner than the mean free path of the hot electron, and by having an asymmetrical barrier at the interface, these hot electrons can collected as a "chemicurrent".

One of the limits of the nanodiode is the lack of energy resolution. Exothermic events on the surface lead to electronic excitations on the order of 1 eV, and Schottky barrier heights are in the same range. The depletion layer within the semiconductor that electrons must go

through is on the order of 100 nm, which rules out the possibility of tunneling. Therefore all that is known about the energies of electrons collected is that they are greater than the Schottky barrier. This makes it difficult to understand the non-adiabatic mechanism that leads to the generation of hot electrons.

Isotopic studies are ideal for studying non-adiabatic phenomena on catalytic nanodiodes. They allow us to perform the same reaction with atoms moving at different speeds while bond energies are practically unchanged, providing us valuable insight for developing a model of non-adiabatic reactions on surfaces. Hydrogen and deuterium are the most practical choice, since the mass ratio between them is very large, and deuterium is readily available.

Previous experiments by Nienhaus have shown changes in chemicurrent yield for D relative to H.[7–9] An H atom impinging on Ag/*n*-Si(111) diodes was found to be 6 times more likely to generate a hot electron than a D atom, with probabilities on the order of 10^{-3}. This is what one would expect, since D is slower than H for the same kinetic energy. The authors rule out the smaller adsorption probability of D as a cause for this, and point instead to the difference in vibrational level energies of D-Ag and H-Ag. Those levels are closer together in D-Ag than in H-Ag, therefore transferring a given amount of energy to a lattice electron involves a higher order vibrational relaxation for D-Ag. Since the transition probability decreases with the order, D atoms would be less efficient at generating hot electrons.[7]

In a later study, H and D adsorption on Ag/*p*-Si was studied with a more accurate measurement of the atom flux on the surface.[8] The yield was found to be 3.7 times higher for D atoms than H, in agreement with theoretical predictions. While chemicurrents collected decrease exponentially with the metal film thickness, the yield ratio for D and H remained the same.

Previous experiments have shown that chemicurrents can be generated not just from adsorption, but also from exothermic catalytic reactions.[10,11] At high enough temperatures, the exothermicity drives the reaction forward, leading to much higher turnover rates and therefore chemicurrents. On Pt/TiO_2 diodes, hydrogen oxidation was found to generate 10^{-4} hot electrons for each reaction event on the surface.

We report here that the chemicurrent from D oxidation is three times higher than for H oxidation. By adjusting for differences in turnover, this would imply a chemicurrent yield that is 40% higher for D oxidation, contrary to adsorption experiments and theoretical expectations. We also find that the ability of the diode to rectify is decreased in deuterium compared to hydrogen, which may explain the differences in current.

Experimental section

The design of nanodiodes tested in this work is described elsewhere.[10] *p*-type (100) silicon wafers with a 500 nm thermally grown silicon oxide film were subjected to a standard piranha clean prior to further processing. The first step consists of depositing a 4×4 mm^2, 150 nm thick film of titanium oxide onto the silicon oxide through an aluminum shadow mask, by reactive direct current (DC) magnetron sputtering. The wafer is then annealed in O_2, using rapid thermal

annealing at 648 K for 5 minutes. A 10 nm film of titanium is then deposited through a second mask using electron beam evaporation. A 50 nm gold film, which constitutes the nanodiode's two ohmic electrodes, is then deposited through the same mask. The titanium serves as an adhesive between the gold and the titanium oxide. Finally, a 5 nm platinum catalyst film is deposited through a third mask, for a total active area of 3 mm^2 per diode. Barrier heights and ideality factors for the nanodiode are obtained by fitting the current-voltage (I-V) curves of diodes to the thermionic emission equation.[10] Typical barrier height and ideality factors for the Pt/TiO_2 nanodiodes are 1.1–1.2 eV, and 1.5–2.0, respectively.

The nanodiode is placed on a ceramic heater, and the temperature is monitored by a thermocouple, fluctuating by less than 0.5 K. The turnover of water molecules was obtained by monitoring the amount of H_2 during the reaction, using a gas chromatograph connected to the chamber by a sample loop equipped with a metal bellows circulation pump. The nanodiode's electrodes are connected to an electrical circuit with gold wires, making it possible to characterize the device by measuring its I-V curve with a Keithley Sourcemeter. The same Sourcemeter is used to measure chemicurrent passing through the diode while the chemical reaction is taking place. No voltage bias is applied to the diode.

Since TiO_2 is quickly (within seconds) reduced by atomic hydrogen, which diffuses through the platinum film,[12] and since the hydrogen/oxygen mixture is explosive in certain conditions, oxygen is used in large excess (>99%). The reaction is conducted in a batch reactor with a volume of about 1 liter, pumped down to 10^{-6} Torr in between runs. The rectifying performance of the diodes degrades with hydrogen exposure because of the spill-over effect as. Under our hydrogen oxidation conditions, however, where we have a large excess of oxygen, the diodes sustain their rectifying behavior. This suggests that the oxygen keeps the semi-conductor part of the diode oxidized, or prevents the hydrogen from diffusing through the platinum. With spill-over largely absent, the Schottky barrier remains constant on the time scale of the experiments.

Results and discussion

A Pt/TiO_2 diode, which we will refer to as diode #1, was placed inside the chamber, which was evacuated down to a pressure of roughly 10^{-5} Torr. The diode was heated to 353 K, 750 Torr O_2 were introduced, an intensity vs. voltage curve was measured from -1 V to +1 V, and finally 6 Torr of H_2 were introduced and mixed in using the circulation pump. In these conditions of temperature and pressure, hydrogen and oxygen react on the surface at a rate measurable by gas chromatography.

Current through the diode is 0 initially then over the course of several minutes decreases to about -10 to -15 nA, and stabilizes. Once the current was stabilized, gases were pumped out, and the same experiment was repeated with deuterium. This sequence was repeated three times, resulting in the graph shown in figure 1. The direction of the current indicates a flow of electrons from the metal to the semiconductor. Current under deuterium oxidation is reproducibly on the order of 3 times that under hydrogen oxidation.

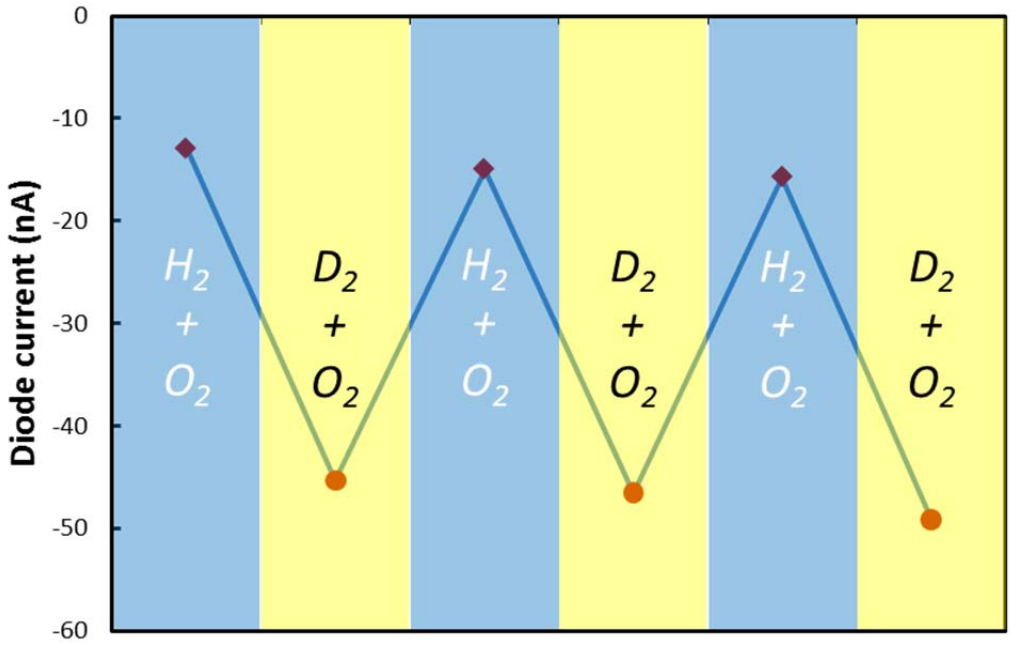

Figure 1 – *Current through Pt/Si nanodiode #1 in alternating hydrogen and deuterium oxidation conditions. Reaction conditions are 6 Torr H_2 / D_2 and 750 Torr O_2 at 353 K. The negative current represents a flow of electrons from the metal to the semiconductor.*

The same device, diode #1, was then used to measure turnover rates in order to determine chemicurrent yields. Since D atoms are heavier than H atoms, their diffusion on a surface or through a lattice is slower, which can influence turnover rates. Rates were measured in the same conditions of pressure of temperature, and in the same reactor, first for D_2 oxidation, then for H_2 oxidation. Figure 2 shows the decrease in the H_2 and D_2 concentration over the course of 200 minutes, showing a rate of H_2 consumption more than twice as high as for D_2. The rate was for D_2 oxidation was measured again after the H_2 oxidation measurement, to determine any activity loss over time. The D_2 oxidation rate was 15 % lower on the second measurement, which makes for a reasonable error in the comparison of D_2 and H_2.

I-V curves were measured throughout the experiment to ensure that rectification was maintained despite the sensitivity of TiO_2 to H_2. Figure 3 shows the I-V curve for the device initially and after each reaction. The first exposure to H_2 dramatically reduces the rectification factor and turn-on voltage, but the device stays rectifying after every subsequent step.

This evidence alone does not show that the current being measured is the result of the surface reaction. H_2 dissociatively adsorbs on Pt and spills over to the TiO_2 surface, which it reduces. The electron flow associated with this process can also be measured as a current. An identical device, diode #2, was subjected to a treatment similar to the previous one: it was exposed to 4 Torr of H_2 in 750 Torr of O_2, at 353 K, and current was measured. It was then exposed to the same conditions, with D_2 instead of H_2, and this cycle was repeated 4 times. The average currents during H_2 and D_2 exposure were 16 nA and 55 nA, respectively, similar to what was obtained for the previous diode. The device was then placed in 4 Torr D_2 and 750 Torr He,

at 353 K, where the current stabilized at -250 nA (see figure 4). After the gases were pumped out and replaced with helium, the current is stable at -270 nA, which is likely due to D still present on the surface. The helium was then pumped out to be replaced with 760 Torr of O_2, yielding a current of 0 nA. At 353 K, trace amounts of D on the surface are quickly converted to H_2O by O_2, which explains the absence of any current. Finally, the O_2 is pumped out, replaced with 4 Torr of H_2 in 750 Torr of He, and the current immediately stabilizes at -300 nA.

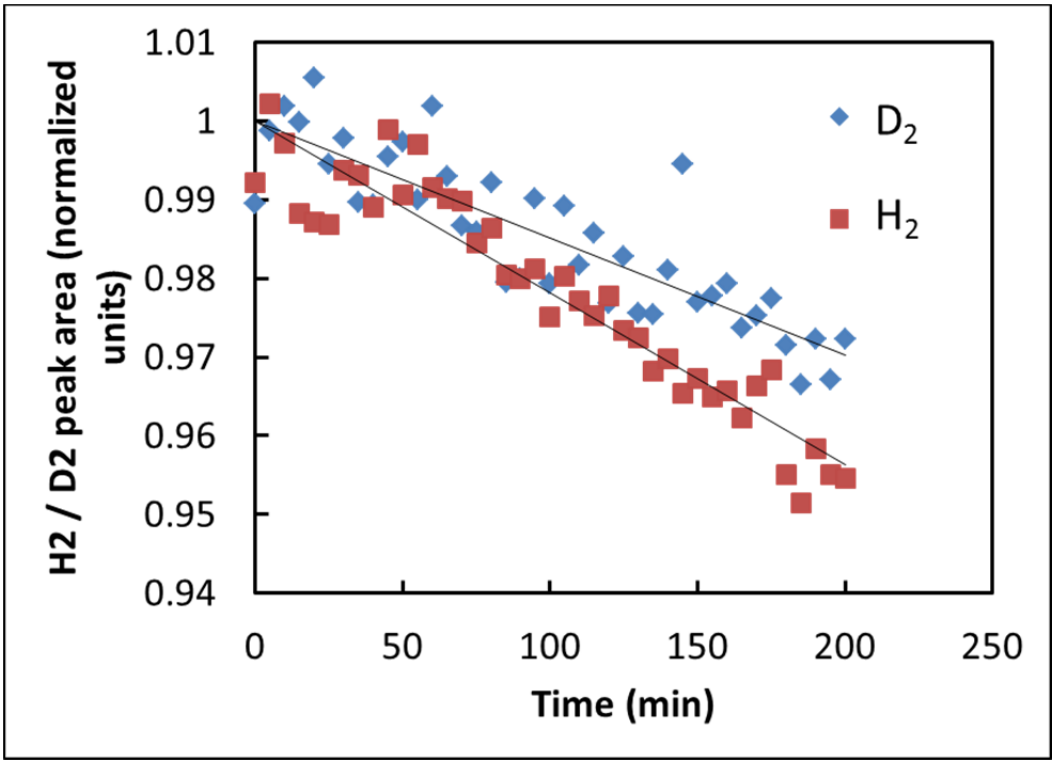

Figure 2 – *Change in the H_2 and D_2 peak areas in H_2 oxidation and D_2 oxidation on diode #1. Reaction conditions are 6 Torr H_2 or D_2 and 750 Torr O_2 at 353 K. Peak areas from gas chromatography are normalized to the initial peak area from linear fit.*

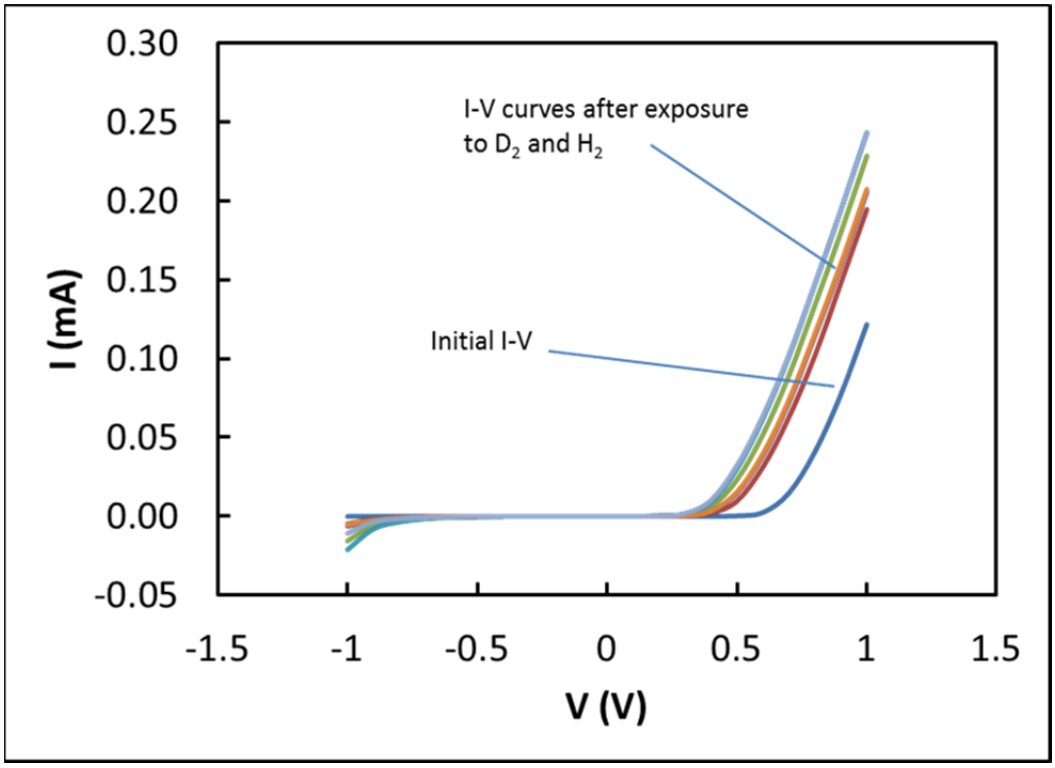

Figure 3 – *I-V curve of diode #1, initially, and after each H_2 and D_2 oxidation reaction. Hydrogen spillover causes a dramatic initial change in the diode's properties after the first exposure, but the diode remains stable in the subsequent steps.*

Sadly, this leaves us with no clear conclusion as to the origin of the current in reaction conditions. The current in H_2 alone and D_2 alone are likely the result of hydrogen spillover from Pt to TiO_2, where reduction occurs.[11] When O_2 is present in large excess, the current is much smaller, either because O_2 outcompetes H_2 on the surface sites that lead to spillover, or because H_2 is likely to react with O_2 before it can spillover. Figure 5 summarizes the currents in different conditions. The difference upon adding O_2 may be from differences in chemicurrent yields for the two isotopes, or it may simply be that O_2 differs in how well it prevents spillover for D_2 and H_2.

Finally, while the diode is stable throughout these experiments, its electronic properties vary in different gas environments. Figure 6 shows the rectification factor for diode #1, as it was exposed alternately to 6 Torr of H_2, 750 Torr of O_2 and 6 Torr of D_2, 750 Torr of O_2, all at 353 K. The rectification factor is defined here as the ratio between the current at +1 V and the current at -1 V. It decreases significantly when switching from H_2 to D_2, and increases back to almost its original value when switching back to H_2. This can occur over many cycles. With the smaller rectification factor in D_2, electrons have less of a barrier to overcome when traveling from the metal to the semiconductor, and a given amount of TiO_2 reduction will produce a higher current relative to H_2.

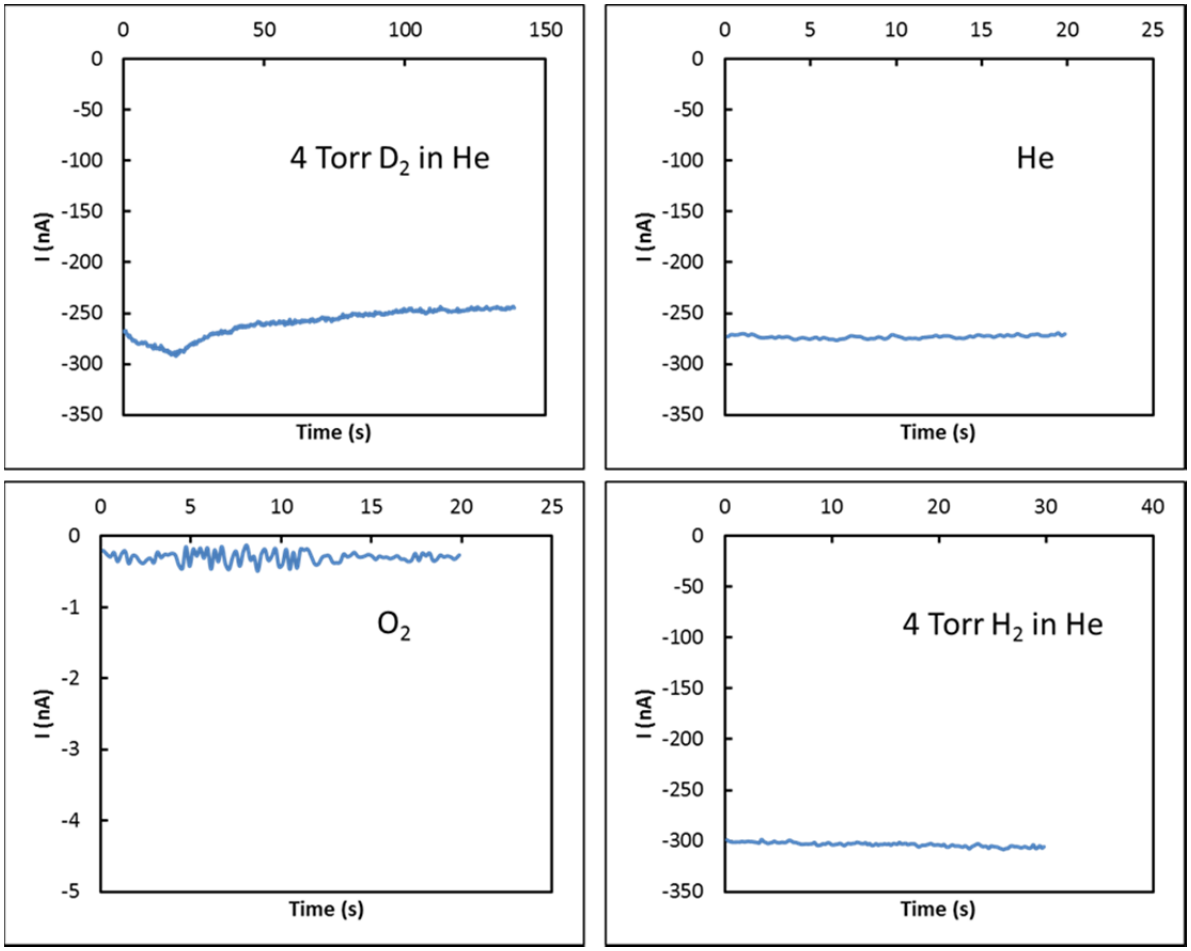

Figure 4 – *Current vs. time graphs for diode #2 in different gas conditions. Both hydrogen and deuterium generate significant current, which remains after the gases have been pumped out and replaced with He. This current disappears after exposure to O_2.*

If the difference between H_2 and D_2 is in fact due to chemicurrent from reaction intermediates non-adiabatically dissipating energy in the Pt lattice, we can compare the chemicurrent yields $Y^{\neq}$ of the two isotopes. If we define $Y^{\neq} = \frac{I}{TOF}$, then we get $\frac{Y^{\neq}_{D_2}}{Y^{\neq}_{H_2}} = 4.8$. Since D_2 is slower than H_2 for a given kinetic energy, we would expect to see instead a higher chemicurrent yield for H_2.

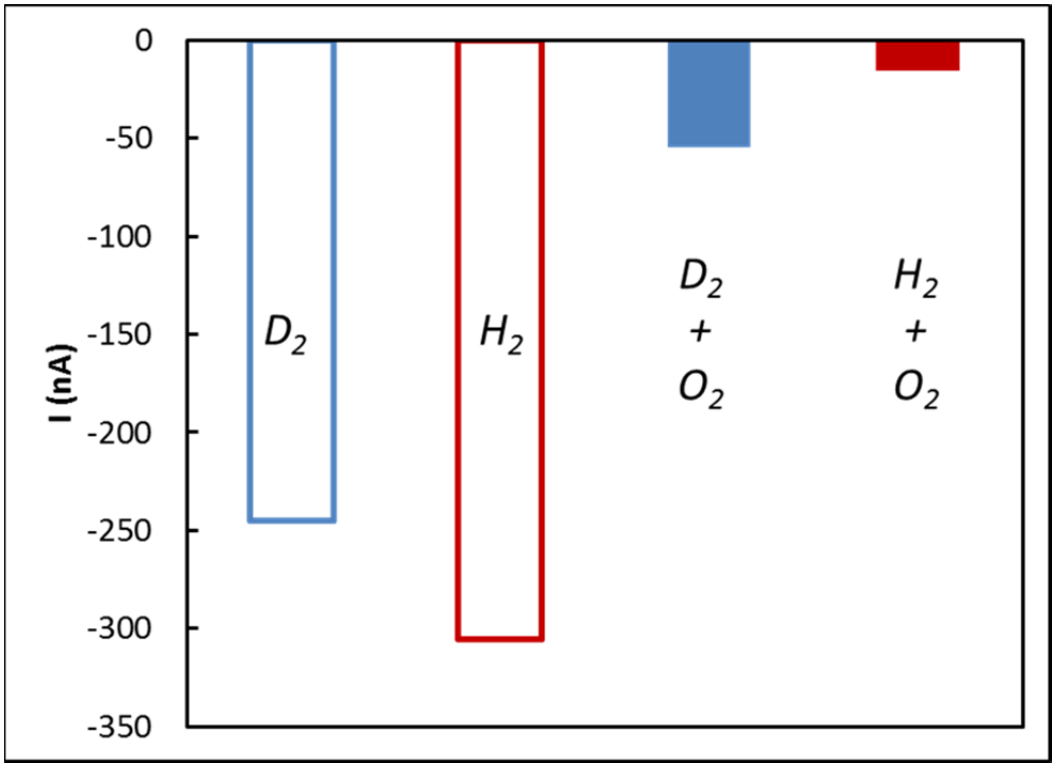

Figure 5 – *Current for diode #2 in 4 Torr H_2 / D_2, 750 Torr He, and for 4 Torr H2 / D_2, 750 Torr O_2 (reaction conditions)*

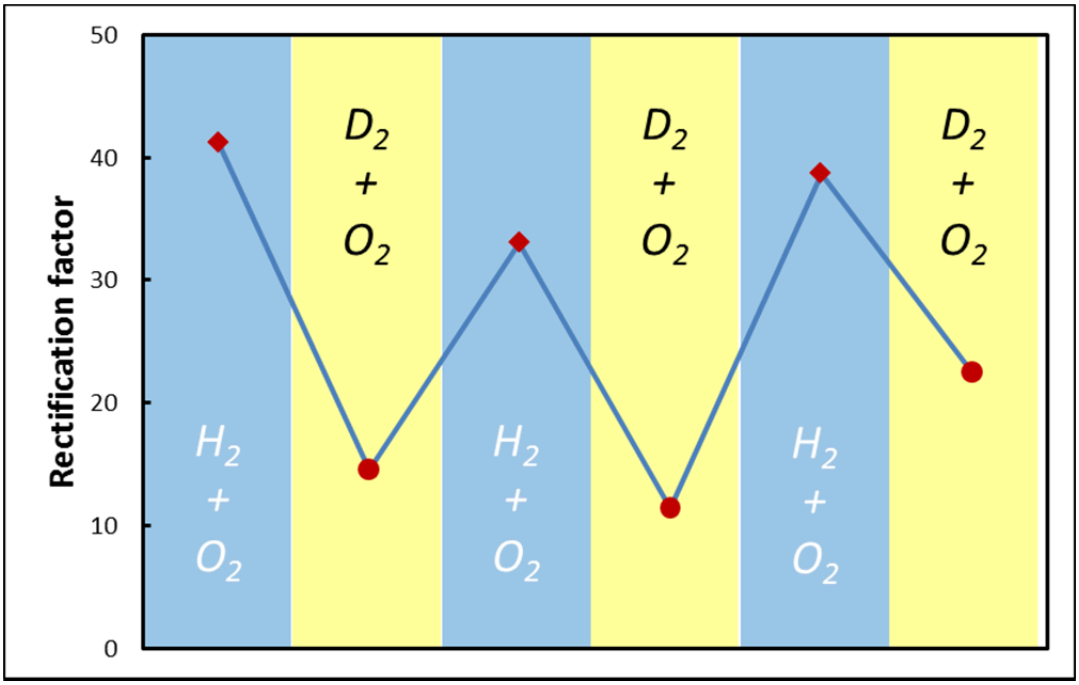

Figure 6 – *Rectification factors for diode #1 in alternating H_2 oxidation and D_2 oxidation conditions. The change in rectification implies a lower barrier height for D_2, which may explain the isotope effect in diode current.*

Conclusion

Charge flow through a Pt/TiO_2 diode was measured under H_2 oxidation and D_2 oxidation conditions, and in H_2 and D_2 without O_2 present. Reaction conditions produce significantly different currents for the two isotopes, which may be due to different efficiencies in chemicurrent productions. However, current is also produced by spillover of dissociatively adsorbed H and D from the Pt to TiO_2, which produces a net flow of electrons from the Pt to TiO_2 that is not distinguishable from chemicurrent. Furthermore, the electronic properties of the diode are different when exposed to H_2 and D_2, which result in different Schottky barrier heights, depending on the gas environment. More experiments are needed to determine with certainty how H_2 and D_2 oxidation differ in generating chemicurrent.

References

(1) Born, M.; Oppenheimer, R. *Annalen der Physik* **1927**, *389*, 457-484.
(2) McDermott, W. E.; Pchelkin, N. R.; Benard, D. J.; Bousek, R. R. *Applied Physics Letters* **1978**, *32*, 469.
(3) Barry, M. D.; Gorry, P. A. *Molecular Physics* **1984**, *52*, 461-473.
(4) Jensen, E.; Keller, J. S.; Waschewsky, G. C. G.; Stevens, J. E.; Graham, R. L.; Freed, K. F.; Butler, L. J. *The Journal of Chemical Physics* **1993**, *98*, 2882.
(5) Hasselbrink, E. *Current Opinion in Solid State and Materials Science* **2006**, *10*, 192-204.
(6) Martin, W. *Surface Science* **1997**, *377-379*, 343-349.
(7) Nienhaus, H.; Bergh, H. S.; Gergen, B.; Majumdar, A.; Weinberg, W. H.; McFarland, E. W. *Phys. Rev. Lett.* **1999**, *82*, 446.
(8) Krix, D.; Nünthel, R.; Nienhaus, H. *Journal of Vacuum Science & Technology A: Vacuum, Surfaces, and Films* **2007**, *25*, 1156.
(9) Krix, D.; Nünthel, R.; Nienhaus, H. *Phys. Rev. B* **2007**, *75*, 073410.
(10) Park, J. Y.; Renzas, J. R.; Hsu, B. B.; Somorjai, G. A. *J. Phys. Chem. C* **2007**, *111*, 15331-15336.
(11) Hervier, A.; Renzas, J. R.; Park, J. Y.; Somorjai, G. A. *Nano Lett.* **2009**, *9*, 3930-3933.
(12) Roland, U.; Braunschweig, T.; Roessner, F. *Journal of Molecular Catalysis A: Chemical* **1997**, *127*, 61-84.

Chapter 5

Light Induced Changes in Turnover Rates for Hydrogen Oxidation on Pt/Si Nanodiodes

We report here that turnover frequency of hydrogen oxidation on a Pt/TiO_2 nanodiode can be decreased by exposing the device to visible light. The magnitude of this effect could not be measured accurately, since the heater used for the experiment desorbed a measurable amount of hydrogen under illumination, which interfered with the measurement. However, applying a reverse bias to the device enhances the effect of light, indicating that the light is in fact modifying catalysis on the surface of the diode.

Introduction

Solar energy is an increasingly attractive alternative to fossil fuels, but it presents the major disadvantage of only being available during the day. One of the solutions to this problem is to use solar energy to drive a chemical reaction on a photocatalytic device. The reaction product can then be used to regenerate electricity when solar energy is unavailable, or as transportation or heating fuel.[1] The device must be able to generate electron-hole pairs from visible light, separate those charges in order to avoid their recombination, and finally use the electrons, the holes, or both to drive a chemical reaction. This is often achieved by placing catalytic particles in contact with a photovoltaic assembly, where it can collect electrons and holes, all of this on the nanoscale.[2–5]

A typical solar cell uses a *p*-*n* junction to separate charges, but nanodiodes have been proposed as an alternative architecture.[6] The Schottky barrier at a metal-oxide interface serves the role of the charge separator. Depending on the direction of the band bending, electrons or holes are injected into the metal, where they can affect surface chemistry. These charges have overcome the Schottky barrier, and have energies in significant excess of the Fermi level. If the metal is thinner than their mean free path, these charges may interact with adsorbates before they relax, providing additional energy to do chemistry. This idea of collecting charge carriers while they are still hot has already been suggested for purely photovoltaic solar cells as a strategy for increasing efficiency.[7]

We report here that a 4 nm Pt film deposited on Si acts as a photodiode and that its catalytic activity can be affected by light. Visible light excites electron-hole pairs in Si, and the holes are injected into Pt. We show that under hydrogen oxidation conditions, the rate of formation of water is decreased under illumination, indicating that the flow of charges to the surface interferes with the reaction mechanism. Unfortunately, illumination of the diode also caused the boron nitride sample heater to desorb H_2 into the reactor. Since the reaction rate

was measured by following the decrease in the amount of H_2 by gas chromatography, this artifact interfered with the observation of the effect of light on the diode.

Nonetheless, the effect of light is enhanced by applying a reverse bias to the Pt/Si diode, which shows that some of the change in reactivity can be attributed to the effect of light.

Experimental

To fabricate the catalytic Schottky diode, Pt was deposited on n-type Si (100) by electron beam evaporation. The n-type Si substrate was phosphorus doped to achieve a conductivity of 1–10 Ω cm. The Pt film was 4 nm thick as measured by quartz crystal microbalance. The chamber base pressure for electron beam deposition was $>1 \times 10^{-5}$ Torr. No etching of the Si native oxide was done prior to Pt deposition, because the native oxide acted as a tunneling barrier to increase the rectification of the diode. Using a shadow mask, the Pt was deposited as a 4 × 6 mm rectangle which served as the device active area.

An aluminum (Al) pad provided ohmic contact to the n-type Si, and a gold (Au) pad provided contact to the Pt active area. Both the Al and Au contact pads were 100 nm thick. A layer of SiO_2 (150 nm) insulated the Au pad from the Si substrate. These Al, Au and SiO_2 layers were each deposited by electron beam evaporation using shadow masks.

The nanodiode is placed on a ceramic heater, and the temperature is monitored by a thermocouple, fluctuating by less than 0.5 K. The turnover of water molecules was obtained by monitoring the amount of H_2 during the reaction, using a gas chromatograph connected to the chamber by a sample loop equipped with a metal bellows circulation pump. Hydrogen oxidation was carried out in 10 Torr H_2, 30 Torr O_2, and 720 Torr He, at 423 K. Prior to reaction, samples were heated to 423 K in 100 Torr O_2 for one hour. This pretreatment led to increased turnover, facilitating the measurements.

The nanodiode's electrodes are connected to an electrical circuit with gold wires, making it possible to characterize the device by measuring its I-V curve. This was done with a Keithley Sourcemeter, which was also used to measure chemicurrent passing through the diode while the chemical reaction is taking place. No voltage bias is applied to the diode.

A halogen lamp was used to illuminate the catalytic diode through a sapphire window on the reaction chamber. Lamp power was 1.35 W, the numerical aperture was 0.3, and the distance from the lamp to the diode was 8 cm. This resulted in approximately 60 mW/cm^2 of radiation over the active area of the diode. The spectral profile of the lamp closely followed the solar spectrum. On a typical diode, current at 443 K was on the order of 0.5 mA in dark conditions, and 1.5 mA under illumination, for an active area of 24 mm^2. Current in dark conditions is likely due to thermionic emission from Pt to Si.

Results & Discussion

Figure 1 shows the rate of hydrogen oxidation on a Pt/Si diode, measured by gas chromatography, in the dark and under illumination at 423 K. Before each on / off cycle, the reactor was evacuated down to a pressure of 10^{-5} Torr, and the mixture introduced was

comprised of 10 Torr H_2, 30 Torr O_2 and 740 Torr N_2. The rate under illumination is consistently lower than in the dark.

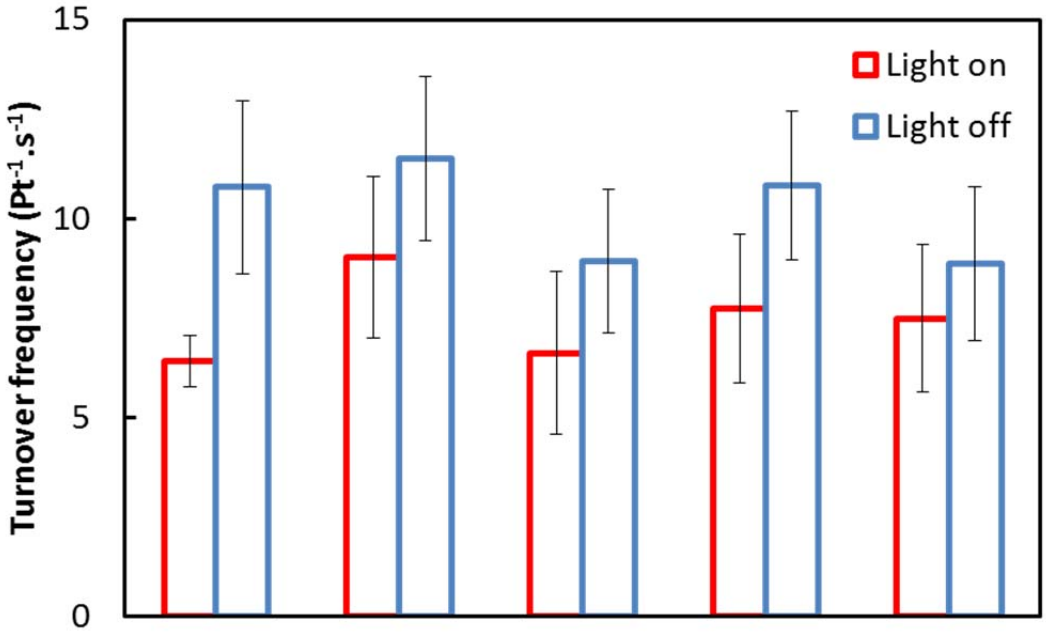

Figure 1 – *Turnover frequency of hydrogen oxidation in 10 Torr H_2, 30 Torr O_2 and 740 Torr He at 423 K. Turnover is calculated based on the rate of decrease of the hydrogen peak height in the chromatogram. In between each on/off cycle, the chamber was pumped down to 10-5 Torr. Error bars represent 95% confidence intervals.*

As a control experiment, the same procedure was carried out in the absence of O_2. In these conditions, no reaction is occurring on the surface of the diode, and yet fluctuations in the H_2 concentration in the reactor still correlate with light exposure, as shown in figure 2. These fluctuations disappeared when the boron nitride sample heater was covered in aluminum foil, suggesting that the heater takes up H_2, and desorbs it continuously under illumination.

Any effect on the reaction from illuminating the diode cannot be separated from this artifact. However, since the diode is connected into a circuit through electrical feedthroughs on the reactor, it can be subjected to a voltage bias. In another set of experiments, H_2 oxidation was performed in the same conditions while different voltage biases were applied to the diode. Figure 3 shows the rates under illumination and in the dark at 0, -0.6, -0.3 and -0.9 V. Again, the rates under illumination are lower than in the dark, but the ratio between the two decreases with applied bias. The ratio of the light on rate to the light off rate is plotted versus voltage in the graph in Figure 4.

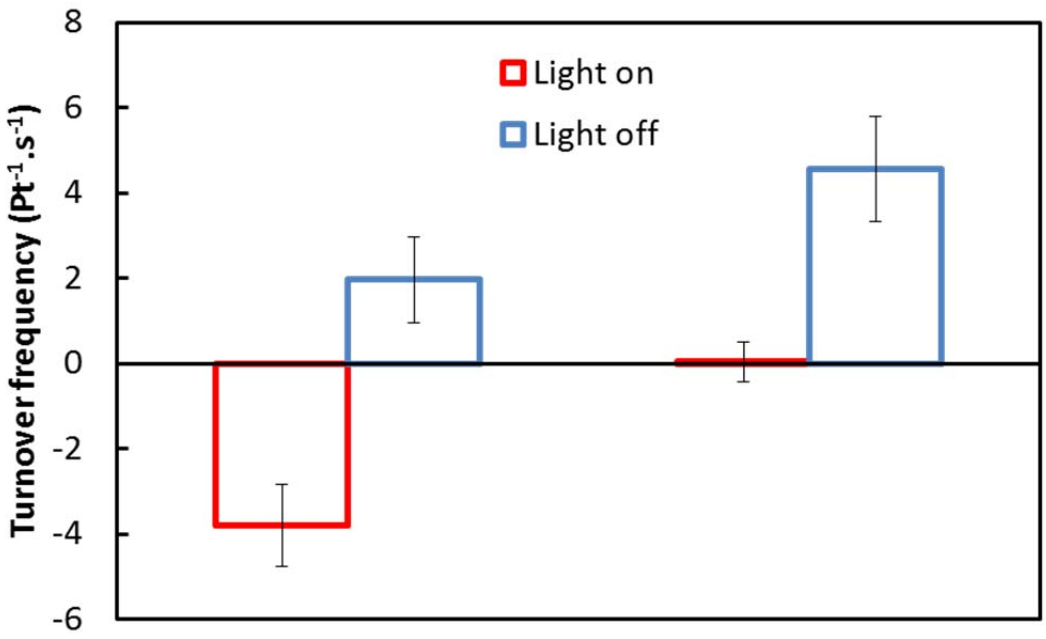

Figure 2 – *Turnover frequency of hydrogen oxidation in 10 Torr H_2, 770 Torr He and no O_2 at 423 K. In the absence of O_2, there should be no turnover, and the non-zero values observed are the result of H_2 leaking from the reactor, reacting with traces of O_2, and desorbing from the heater under illumination.*

Turnover rates tend to change over time: the active surface area and the surface coverage may change as a poison takes up surface sites, and the film may anneal or oxidize under the harsh conditions used for the reaction. To avoid confusing any of these effects with the effect from bias, the voltages were not applied in decreasing order, but instead in the following order: 0, -0.6, -0.3 and -0.9 V. The decrease in turnover by light is enhanced with greater reverse bias. A final measurement was then performed at 0 V again, and showed a value similar to the initial 0 V measurement.

The effect from bias shows that the light does affect the surface chemistry of the diode. The Pt film is 4 nm thick, and transmits most of the light through to the Si substrate. Si, with its bandgap of 1.1 eV, absorbs visible light, resulting in the formation of electron hole pairs.[9] The direction of band bending in a Pt/*n*-Si is such that excited electrons in the conduction band remain in the silicon, while excited holes are accelerated towards the metal.

The Si wafers used were covered in an insulating layer of SiO_2 several nanometers thick. The bandgap of SiO_2 is 9 eV, so excited holes in Si must tunnel through this native oxide to reach the Pt film.[10] This decreases the efficiency of the diode. The SiO_2 film can be etched away with HF. However, this film grows back to 1 nm thickness in air in only 1 hour.[11] Fabricating a diode with no tunneling barrier for the holes is therefore quite difficult. Since photocurrent obtained with the native oxide present is substantial enough to affect the catalysis, no attempt was made to remove it.

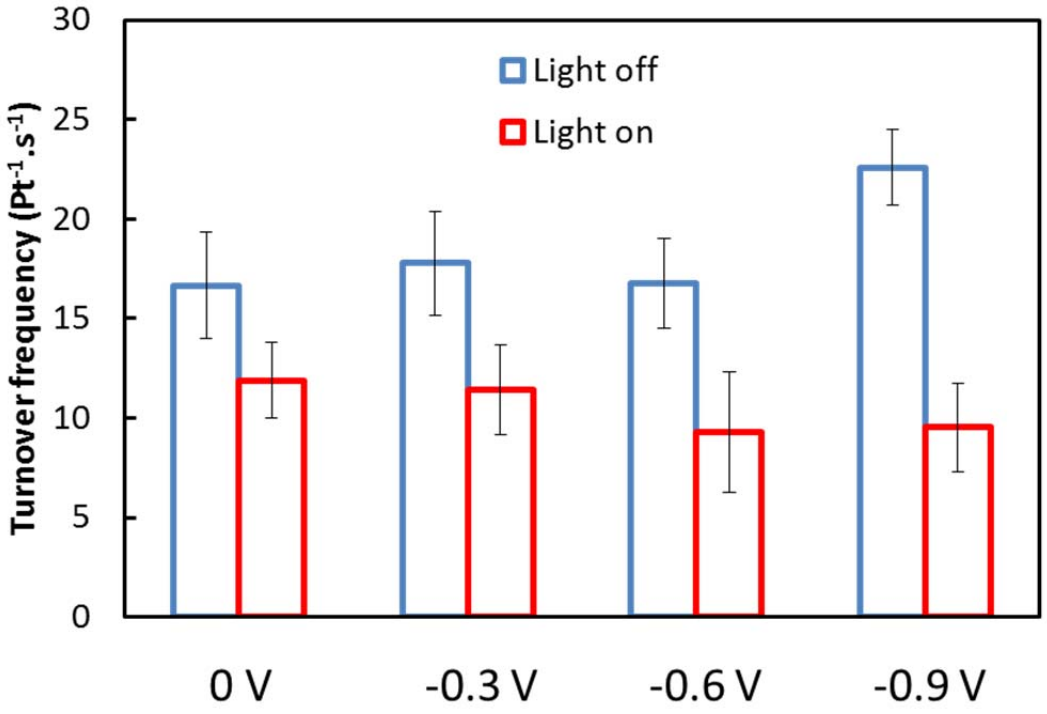

Figure 3 – *Turnover frequency for hydrogen oxidation in 10 Torr H_2, 30 Torr O_2 and 740 Torr He at 423 K, over a series of on / off cycles with different bias voltages applied to the diode. In order to avoid artifacts in device history, the chronological order of the voltages applied was 0 V, -0.6 V, -0.3 V and -0.9 V.*

Illuminating the diode would also increase its temperature, from photon absorption, and from Joule heating due to the photocurrent. This can safely be ruled out as a cause of the change in turnover, since an increase in temperature under illumination would increase turnover, not decrease it.

It would be useful to know the efficiency of the process by which light hinders turnover in order to understand the mechanism at play. The efficiency for generation of photocurrent in the diode is known, as is the number of reaction events occurring on the surface. It would therefore be possible to know how many reaction events are prevented for each hole that is injected from Si into Pt. Desorption of H_2 from the sample heater unfortunately prevents us from making this calculation, and more experiments are needed to better understand this phenomenon. Chapter 6 covers similar, more succesful experiments performed with CO oxidation.

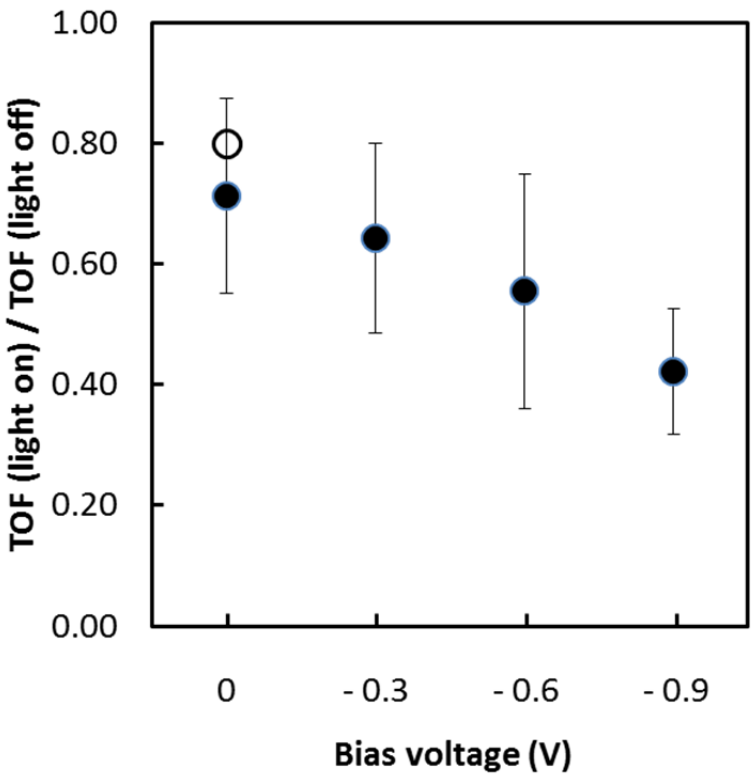

Figure 4 – *Ratio of turnover frequency under illumination to turnover frequency in the dark at different bias voltages, calculated from the values plotted in figure 3 (full circles). Empty circle represents a final on/off cycle at 0 V carried out after the four others.*

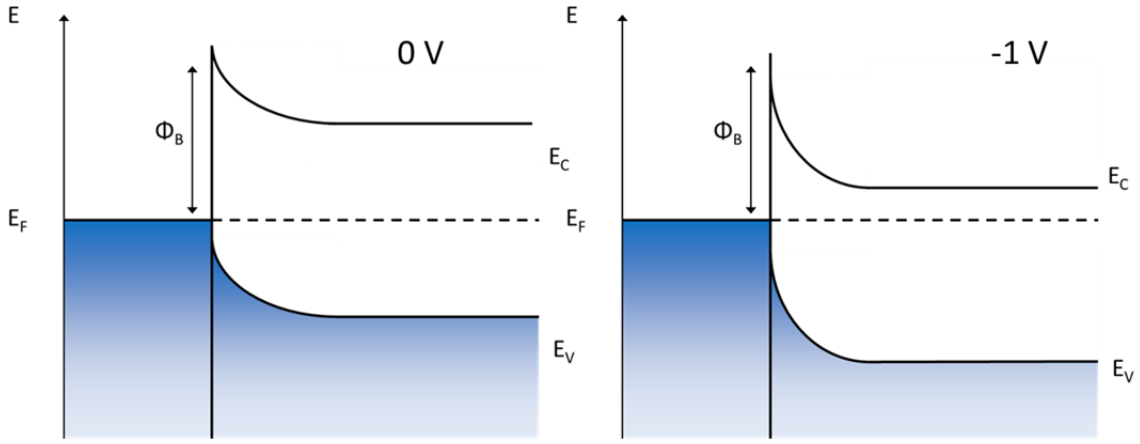

Figure 5 – *Schematic band energy diagrams for a Pt/Si diode at 0 V and -1V voltage biases, respectively.*

Conclusion

Despite the sample heater interfering with the results, we have shown that turnover for hydrogen oxidation can be significantly reduced on a Pt/TiO_2 photodiode by exposing the diode to visible light. This is not due to heating of the catalyst under illumination, but instead to a steady-state flow of hot holes to the surface. The mechanism for this process is not well understood, and further experiments are required. Without the effect of H_2 desorbing from the heater under illumination, it would be possible to calculate an efficiency for this process, which would be useful in understanding the mechanism. A comparison of D_2 and H_2 oxidation would also be particularly useful in this regard.

This shows that a catalytic device can be designed that allows us to tune surface chemistry with light. Using different diode materials, and with a different reaction, it may be possible to use light to increase activity, or achieve higher selectivity in the case of a multi-path reaction.

References

(1) Lewis, N. S.; Nocera, D. G. *Proceedings of the National Academy of Sciences* **2006**, *103*, 15729 -15735.
(2) Yan, H.; Yang, J.; Ma, G.; Wu, G.; Zong, X.; Lei, Z.; Shi, J.; Li, C. *Journal of Catalysis* **2009**, *266*, 165-168.
(3) Amirav, L.; Alivisatos, A. P. *J. Phys. Chem. Lett.* **2010**, *1*, 1051-1054.
(4) Maeda, K.; Xiong, A.; Yoshinaga, T.; Ikeda, T.; Sakamoto, N.; Hisatomi, T.; Takashima, M.; Lu, D.; Kanehara, M.; Setoyama, T.; Teranishi, T.; Domen, K. *Angewandte Chemie International Edition* **2010**, *49*, 4096-4099.
(5) Zong, X.; Han, J.; Ma, G.; Yan, H.; Wu, G.; Li, C. *J. Phys. Chem. C* **2011**, *115*, 12202-12208.
(6) McFarland, E. W.; Tang, J. *Nature* **2003**, *421*, 616-618.
(7) Ross, R. T. *Journal of Applied Physics* **1982**, *53*, 3813.
(8) Park, J. Y.; Renzas, J. R.; Hsu, B. B.; Somorjai, G. A. *J. Phys. Chem. C* **2007**, *111*, 15331-15336.
(9) Kittel, C. *Introduction to solid state physics*; Wiley, 2005.
(10) DiStefano, T. H.; Eastman, D. E. *Solid State Communications* **1971**, *9*, 2259-2261.
(11) Raider, S. I.; Flitsch, R.; Palmer, M. J. *J. Electrochem. Soc.* **1975**, *122*, 413-418.

Chapter 6

Solid State Charge-Based Device for External Control of Catalytic Chemistry

It is well known that the catalytic activity of metal particles is strongly influenced by electronic properties at the metal/support interface, and interactions at this interface often give rise to highly active and selective reaction pathways. The ability to control these effects to develop new efficient catalysts is a major focus in science and industry. An unexplored approach is to use a solid state device to control catalytic chemistry by externally tuning the electronic structure and charge flow at the metal/support interface. We demonstrate the viability of this approach using a Pt/Si catalytic diode to control the rate of CO oxidation. We show that the catalytic reaction can be turned on and off by alternating between bias states of the device. Additionally, we show that the reaction rate is sensitive to photocurrent induced by visible light. The effects of both bias and light show that negative charge on the Pt increases catalytic activity, while positive charge on the Pt decreases catalytic activity for CO oxidation. This is the first time that a solid state device has been used for external control of catalytic chemistry.

Introduction

Many industrial catalysts consist of metal nanoparticles dispersed on a porous support. Because the support is often inert without the metal, the metal is usually considered the active catalyst. However, numerous studies have demonstrated that the electronic properties of the support play a major role in determining the activity and selectivity of the metal/support system.[1–6] This complex interaction between a metal and its support has been widely studied and is commonly called the strong metal-support interaction (SMSI).[7–11] We are interested in SMSI because these interactions often give rise to highly active and selective reaction pathways.[12,13]

SMSI affects a wide range of catalytic reactions, including carbon monoxide (CO) and carbon dioxide (CO_2) hydrogenation[10–12], selective hydrogenation[14–16], CO oxidation[17–21], and selective partial oxidation reactions[22–25]. We have recently demonstrated that for CO oxidation and methanol oxidation, the metal/support interaction is controlled by the electronic structure of the support, which can be tuned by chemical doping.[21,25]

In addition to SMSI, acid/base chemistry also relies on the charge transfer properties of a catalyst.[26–28] Solid acids and bases (i.e. zeolite catalysts) are of major industrial importance for hydrocarbon refining because of their ability to catalyze C-C bond isomerization.[29] These

catalysts work by generating ionic intermediates that act as the active species for C-C bond rearrangement.

A largely unexplored approach to catalytic chemistry is to use a solid state charge-based device to control the electric field and charge flow at a metal/support interface in order to control the catalytic reaction.[30–32] From SMSI and acid/base catalysis, it is clear that charge flow at the metal/support interface has a major influence on the rate and selectivity of a catalytic reaction. If this approach is viable, solid state device technology could soon find major applications in the field of catalysis for tunable control of selective surface chemistry.

We have previously reported the production of hot electron flow during CO oxidation using a catalytic nanodiode.[33,34] In that work a catalytic reaction was used to drive a current flow across a nanodiode. We now demonstrate that the opposite is also possible: using a catalytic nanodiode, an externally applied bias and a photo-induced current flow are used to control the rate of the catalytic reaction. This is the first time that a solid state device has successfully been used to achieve control of a catalytic reaction.

Experimental section

To fabricate the catalytic Schottky diode, Pt was deposited on n-type Si (100) by electron beam evaporation. The n-type Si substrate was phosphorus doped to achieve a conductivity of 1–10 Ω cm. The Pt film was 4 nm thick as measured by quartz crystal microbalance. The chamber base pressure for electron beam deposition was $>1 \times 10^{-5}$ Torr. No etching of the Si native oxide was done prior to Pt deposition, because the native oxide acted as a tunneling barrier to increase the rectification of the diode. Using a shadow mask, the Pt was deposited as a 4 × 6 mm rectangle which served as the device active area.

An aluminum (Al) pad provided ohmic contact to the n-type Si, and a gold (Au) pad provided contact to the Pt active area. Both the Al and Au contact pads were 100 nm thick. A layer of SiO_2 (150 nm) insulated the Au pad from the Si substrate. These Al, Au and SiO_2 layers were each deposited by electron beam evaporation using shadow masks.

A halogen lamp was used to illuminate the catalytic diode through a sapphire window on the reaction chamber. Lamp power was 1.35 W, the numerical aperture was 0.3, and the distance from the lamp to the diode was 8 cm. This resulted in approximately 60 mW/cm^2 of radiation over the active area of the diode. The spectral profile of the lamp, shown in figure 1, closely followed the solar spectrum.

A batch mode reactor with a boron nitride substrate heater was used to determine activity of the catalytic diode for CO oxidation. A 2:5 ratio of CO to O_2 was used in the chamber in a background of He. A metal bellows circulation pump provided gas mixing. Reactions were performed at several temperatures between 423 and 443 K as measured by a type-K thermocouple. CO_2 production was monitored as a function of time using a gas chromatograph with a thermal conductivity detector.

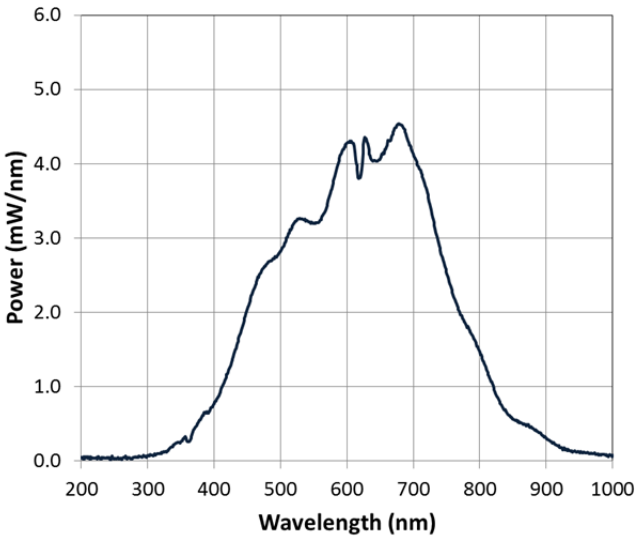

Figure 1 – *Spectral profile of halogen lamp used to illuminate the catalytic diode through a sapphire window on the reaction chamber. Lamp power was 1.35 W, the numerical aperture was 0.3, and the distance from the lamp to the diode was 8 cm. This resulted in approximately 60 mW/cm^2 of radiation over the active area of the diode. The spectral profile of the lamp closely followed the solar spectrum.*

Electrical connections were made between the contact pads of the device and BNC feedthroughs on the chamber using Au wire. Depending on the activity of the catalytic diode for a given reaction condition, up to three diodes were connected in parallel to increase the catalytic device area. A Keithley 2400 Sourcemeter was used to control the electrical bias across the device, measure photocurrent, and obtain IV curves of the device during reaction.

Reaction rates are reported in turnover frequency (TOF) as CO_2 molecules produced per Pt site per minute. All error bars represent the 95% confidence interval based on the rate of CO_2 production normalized to the estimated number of Pt sites. The number of Pt sites was estimated by assuming a uniform (111) surface structure over the entire catalyst area.

Although this calculation is approximate, it provides a consistent normalization to the catalyst area and yields a reasonable estimate of the absolute TOF.

Results and Discussion

CO oxidation served as a model reaction. The catalytic nanodiode was fabricated by depositing platinum (Pt) onto n-type silicon (Si). The Pt served as the catalyst, and a Schottky barrier formed at the Pt/Si interface. The Pt film was 4 nm thick. We found this was thin enough to transmit visible light, so the device was also an efficient photodiode showing power conversion efficiency (PCE) of ~1.5% and a spectrally averaged incident photon to current conversion efficiency (IPCE) of ~15%. Figure 2A shows the device architecture; figure 2B shows the current-voltage (IV) curves of the device in the dark and during illumination by a halogen lamp (~60 mW/cm^2).

Figure 3A shows the effect of applied bias on the catalytic activity of the device for CO oxidation. The experiment was performed in 40 Torr CO and 100 Torr O_2 at 443 K. In this experiment the device is initially active in open circuit (i.e. no applied bias) showing a TOF of ~3.4 CO_2 molecules/Pt site/min. However, the catalyst deactivates, and after approximately 10 h of reaction, the catalyst is entirely inactive. At this point in the reaction, we find that the catalyst activity can be enhanced by applying a bias across the device. As shown in figure 3A this effect is reversible, so that the reaction rate can be turned on and off simply by switching the applied bias. In the experiment shown, a 1 V reverse bias is used to enhance the catalytic reaction rate, and the device is switched back and forth between an applied bias and an open circuit (i.e. no applied bias) state corresponding to high catalyst activity and no activity, respectively.

We attempted to perform similar experiments to observe how the magnitude of applied bias affects the catalyst activity. For example, we may assume that applying a 0.5 V bias rather than a 1 V bias would result in a smaller rate enhancement, while a 2 V bias would yield a greater rate enhancement. The major challenge of this experiment is the hysteresis of the device in reaction. We find that both the catalyst activity and the effect of bias strongly depend on the state of the device which is prone to constant change under reaction conditions. Consequently, we could not quantify the magnitude of rate enhancement as a function of applied bias in a way that is statistically significant.

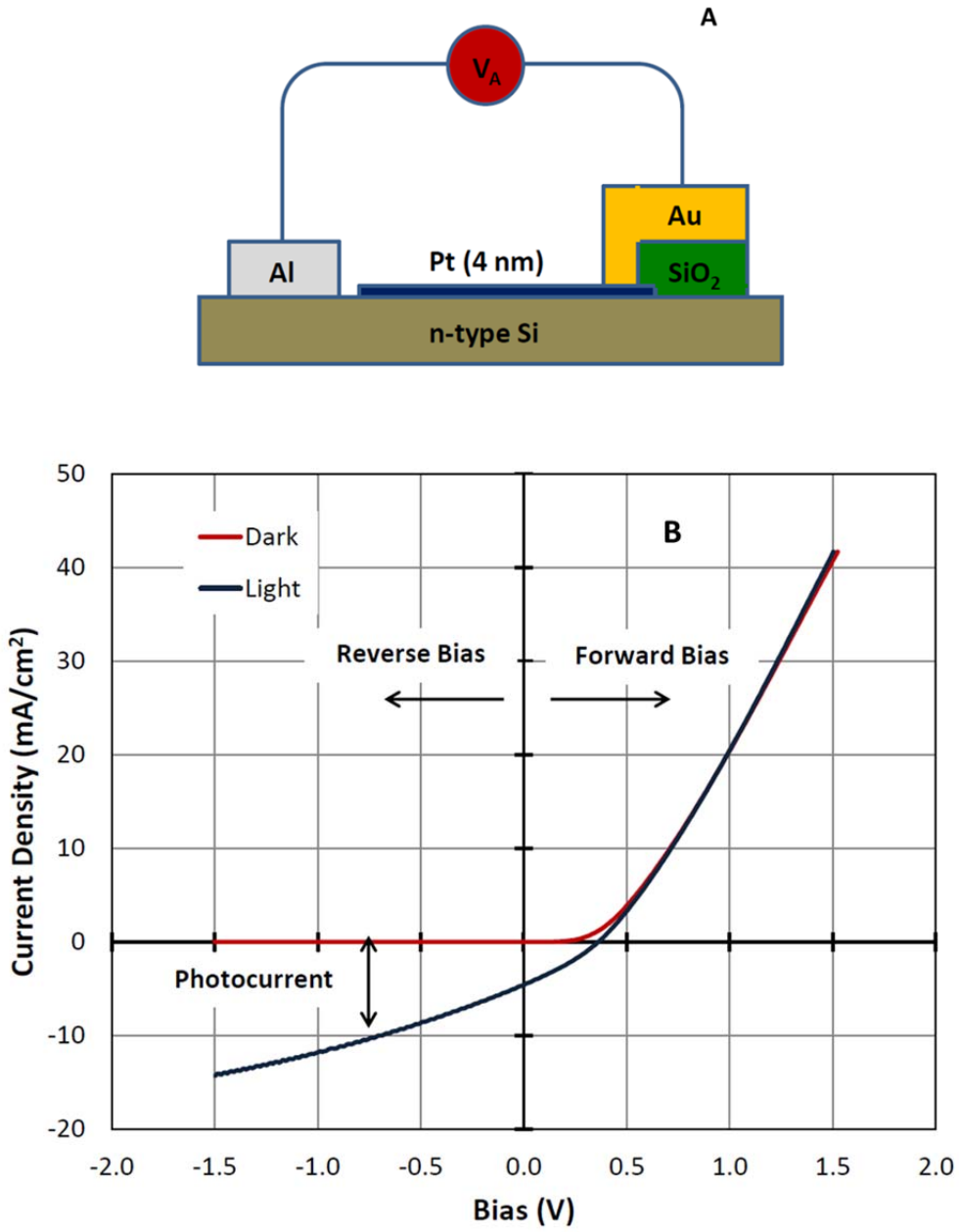

Figure 2 – *(A) Schematic of the catalytic nanodiode. The rectifying interface is made by depositing Pt (4 nm) on n-type Si. An Al pad (100 nm) makes ohmic contact to the Si, and an Au pad (100 nm) makes contact to the Pt. A layer of SiO_2 (150 nm) insulates the Au pad from the Si substrate. The 4 nm Pt layer is thin enough to transmit visible light, so the device is also a photodiode. (B) IV curves of the catalytic nanodiode in the dark (red curve) and during illumination with visible light (blue curve). As seen in the dark curve, forward bias induces a flow of electrons from the Si substrate to the Pt. Reverse bias does not induce a current flow, but a field is generated at the Pt/Si interface. The difference between the blue and red curves represents the photocurrent which increases with reverse bias. The light source is a halogen lamp emitting 60 mW/cm^2 with a spectral profile similar to the solar spectrum.*

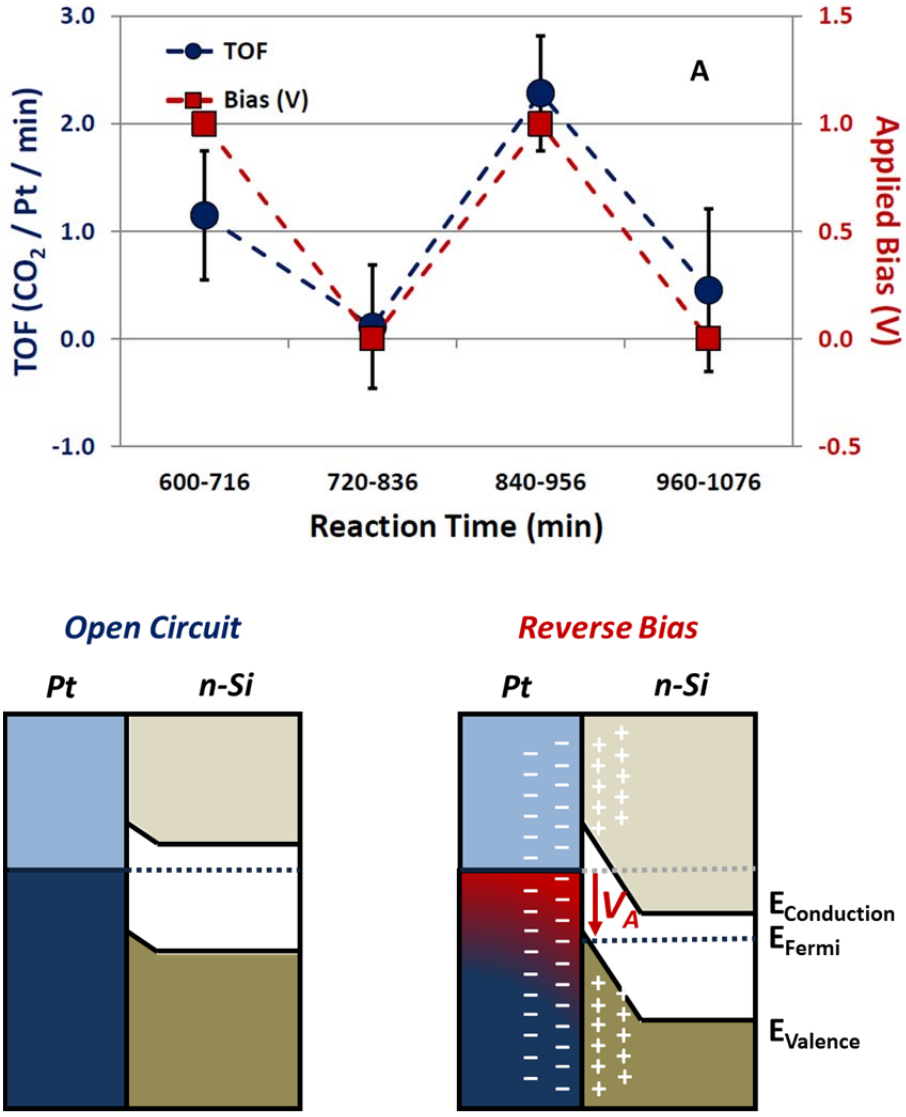

Figure 3 – *(A) Effect of bias on the catalytic activity of the nanodiode for CO oxidation. Red squares show the reverse bias that was externally applied to the device during CO oxidation. Blue circles show the corresponding turnover frequencies (TOF). TOF is given as the number of CO_2 molecules produced per Pt site per minute. The error bars represent 95% confidence intervals for the TOF measurements. The reaction was run in 40 Torr CO and 100 Torr O_2 at 443 K. The device was cycled between 1 V reverse bias and open circuit (i.e. no applied bias). As shown, the TOF strongly depends on the bias state of the device, and the activity could be turned on and off by switching between reverse bias and no bias, respectively. (B) Band diagrams of the nanodiode in open circuit and during reverse bias. During reverse bias, positive charge builds-up on the Si and negative charge builds-up on the Pt. This increases band bending in the Si and results in a high electric field at the Pt/Si interface. It appears that the negative charge on the Pt enhances catalytic activity presumably by electronic activation of the Pt-O bond.*

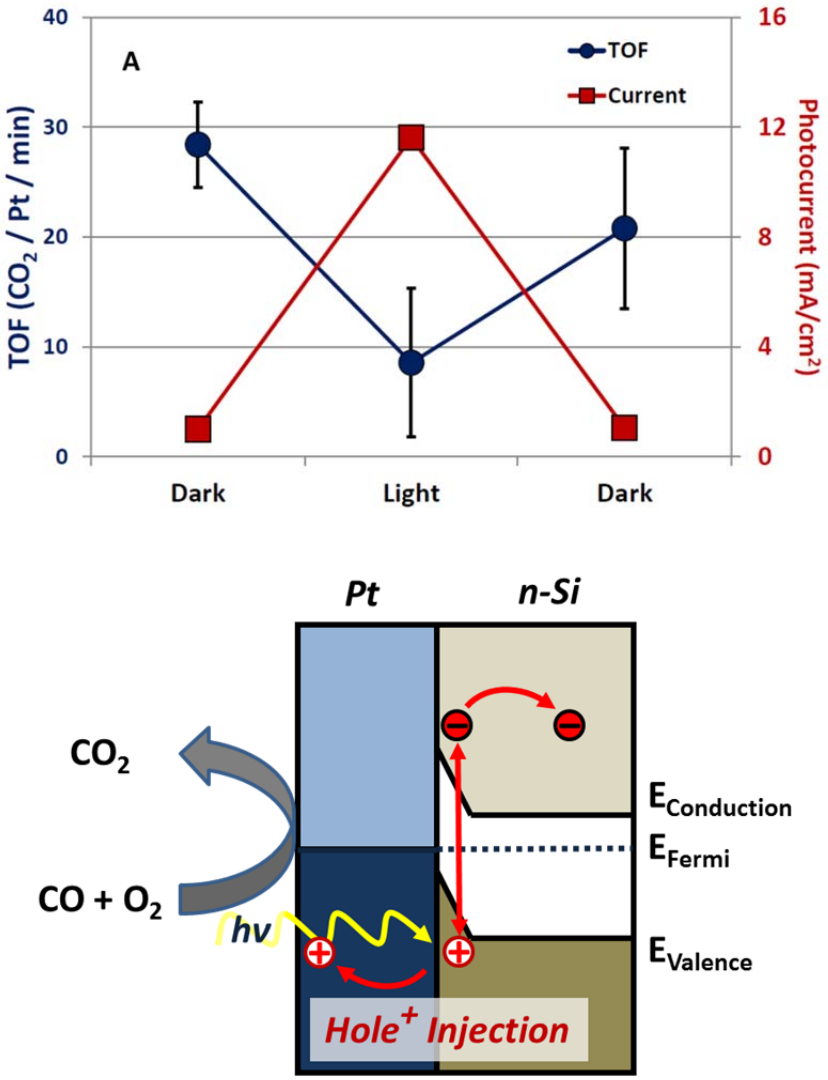

Figure 4 – *(A) Effect of photocurrent on the catalytic activity of the nanodiode for CO oxidation. Red squares show the current flow across the device in the dark and during illumination under reaction conditions. Blue circles show the corresponding TOF. The error bars represent 95% confidence intervals for the TOF measurements. The reaction was run in 8 Torr CO and 20 Torr O_2 at 423 K. During this experiment, the reverse bias was kept fixed at 0.6 V. The role of the bias was to increase the efficiency of photocurrent generation. As shown, the photocurrent reversibly decreases the reaction rate by a factor of ~3. Prior to the reaction, the device was subjected to an oxidizing pretreatment at 423 K. We found that the oxidizing pretreatment greatly increased the reaction rate at reverse bias and was necessary to observe an effect by light on the reaction rate. (B) Band diagram of the device showing the mechanism of photocurrent generation. The 4 nm Pt film is thin enough to transmit visible which is absorbed in the Si, generating electron-hole pairs. Because of the interface potential, the holes move across the Pt/Si interface resulting in a flow of positive charge to the Pt surface. Above we showed that a negative bias on the Pt increases the reaction rate; now we show that a flux of positive charge to the Pt surface decreases the reaction rate.*

The direction of the applied bias is important because of the rectifying nature of the diode. A forward bias induces a current flow, and we find that under conditions of high current flow induced by a forward bias, the device is extremely unstable in reaction. However, because of the Schottky barrier between the Pt and n-type Si, a reverse bias does not induce a current flow. Rather an electric field is generated at the Pt/Si interface with a negative charge build-up on the Pt and a positive charge build-up on the Si as shown in figure 3B. It appears that the negative charge on the Pt enhances catalytic activity, presumable by electronic activation of the Pt-O bond.

We also explored the possibility of using a photo-induced current flux to control the reaction rate. Figure 4A shows the reaction rate for CO oxidation on the catalytic device first in the dark, then under illumination, then in the dark again. Figure 4A also shows the corresponding photocurrent measurements made during the reaction. The results show that the photocurrent decreases the reaction rate by a factor of ~3. As with the bias, this effect is reversible, and the rate increases again when the light is turned off. The final dark rate is slightly lower than the initial dark rate; this is not an effect of the light, but rather is consistent with catalyst deactivation over time in reaction.

The photochemistry experiment was performed in 8 Torr CO and 20 Torr O_2 at 423 K. During this experiment, the reverse bias was kept fixed at 0.6 V. The role of the bias was to increase the reaction rate as well as the efficiency of photocurrent generation which scales with reverse bias. It is important to note that prior to the reaction, the device was subjected to an oxidizing pretreatment at 473 K. We found that the oxidizing pretreatment greatly increased the reaction rate at reverse bias and was necessary to observe an effect by light on the reaction rate.

The mechanism of photocurrent flux is generation of an electron-hole pair in the Si followed by hole injection to the Pt as shown in figure 4B. Accordingly, photocurrent represents a flux of positive charge to the Pt catalyst and negative charge to the Si support. By bias we showed that a negative charge on the Pt increases the reaction rate; now we show that a flux of positive charge to the Pt decreases the reaction rate.

We found the history of the device in reaction conditions played a major role in determining both the bias effect and the photon effect, as explained below. In reaction conditions the device is subject to irreversible changes, and the effects of bias and photocurrent depend heavily on the state of the diode. Consequently, working outside of the specified reaction conditions, we do not observe the same effect of bias and light on the reaction rate. Additionally, the effect we demonstrate is relatively short-lived because the device is undergoing constant change. The bias effect shown in figure 3A was reversible for about 8 h prior to losing control of the device. The photon effect shown in figure 4A was even shorter, lasting for only about 1 h. However, in both cases, the device was effective long enough to control the chemistry for at least several hundred turnover events per active site.

We observed switching behavior by the device induced by treatment in oxidizing conditions, especially during forward bias. Figure 5 shows the IV curve of the device under reaction

conditions initially and again following extended time in reaction conditions. We find that the same switching occurs following extended treatment in pure O_2 at reaction temperature (443 K). The initial state of the device, which we call state A, is characterized by a high forward bias current and good rectification. The final state of the device, which we call state B, is characterized by a low forward bias current and an almost symmetrical IV curve with respect bias. We found that the longer the device was exposed to oxidizing conditions, the more likely it was to fall into state B, although, there were several instances that we were able to induce a switch back to state A for a short amount of time by applied bias. The exact oxidizing treatment required to induce the switch from state A to B was not always the same between devices.

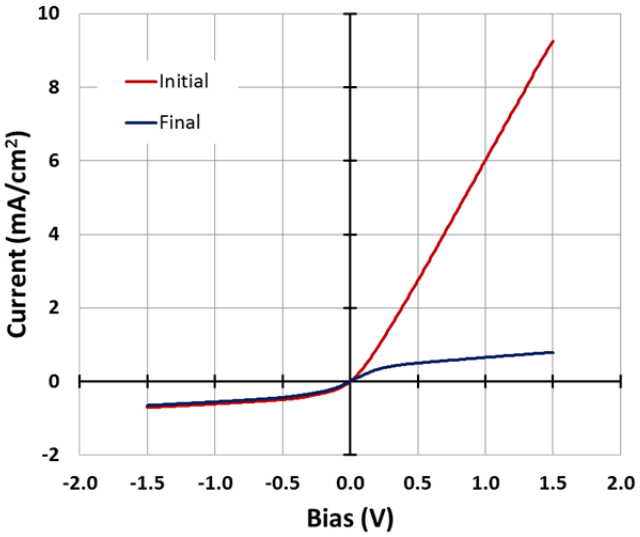

Figure 5 – *Current-voltage curves of the device initially and after extended time in reaction conditions.*

Forward bias seems to promote the switching behavior. Figure 6 shows a current-time (IT) curve of the device under reaction condition at a fixed forward bias. The sudden drop in current at 14 s indicates the switch from state A to B. Figure 7 shows the same type of switch occur during an IV curve measurement where at 0.7 V forward bias, the device suddenly switches from state A to B. We hypothesize that the switch from state A to B corresponds to the incorporation of subsurface O into the Pt catalyst. This hypothesis explains why extended treatment in oxidizing conditions is necessary to induce the switch and explains the drop in forward bias conductivity after the switch.

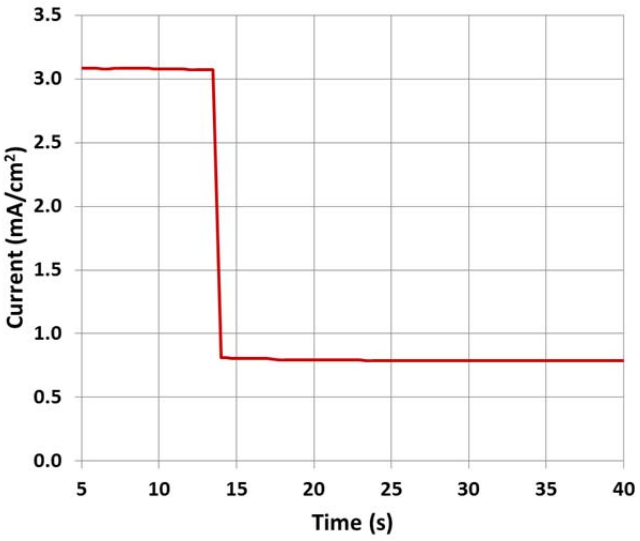

Figure 6 – *Current-time curve at 1 V forward bias showing a sudden switch of the device from its initial conductive state to an insulating state.*

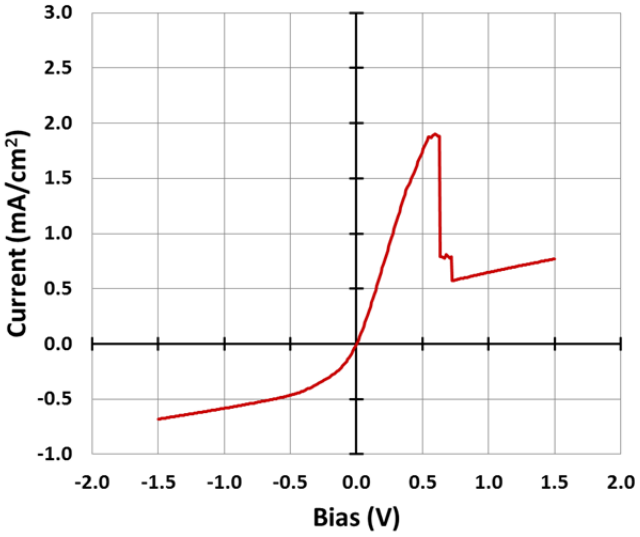

Figure 7 – *Current-voltage curve of the device showing a sudden switch from a conductive state to an insulating state at 0.7 V forward bias.*

We find that the switch also corresponds with a major change in the catalytic behavior of the device. Figure 8 shows the reaction rate measured over time while the device is alternated between open circuit and a 1 V reverse bias. Each time the bias was changed, the IV curve of the device was measured to determine its state, and the switch from state A to B occurred at 596 min of time in reaction. Before the switch, we find that the device is catalytically active in open circuit, and the activity is decreased when a reverse bias is applied. However, after the switch, the device is inactive in open circuit, and the activity is increased when a reverse bias is applied.

We suggest the following explanation: Initially the Pt is metallic and the CO oxidation reaction is rate limited by activation of the Pt-C bond of the adsorbed CO. It was recently demonstrated by Wolf and coworkers that in a similar Pt/TiO_2 Schottky diode system, a reverse bias results in a red shift of the vibration frequency of adsorbed CO.[32] This red shift corresponds to electron back donation to the π^* orbital of the CO. This orbital is anti-bonding with respect to C-O, but is bonding with respect to Pt-C. Consequently, we can assume that the effect of reverse bias is to weaken the C-O bond but to strengthen the Pt-C bond. On metallic Pt where the reaction rate is limited by activating adsorbed CO, strengthening the Pt-C bond by reverse bias results in a decreased reaction rate.

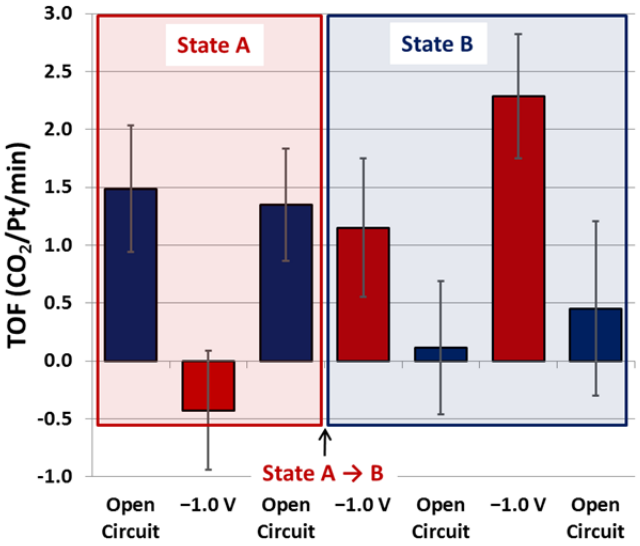

Figure 8 – *Turnover frequency (TOF) for CO oxidation on the catalytic diode as the bias is switched between open circuit and 1 V reverse bias. Between each TOF measurement a current-voltage curve is measured to determine the state of the device. A switch occurs from state A (conductive) to state B (insulating) during the experiment. We find that the effect of bias on catalytic activity depends strongly on the state of the device.*

However, the reaction kinetics change upon incorporation of subsurface O in the Pt. If we assume that the reaction mechanism in this case is reaction of CO with O in the Pt lattice, then O activation is likely rate limiting. Our group and others have demonstrated that metal-O bond activation occurs by negative charge.[21,35,36] This explains why in state B, the device is only active when a negative bias is applied to the Pt, and the activity decreases during illumination when a flux of positive charge moves from the Si substrate to the Pt surface.

Conclusion

This work demonstrates direct control of catalytic CO oxidation using a catalytic nanodiode. This is the first time that a charge-based device has been shown to provide external control of a surface chemical reaction, and this was achieved using both applied bias and visible light. Previously, we demonstrated that a catalytic reaction can drive a current flow across a nanodiode. Now we show the reverse: that an external bias or current flow across a nanodiode

can drive a surface chemical reaction. Based on these results, we hope that charge-based device technology will be further developed for catalytic applications in energy conversion and selective chemistry.

References

(1) Herrmann, J.-M.; Pichat, P. *Journal of Catalysis* **1982**, *78*, 425-435.
(2) Mériaudeau, P.; Ellestad, O. H.; Dufaux, M.; Naccache, C. *Journal of Catalysis* **1982**, *75*, 243-250.
(3) Sexton, B. A.; Hughes, A. E.; Foger, K. *Journal of Catalysis* **1982**, *77*, 85-93.
(4) Resasco, D. E.; Haller, G. L. *Journal of Catalysis* **1983**, *82*, 279-288.
(5) Benvenutti, E. V.; Franken, L.; Moro, C. C.; Davanzo, C. U. *Langmuir* **1999**, *15*, 8140-8146.
(6) Jochum, W.; Eder, D.; Kaltenhauser, G.; Kramer, R. *Topics in Catalysis* **2007**, *46*, 49-55.
(7) Schwab, G.-M. *Trans. Faraday Soc.* **1946**, *42*, 689-697.
(8) Tauster, S. J.; Fung, S. C.; Garten, R. L. *J. Am. Chem. Soc.* **1978**, *100*, 170-175.
(9) Tauster, S. J.; Fung, S. C.; Baker, R. T. K.; Horsley, J. A. *Science* **1981**, *211*, 1121 -1125.
(10) Tauster, S. J. *Acc. Chem. Res.* **1987**, *20*, 389-394.
(11) Somorjai, G. A.; Li, Y. *Introduction to Surface Chemistry and Catalysis*; John Wiley and Sons, 2010.
(12) Boffa, A.; Lin, C.; Bell, A. T.; Somorjai, G. A. *Journal of Catalysis* **1994**, *149*, 149-158.
(13) Yamada, Y.; Tsung, C.-K.; Huang, W.; Huo, Z.; Habas, S. E.; Soejima, T.; Aliaga, C. E.; Somorjai, G. A.; Yang, P. *Nat Chem* **2011**, *3*, 372-376.
(14) Vannice, M. A.; Sen, B. *Journal of Catalysis* **1989**, *115*, 65-78.
(15) Lin, S. D.; Sanders, D. K.; Albert Vannice, M. *Applied Catalysis A: General* **1994**, *113*, 59-73.
(16) Malathi, R.; Viswanath, R. P. *Applied Catalysis A: General* **2001**, *208*, 323-327.
(17) Oh, S. H.; Eickel, C. C. *Journal of Catalysis* **1988**, *112*, 543-555.
(18) Zhu, H.; Qin, Z.; Shan, W.; Shen, W.; Wang, J. *Journal of Catalysis* **2004**, *225*, 267-277.
(19) Chen, M. S.; Goodman, D. W. *Science* **2004**, *306*, 252 -255.
(20) Goodman, D. W. *Catalysis Letters* **2005**, *99*, 1-4.
(21) Baker, L. R.; Hervier, A.; Seo, H.; Kennedy, G.; Komvopoulos, K.; Somorjai, G. A. *J. Phys. Chem. C* **2011**, *115*, 16006-16011.
(22) Enache, D. I.; Edwards, J. K.; Landon, P.; Solsona-Espriu, B.; Carley, A. F.; Herzing, A. A.; Watanabe, M.; Kiely, C. J.; Knight, D. W.; Hutchings, G. J. *Science* **2006**, *311*, 362 -365.
(23) Edwards, J. K.; Solsona, B. E.; Landon, P.; Carley, A. F.; Herzing, A.; Kiely, C. J.; Hutchings, G. J. *Journal of Catalysis* **2005**, *236*, 69-79.
(24) Nakagawa, K.; Ikenaga, N.; Suzuki, T.; Kobayashi, T.; Haruta, M. *Applied Catalysis A: General* **1998**, *169*, 281-290.
(25) Hervier, A.; Baker, L. R.; Komvopoulos, K.; Somorjai, G. A. *J. Phys. Chem. C* **2011**.
(26) Jencks, W. P. *Acc. Chem. Res.* **1980**, *13*, 161-169.
(27) Kazansky, V. B.; Senchenya, I. N. *Journal of Catalysis* **1989**, *119*, 108-120.
(28) Greeley, J.; Nørskov, J. K.; Mavrikakis, M. *Annual Review of Physical Chemistry* **2002**, *53*, 319-348.
(29) Olah, G. A.; Molnár, Á. *Hydrocarbon chemistry*; John Wiley & Sons, 2003.

(30) Gadzuk, J. W. *Phys. Rev. Lett.* **1996**, *76*, 4234-4237.
(31) Zhang, Y.; Kolmakov, A.; Chretien, S.; Metiu, H.; Moskovits, M. *Nano Lett.* **2004**, *4*, 403-407.
(32) Deshlahra, P.; Schneider, W. F.; Bernstein, G. H.; Wolf, E. E. *J. Am. Chem. Soc.* **2011**.
(33) Park, J. Y.; Somorjai, G. A. *ChemPhysChem* **2006**, *7*, 1409-1413.
(34) Hervier, A.; Renzas, J. R.; Park, J. Y.; Somorjai, G. A. *Nano Lett.* **2009**, *9*, 3930-3933.
(35) Bonn, M.; Funk, S.; Hess, C.; Denzler, D. N.; Stampfl, C.; Scheffler, M.; Wolf, M.; Ertl, G. *Science* **1999**, *285*, 1042 -1045.
(36) Zhang, Z.; Yates, J. T. *J. Am. Chem. Soc.* **2010**, *132*, 12804-12807.

Chapter 7

An Introduction to Oxide Support Effects in Heterogeneous Catalysis

1. Introduction

While nanoparticles comprise the active part of a catalyst, they cannot be used on their own: once they are exposed to the temperatures required for typical catalytic reactions, they will quickly aggregate, and the turnover frequency will drop as the catalyst surface area vanishes. This is why metal nanoparticles are ordinarily dispersed on a porous oxide or carbonaceous support in industrial applications.[1] Usually not active on its own, the support materials tend to maintain the metal catalysts in a highly dispersed state during catalytic applications.[2] However, it has been known for decades that the choice of support also has dramatic effects on surface chemistry, an effect widely and loosely referred to as the "Strong Metal Support Interaction" (SMSI).

In the original sense, the term SMSI described a specific phenomenon observed in catalysts synthesized by the incipient wetness impregnation method. Tauster and Fung first observed that upon reduction in H_2 at high temperatures, noble metal catalysts supported on TiO_2 almost completely lost their ability to adsorb CO and H_2 without significant change in catalyst surface area.[3] Electron microscopy and X-Ray diffraction showed that the loss of adsorption ability was not due to aggregation of the platinum particles. Hence, the intriguing factors that contributed to the unexpected activity loss became an attractive topic of study.

Despite having been studied for decades with hundreds of relevant publications, the SMSI phenomenon is still in need of experimental investigation to fully understand the effect. Most studies deal with the more general question of understanding how oxide supports interact with the metal catalysts, regardless of whether or not the support materials have been reduced in H_2 at high temperatures. The distinct chemical nature of various supports and the diversity of metal/oxide interactions further complicate the picture. A recent example has revealed that gold nanoparticles with identical sizes exhibited dramatically different behaviors for CO oxidation reaction depending on the type of oxide support used.[4] So far, several valid models that are not mutually exclusive have been proposed in regards to the effects at metal/oxide interface.

2. Decoration/encapsulation

Tauster and Fung described their catalysts as being in an "SMSI state" after reduction in hydrogen at 773 K, a state in which there was virtually no adsorption of CO and H_2. The authors

ruled out a possible explanation of metal encapsulation by the oxide because the effect was reversible while the total surface area of the catalyst was unchanged[3]. However, evidence to the contrary has been become available since then.

Baker *et al.* reduced Pd/TiO_2 catalysts at 973 K and suggested that TiO_2 was reduced to Ti_4O_7 which subsequently migrated over the Pd surface, based on TEM images and H_2 adsorption results.[5] In a similar experiment, Komaya *et al.* provided high resolution TEM images of reduced Rh/TiO_2 catalysts, demonstrating that Rh particles were partially covered by an amorphous titania overlayer after reduction at 573 K. The titania completely covered Rh particles upon reduction at 773K.[6] The decoration of Rh by TiO_2 agreed with an uptake drop in H_2 adsorption experiments. As TEM resolution has continuously improved, evidence for encapsulation became unquestionable: Figure 1 illustrates a Rh particle encapsulated with $CeTbO_x$ after reduction at 1173 K[7].

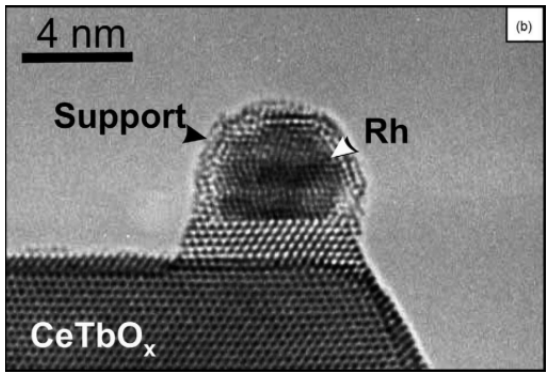

Figure 1 – *HREM images of a 0.5% $Rh/Ce_{0.8}Tb_{0.2}O_{2-x}$ catalyst reduced at 1173 K*[7].

It is generally agreed that surface tension is the driving force behind encapsulation. Leyrer *et al.* showed that the ability of an oxide to wet the surface of the metal catalyst correlated with its surface energy.[8] However, the fact that support effects could be observed at reduction temperatures lower than those required to cause encapsulation greatly challenged the explanation.[9] As a consequence, encapsulation is not considered to be the only contributing factor to these SMSI effects.

3. Spillover

Various catalysts differ in their ability to physisorb and chemisorb gaseous species. By combining two different surfaces, species adsorbed on one surface are capable of migrating onto the other, provided that a large enough interface area is provided by a high dispersion of metal nanoparticles on the oxide supports. Since the first hypothesis of spillover as early as 1940 by Emmett[10], many supportive phenomena have been reported.

Kuriacose *et al.* first reported that the presence of Pt accelerated the decomposition of GeH_4 to Ge.[11] Taylor later suggested that the Pt surface provided recombination sites for atomic H to form H_2 that readily desorbs.[12] Lately, spillover was directly observed for the first time

using scanning tunneling microscopy (STM) on methanol adsorption onto the $Pt/TiO_2(110)$ catalyst.[13] The sequential STM images in Figure 2 showed the formation of bright spots at the interface between the Pt particles and the TiO_2 surface and the migration along the fivefold-coordinated Ti rows away from Pt. TPD measurements indicated that these spots corresponded to $CH_3O_{(a)}$, even though $TiO_2(110)$ alone cannot dissociatively adsorb CH_3OH at room temperature. As a result, spillover might lead reactions to occur through pathways whose activation barriers are too high without the existence of these interfaces. On the other hand, spillover can complicate the task of measuring surface area for calculating turnovers. On Rh/TiO_2, for example, dissociatively adsorbed H atoms on Rh can spill over onto the TiO_2 surface, resulting in an overestimate of the number of active Rh surface sites.[6]

4. Charge transfer

It was proposed early on that certain forms of charge transfer, which occurred on or within the catalyst, played a significant role in oxide support effects. However, the various possible forms of charge transfer lead to a poor current understanding of such effects.

4.1. Charge transfer at the metal/oxide heterojunction

4.1.1. Steady state charge transfer

It is well known that when the surfaces of two materials are brought into contact, the difference in Fermi levels drives electrons to flow from the one with the higher Fermi level to the other until equilibrium is reached. The phenomenon is the basis not only for the electronics industry but also for the catalysis at metal/oxide interfaces.

Fung characterized thin films of Pt on SiO_2 and TiO_2 by XPS before and after reduction in H_2 at 623 K and 873 K.[14] The Pt4f peak was shifted down in binding energy by 1.6 eV following treatment at both temperatures, whereas no such shift occurred for the Pt thin film supported on SiO_2. Instead of the direct reduction of the metal by hydrogen, Fung ascribed the shift to electron transfer from the TiO_2 support to metal. Nevertheless, contradictory proofs were later reported by Sexton *et al.*, who pointed out that the surprisingly high downshift would correspond to the transfer of 1.5 electrons per platinum atom.[15] They found that reduction in hydrogen led to a small shift, on the order of 0.04 eV. The energy shift was only partially reversible upon re-oxidation, perhaps on account of sintering of the metal particles. The reversible contribution to the binding energy downshift was hence only 0.02 eV, two orders of magnitude smaller than Fung's reports.

The suggestion of such a small transfer of electrons to the metal could affect catalysis was met with skepticism by Ponec[16], since the charge screening length in a metal is on the order of a single bond length.[17] Nonetheless, Resasco and Haller found that the kinetics of ethane hydrogenolysis and cyclohexane dehydrogenation on Rh/TiO_2 could be explained by a model that involved two kinds of charge transfer.[18] After a low temperature reduction in H_2 at 473 K or 523 K, the metal particles donated electrons to the support, which was more noticeable for smaller particles. After a high temperature reduction in H_2 at 773 K, the electron transfer occurred from the oxide to the metal, and became localized. This amounted to stating that a chemical bond formed between the oxide and the metal, suggesting that the oxide covered up

the active metal sites, a combination of the charge transfer model and the encapsulation model.

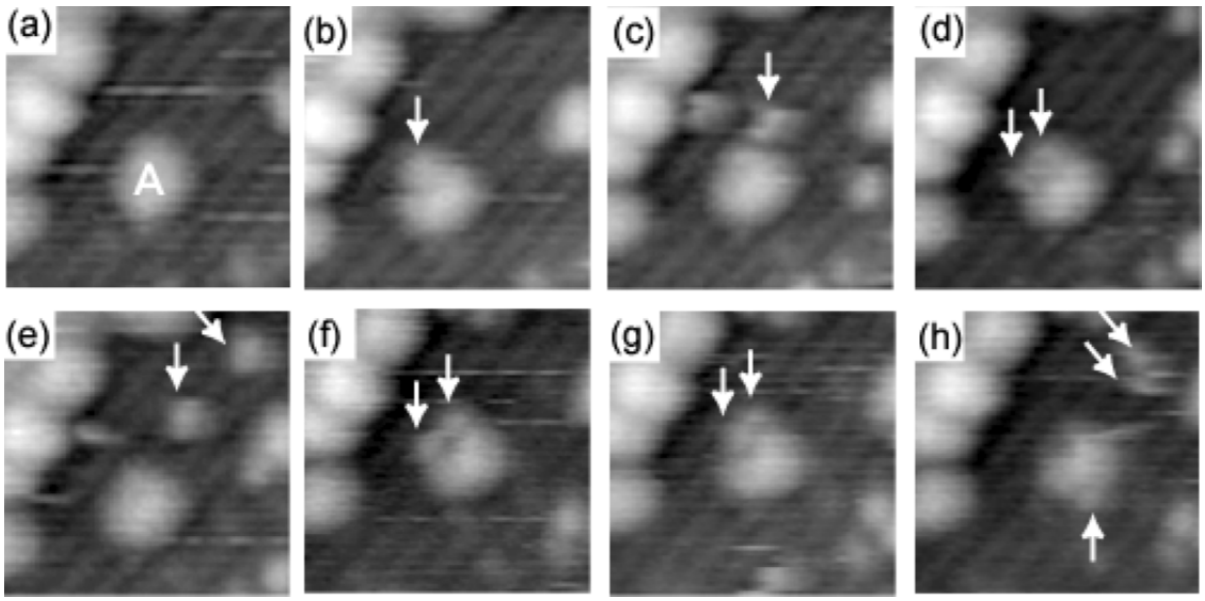

Figure 2 – *Snapshots of sequential STM measurements of the methanol adsorption process on a $Pt/TiO_2(110)$ surface. 6.4 × 6.4 nm^2; V_s, +1.0 V; I_t, 0.30 nA. Image (a) was captured just after introduction of methanol vapor into the STM chamber by backfilling. The vapor pressure was kept at 1.2 × 10^{-7} Pa during the measurement. Images (b-h) were acquired 170, 225, 280, 335, 775, 830, and 885 s, respectively, after image (a) was acquired. Reproduced from* [13]

4.1.2. Charge transfer during a reaction

Work in our laboratory showed that charge transfer from the metal to the oxide could also occur as a direct result of the reaction occurring on the surface. The nanodiode, consisting of a metal film deposited onto a semiconductor, was employed as the solid state model catalyst to observe the charge transfer occurring as a dynamic event.

As explained previously, the mismatch in Fermi levels leads to charge transfer between the metal and the semiconductor, which in turn causes the energy bands to bend at the interface. Contacts can be either Ohmic or Schottky-type with a transport barrier. The barrier serves as a high energy filter, letting through only hot electrons, i.e., electrons with energy significantly higher than the Fermi level in the case of an *n*-type semiconductor. The same concept can also be applied to hot holes when using *p*-type semiconductors. By connecting the diode to a circuit, it becomes possible to measure the flow of hot electrons or holes under reaction conditions. This chemicurrent is measurable if the metal film is thin enough for electrons to reach the Schottky barrier without dissipating their excess energy. Typical mean free paths for electrons with excess energies of 1 eV in metals are in the order of a few nanometers.[19]

The mechanism was recognized for two exothermic reactions, CO oxidation over both Pt/TiO_2 and Pt/GaN diodes, and H_2 oxidation over Pt/TiO_2 diodes, which was described in detail

in Chapter 3.[20,21] In both cases, the activation energies measured for the currents were in agreement with the activation energies of the reaction, indicating that the reaction on the surface dissipates energy into the metal by exciting electrons. In a true catalyst where no circuit is present to shuttle charges back to the metal, eventually an electrical field appears to prevent any further charge flow. These experiments lead to the important conclusion that if a reaction leads to a current between the metal and the oxide, applying current to a catalytic nanodiode may affect the surface chemistry by the reverse mechanism.

4.2. Charge transfer from the oxide to the adsorbate

More recently, we have found evidence of charge transfer occurring from titanium oxide to surface oxygen during CO oxidation[22] and methanol oxidation.[23] These results out presented in detail in the following chapters. Briefly, TiO_x films were annealed under different conditions to obtain various stoichiometries, such as $TiO_{1.7}$, $TiO_{1.9}$, and TiO_2, determined by XPS. Oxygen vacancies in TiO_2 create electronic states about 0.5–1.0 eV below the bottom of the conduction band.[24] The midgap states act as a conduction channel, and the conductivity of the film increases by orders of magnitude.[25,26] One titanium oxide film of each sample was also doped in SF_6 plasma, yielding six types of oxide support: $TiO_{1.7}$, $TiO_{1.9}$, and TiO_2, both doped and undoped. F was found to bind to Ti by filling oxygen vacancies, slightly offsetting the increased

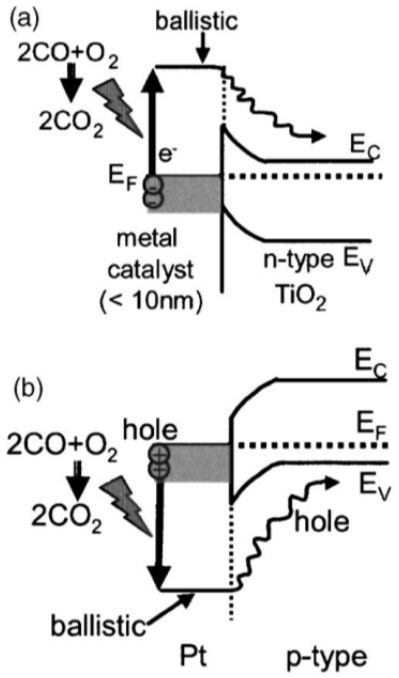

Figure 3 – *Scheme for the detection of ballistic hot charge carriers in reaction using a catalytic metal semi-conductor Schottky diode. (a) Band bending at the interface leads to hot electron collection when the semi-conductor has a higher Fermi level than the metal. (b) Hot holes are collected when the semi-conductor has a lower Fermi level than the metal.*[20]

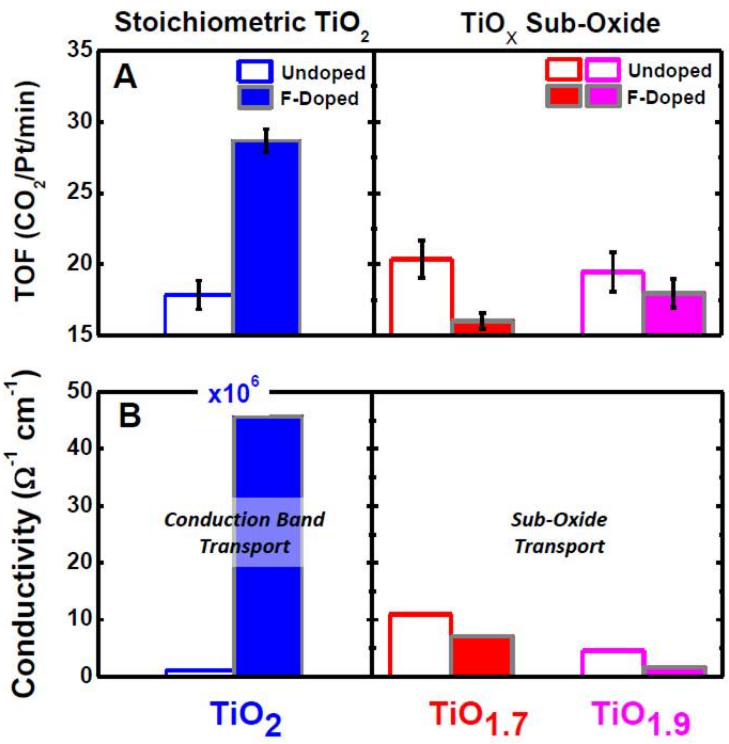

Figure 4 – *(A) Turnover frequencies (TOF) for CO oxidation on Pt nanoparticles supported on the six titanium oxide supports: TiO_2, $TiO_{1.9}$, and $TiO_{1.7}$, each with and without F insertion. Reaction occurred in 40 Torr CO, 100 TorrO_2, and 620 Torr He at 443 K. TOF data reflect the stable rate after ~30 min of deactivation. Error bars represent 95% confidence intervals. (B) Surface conductivity measurements for all six titanium oxide supports before Pt nanoparticle deposition. In the case of TiO_2, F insertion increased surface conductivity by a factor of 40 by acting as an extrinsic n-type donor. However, in the case of $TiO_{1.7}$ and $TiO_{1.9}$, F insertion slightly decreased the conductivity because F binds to Ti at O vacancy sites, resulting in the removal of subgap states that act as a transport channel in these samples. Note that TiO_2 with and without F is magnified by 10^6. This reflects the insulating nature of TiO_2 without the presence of a sub-band conduction channel. Comparison of panels A and B shows a surprising similarity between the effect of F on the TOF and on the surface conductivity.*

conductivity. However, F also acts as an *n*-type donor, forming donor levels just beneath the conduction band. For TiO_2, this increases conductivity 40-fold, as shown in Figure 4B. In the presence of oxygen vacancies, the vacant midgap states 0.5-1.0 eV below the bottom of the conduction band capture any donor electrons, and F doping slightly decreases the conductivity of the $TiO_{1.7}$ and $TiO_{1.9}$ films.[22]

While both types of electronic structure modification can increase the film conductivity, the resulting conduction channels are about 1.0 eV apart in energy. This energy difference correlates with the surface chemistry of the Pt/TiO_x catalysts. Although turnover increases nearly two-fold when stoichiometric TiO_2 is F-doped, no increase is observed with the non-stoichiometric $TiO_{1.7}$ and $TiO_{1.9}$ films, as demonstrated in Figure 4A.

Since CO oxidation on platinum is limited by activation of the Pt-O bond in the conditions used, the increase in turnover rate may be attributed to electron transfer from the oxide to surface O. Non-stoichiometric TiO_x does not show similar effects because the conduction channel formed by midgap states is much lower in energy. Electrons in those states have insufficient energy to transfer to surface O. Similar work was then carried out for methanol oxidation, and is described in Chapter 10.[23] The same work was then carried out for methanol oxidation, showing similar results. In the conditions used, the three products of the reaction are the total oxidation product, CO_2, and the partial oxidation products, methyl formate and formaldehyde. After fluorine doping, turnover for all three products increased significantly, and selectivity toward partial oxidation products increased from 17% to 35%. When non-stoichiometric TiO_2 was used, fluorine doping decreased catalytic activity, and the selectivity toward partial oxidation decreased or did not change significantly, depending on the oxygen vacancy concentration.

All of this data suggests that modifying the electronic structure of the support, in this case by fluorine doping, makes it possible to tune both the activity and the selectivity of a catalyst.

References

(1) Hayek, K.; Kramer, R.; Paál, Z. *Applied Catalysis A: General* **1997**, *162*, 1-15.
(2) Muetterties, E. L.; Krause, M. J. *Angewandte Chemie International Edition in English* **1983**, *22*, 135-148.
(3) Tauster, S. J.; Fung, S. C.; Garten, R. L. *J. Am. Chem. Soc.* **1978**, *100*, 170-175.
(4) Comotti, M.; Li, W.-C.; Spliethoff, B.; Schüth, F. *J. Am. Chem. Soc.* **2005**, *128*, 917-924.
(5) Baker, R. T. K.; Prestridge, E. B.; McVicker, G. B. *Journal of Catalysis* **1984**, *89*, 422-432.
(6) Komaya, T.; Bell, A. T.; Wengsieh, Z.; Gronsky, R.; Engelke, F.; King, T. S.; Pruski, M. *Journal of Catalysis* **1994**, *149*, 142-148.
(7) Bernal, S.; Calvino, J. J.; Cauqui, M. A.; Gatica, J. M.; López Cartes, C.; Pérez Omil, J. A.; Pintado, J. M. *Catalysis Today* **2003**, *77*, 385-406.
(8) Leyrer, J.; Margraf, R.; Taglauer, E.; Knözinger, H. *Surface Science* **1988**, *201*, 603-623.
(9) Jochum, W.; Eder, D.; Kaltenhauser, G.; Kramer, R. *Topics in Catalysis* **2007**, *46*, 49-55.
(10) Emmett, P. In *Twelfth report of the Committee on catalysis, National Research Council*; National Academies, 1940; pp. 53-67.
(11) Kuriacose, J. *Indian Journal of Chemistry 5*, 646.
(12) Taylor, H. *Annual Review of Physical Chemistry* **1961**, *12*, 127-150.
(13) Takakusagi, S.; Fukui, K.-ichi; Tero, R.; Asakura, K.; Iwasawa, Y. *Langmuir* **2010**, *26*, 16392-16396.
(14) Fung, S. *Journal of Catalysis* **1982**, *76*, 225-230.
(15) Sexton, B. A.; Hughes, A. E.; Foger, K. *Journal of Catalysis* **1982**, *77*, 85-93.
(16) Ponec, V. In *Studies in Surface Science and Catalysis*; Elsevier, 1982; Vol. Volume 11, pp. 63-75.
(17) Smith, J. R.; Arlinghaus, F. J.; Gay, J. G. *Phys. Rev. B* **1982**, *26*, 1071-1074.
(18) Resasco, D. E.; Haller, G. L. *Journal of Catalysis* **1983**, *82*, 279-288.
(19) Sze, S. M. *Journal of Applied Physics* **1966**, *37*, 2690.

(20) Park, J. Y.; Somorjai, G. A. *Journal of Vacuum Science & Technology B: Microelectronics and Nanometer Structures* **2006**, *24*, 1967.
(21) Hervier, A.; Renzas, J. R.; Park, J. Y.; Somorjai, G. A. *Nano Lett.* **2009**, *9*, 3930-3933.
(22) Baker, L. R.; Hervier, A.; Seo, H.; Kennedy, G.; Komvopoulos, K.; Somorjai, G. A. *J. Phys. Chem. C* **2011**, *115*, 16006-16011.
(23) Hervier, A.; Baker, L. R.; Komvopoulos, K.; Somorjai, G. A. *J. Phys. Chem. C* **2011**.
(24) Cronemeyer, D. C. *Phys. Rev.* **1959**, *113*, 1222.
(25) Bilmes, S. A.; Mandelbaum, P.; Alvarez, F.; Victoria, N. M. *J. Phys. Chem. B* **2011**, *104*, 9851-9858.
(26) Seo, H.; Baker, L. R.; Hervier, A.; Kim, J.; Whitten, J. L.; Somorjai, G. A. *Nano Lett.* **2011**, *11*, 751-756.

Chapter 8

Generation of Highly *n*-Type Titanium Oxide Using Plasma Fluorine Insertion

True n-type doping of titanium oxide without formation of mid-gap states would expand the use of metal oxides for charge-based devices. We demonstrate that plasma-assisted fluorine insertion passivates defect states and that fluorine acts as an n-type donor in titanium oxide. This enabled us to modify the Fermi level and transport properties of titanium oxide outside the limits of O vacancy doping. The origin of the electronic structure modification is explained by *ab initio* calculation.

Introduction

The application of transition metal oxide (TMO) semiconductors for charge-based devices is becoming prevalent for chemical, electrical, and energy applications.[1–3] Among TMOs, titanium oxide has been widely studied for photocatalysis,[4] light harvesting,[5] resistive switching memory,[6] and chemical sensing,[7] as an intrinsic n-type semiconductor. The charge transport/transfer in titanium oxide is highly sensitive to O vacancy defects that exist as the lattice bonding defects in single-crystals and as surface and grain boundary defects in polycrystalline films.[8] In previous studies, O vacancies, equivalent to Ti^{3+} states, have been used as intrinsic donors to create a transport channel for increased conductivity.[9,10]

O vacancies give rise to partially occupied Ti^{3+} states below the conduction band (CB) edge and act as n-type donors. Consequently, limited control of titanium oxide conductivity and Fermi level (E_F) is possible by the manipulation of O vacancies. However, the intrinsic doping of titanium oxide through Ti^{3+} defect sites is equivalent to the formation of a reduced oxide. Although, the reduced oxide is often highly conductive, Ti^{3+} mid-gap states act as a barrier to CB transport and result in E_F pinning.[11] Additionally, the electric activity (e.g. charge trapping) and chemical reactivity of O vacancies create problems for material reliability. Consequently, highly conductive titanium oxide is seldom useful for device architecture, and fabrication of highly conductive, defect-free titanium oxide remains an important challenge.

The extrinsic chemical doping of titanium oxide using impurity dopants (e.g. N, S, and C) by colloidal synthesis methods to modify the electronic structure and achieve visible light absorption has been actively studied for photocatalytic applications.[12,13] Additionally, metal impurity (e.g. V, Ni, and Nb) doping to titanium oxide has been used to modify E_F and increase the conductivity.[14,15] However, in each of these cases, the semiconductor properties of titanium oxide are compromised by the formation of metallic mid-gap states. To the best of our knowledge, no one has reported n-type doping of a metal oxide without simultaneously

decreasing the bandgap. This ability would be analogous to phosphorus or arsenic doping of silicon where carrier concentration is changed without significant band structure modification.

Here we report the use of plasma-assisted fluorine (F) insertion to passivate defects and act as an extrinsic n-type donor in titanium oxide. Electrical analysis shows that F insertion is an excellent method to achieve highly conductive, low defect titanium oxide suitable for TMO device applications. Theoretical calculations also investigate the concept of n-type doping to metal oxides by F insertion and suggest the mechanism by which F generates a highly conductive surface channel.

Results & Discussion

We deposited titanium oxide thin films by direct current magnetron sputtering. As deposited, these films were highly oxygen deficient. We tuned the oxygen vacancy concentration by rapid thermal annealing in O_2 at various temperatures; in this way we prepared three pre-conditions for F insertion with variable amounts of O vacancies. Based on the relative intensities of the Ti^{3+} and Ti^{4+} states in the Ti2p XPS spectrum, we refer to the three pre-conditions to F insertion as $TiO_{1.7}$, $TiO_{1.9}$, and TiO_2 (see figure 1). F insertion is achieved by treatment in N_2 plasma with trace SF_6. Process pressure was 50 mTorr with SF_6 partial pressure < 5 mTorr. Plasma power is 20 W with a 130 V DC substrate bias. Treatment times ranged between 1.5 and 4.5 minutes.

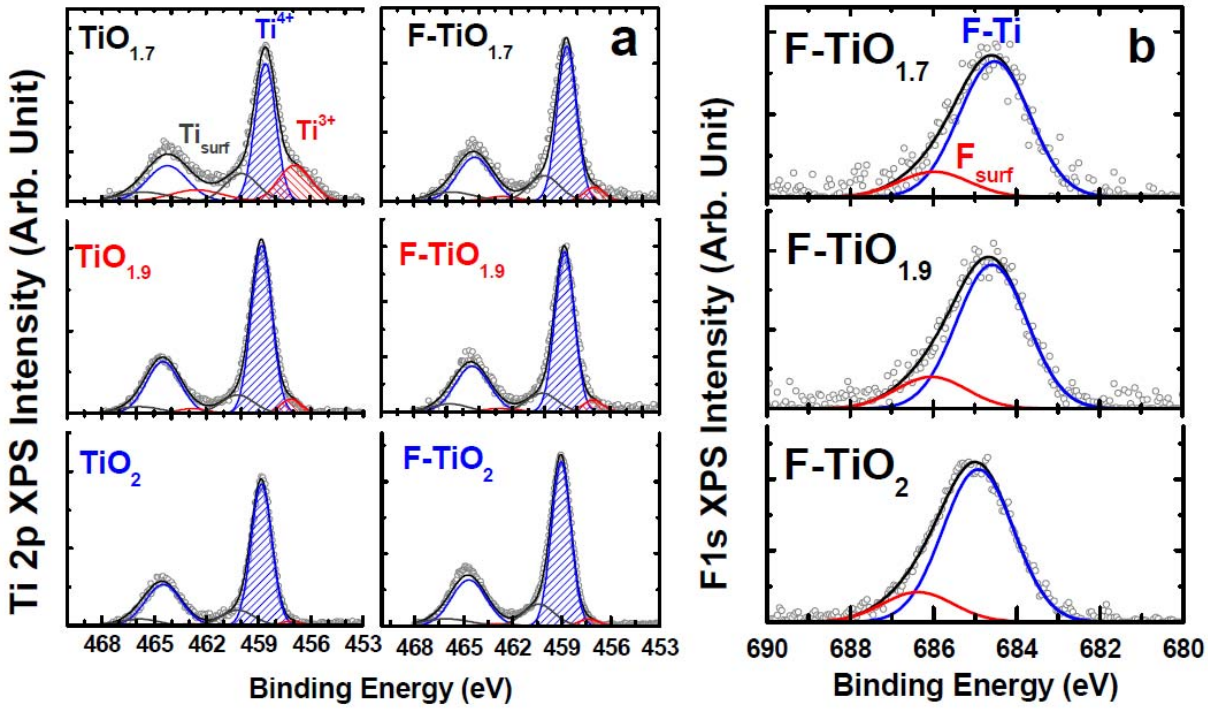

Figure 1 – ***(a)*** *Ti2p and* ***(b)*** *F1s XPS spectra of undoped and F-doped $TiO_{1.7}$, $TiO_{1.9}$, TiO_2. Open circles show the raw data, and lines show the results of a Gaussian deconvolution.*

Figure 2A shows surface conductivity measurements at room temperature for $TiO_{1.7}$ and TiO_2 before and after F insertion. In the case of $TiO_{1.7}$, the high density of suboxide states associated with the O vacancies leads to a metallic conduction (resistivity ~0.1 Ω·cm) but the conductivity decreases slightly with F insertion. This is because F passivation of O vacancies decreases the density of suboxide states used for transport in these materials. However, in the case of TiO_2, F insertion increased conductivity (i.e., decreased resistivity) by a factor of 40. Before discussing these results, it is insightful to note that for O vacancy doped TiO_X, transport occurs in the suboxide band structures induced by O vacancy defects. This is clearly evident in the activation energy of charge transport which is < 0.1 eV for these samples (see figures 2B and 3). Polycrystalline TiO_2 will always show activation energy for CB transport of ~ 0.3 eV because of localized electron traps at grain boundaries.[16] We cannot measure the activation energy for transport in the TiO_2 sample because it is highly insulating. This serves to illustrate that in oxide materials true CB transport is almost impossible to observe because high conductivity in oxides is usually only achievable by reducing the O stoichiometry to create a suboxide band structure. For the F inserted TiO_2 (F-TiO_2) sample we observe a transport activation energy of 0.3 eV consistent with CB transport in polycrystalline TiO_2 (see figure 3).

It is likely that this conduction is highly localized to the surface of the film. Due to the method for F insertion, we consider that F incorporates in the film primarily in the top 3 ± 1 nm as confirmed in the XPS depth profile. By acting as an n-type donor (to be discussed later) to raise E_F toward CB edge, F represents a positive space charge in the near surface region resulting in downward band bending toward the surface. If the band bending is such that the CB drops below E_F, then a shallow 2-dimensional electron gas (2DEG) forms. We suggest that the 2DEG is the mechanism for the dramatic increase in conductivity for the F-TiO_2 sample. According to this theory, the surface channel resistivity is much lower than shown in figure 2A, where we conservatively consider the entire film thickness (100 nm) in determining the area of the transport channel. If the 2DEG is localized to the top 1 nm of the film as is likely, then true resistivity calculated from the device channel area could easily be two orders lower (~ 10^2 Ω·cm) than that determined by considering the entire film thickness (~10^4 Ω·cm). Note that the F appears to be stable over long periods of time. We have repeated surface conductivity measurements after storing the samples in dry N_2 for 5 months and observe no measurable loss in surface conductivity induced by F. The purpose of storing in dry N_2 is to prevent water adsorption that significantly modifies the surface electronic structure of titanium oxide.

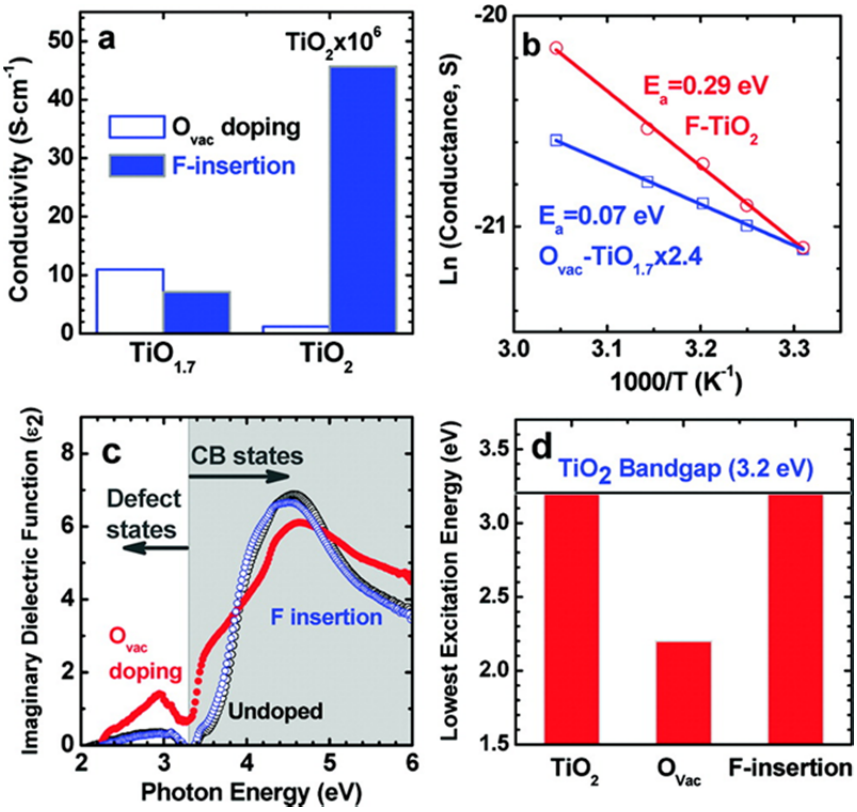

Figure 2 – ***(a)*** *Conductivity ($S \cdot cm^{-1}$) measurements at room temperature for 100 nm TiO_X on insulating substrates. Note that the enhanced surface conductivity induced by F in TiO2 is stable over time with no measurable loss in conductivity after 5 months.* ***(b)*** *Ln (Conductance, S) as a function of temperature for O vacancy doped $TiO_{1.7}$ and F-inserted TiO_2 diodes. The Ln (S) values of O vacancy doped $TiO_{1.7}$ is normalized to the value of F-inserted TiO_2 at 28.7 °C (i.e. 1000/T = 3.31 K^{-1}). The slope is proportional to the activation energy (E_a) for transport (see figure 3). E_a less than 0.1 eV indicates transport in semi-metal suboxide states, while E_a about 0.3 eV indicates CB transport with grain boundary defects acting as barriers. For $TiO_{1.7}$, F insertion slightly decreases conductivity by removing the suboxide states that provide the primary path for charge transport. For TiO_2, F insertion increases conductivity by a factor of 40 and shows E_a consistent with CB transport. We conclude that while F decreases suboxide transport, it produces a surface channel for enhanced CB transport.* ***(c)*** *Imaginary dielectric functions (ε_2) as a function of photon energy for undoped TiO_2, O vacancy doped $TiO_{1.7}$, and F inserted TiO_2 taken by spectroscopic ellipsometry measurements. CB absorption (shaded in grey) shows an onset at 3.2 eV and is nearly identical for the F inserted and undoped TiO_2 sample indicating that F insertion does not significantly modify the CB structure. At photon energies below 3.2 eV, absorption is due to O vacancy associated mid-gap states.* ***(d)*** *Lowest excitation energy of TiO_2, O vacancy doped $TiO_{1.7}$, and F inserted TiO_2 from absorption coefficient spectra (see figure 7). The reference absorption onset for each excitation is ~ 10^5 cm^{-1}.*

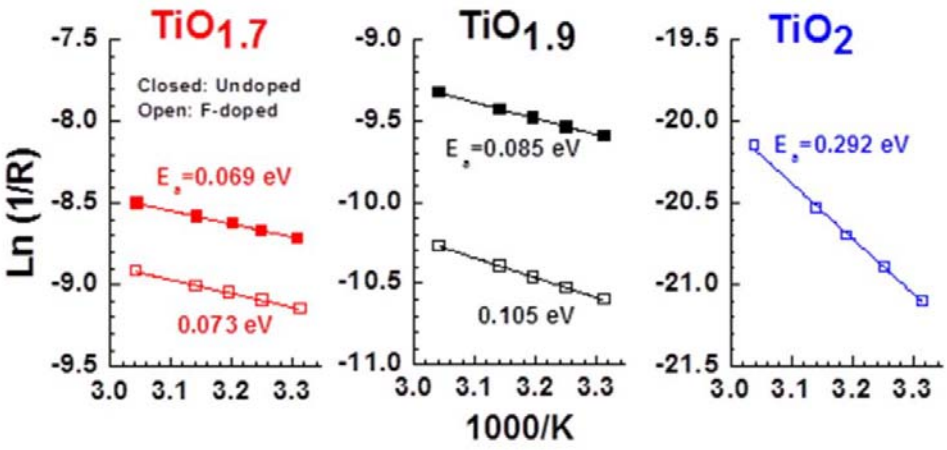

Figure 3 – *Arrhenius Plot of Ln(1/resistance, Ω^{-1}) against 1000/temperature (K) for undoped and F-doped $TiO_{1.7}$, $TiO_{1.9}$, TiO_2. Squares show raw data, and lines show linear fits. The slope of the fit is proportional to the activation energy for thermally activated charge transport.*

Figure 2C shows the photon energy dependent imaginary dielectric functions obtained by spectroscopic ellipsometry for undoped titanium oxide (i.e. TiO_2), O vacancy doped titanium oxide (i.e. $TiO_{1.7}$), and titanium oxide after F insertion (i.e F-TiO_2). This allows us to compare the effects of O vacancy doping and F insertion on the CB structure and minimum excitation energy. The CB edge shows an onset at 3.2 eV for TiO_2 and F-TiO_2 samples, indicating that F insertion does not change the bandgap. Absorption at photon energies below 3.2 eV is the result of electron excitation from the valence band (VB) to mid-gap states associated with a suboxide band structure. By looking at the relative absorption coefficients converted from the dielectric functions, it is possible to compare the density of mid-gap states induced by O vacancy doping and by F insertion under the joint density of states theory (see below). The relative absorption of mid-gap states in $TiO_{1.7}$ (~10^5 cm^{-1}) is an order of magnitude higher than that (~10^4 cm^{-1}) of TiO_2. The lowest excitation energy for each film in figure 2C is plotted in figure 2D. While O vacancy doped $TiO_{1.7}$ shows the significant destabilization of intrinsic TiO_2 band structure with the low excitation energy (from top of VB to empty subgap O vacancy states) at 2.2 eV, F insertion does not induce any of change in CB edge states, stabilizing the bandgap energy at 3.2 eV. As will be discussed later, this stabilized CB edge state of F-TiO_2 is due to the higher excitation energy of molecular orbital states of Ti-F bonds than 3.2 eV bandgap energy of TiO_2.

The conduction band (CB) edge states of titanium oxide thin films were analyzed from the absorption spectra taken by a rotating compensator enhanced spectroscopic ellipsometry (SE) measurement with a spectral resolution of 15 meV. SE determines the complex reflectance ratio, $\rho=r_p/r_s$, where r_p and r_s are the complex reflectance of waves in the polarized light that are parallel (p) and perpendicular (s) to the plane of incidence, respectively. Monochromatic light from a xenon lamp provides visible and ultraviolet light having an energy range from 1.5

eV (8267 Å) to 6 eV (2066 Å). This light excites electrons from the top of the valence band to the conduction band in the overlayer (i.e. titanium oxide) material. From ρ, optical properties such as index of reflection (*n*), extinction coefficient (*k*), and dielectric function (ε) are determined. To extract the dielectric function of the titanium oxide overlayer from the pseudodielectric function of the whole stack (air/TiO_2/Si) a three phase model was applied such that the dielectric function of Si was analyzed first, and the dielectric functions of the titanium oxide overlayer was subsequently extracted. The generalized equation for the optical three phase model is expressed as follows:

$$<\varepsilon>=\varepsilon_s+\frac{4\pi d n_a}{\lambda}\frac{\varepsilon_s(\varepsilon_s-\varepsilon_o)(\varepsilon_o-\varepsilon_a)}{\varepsilon_o(\varepsilon_s-\varepsilon_a)}\left(\frac{\varepsilon_s}{\varepsilon_a}-\sin^2\phi\right)^{1/2} \qquad \text{(A1)}$$

where $<\varepsilon>$ is the measured pseudo dielectric function, ε_s is the substrate (Si) dielectric function, ε_a is the air dielectric function, ε_o is the overlayer (titanium oxide) dielectric function, *d* is the overlayer thickness, n_a is the index of reflectance for air, λ is the wavelength of incident polarized light, and φ is the angle of incidence (fixed at 67.08°). Because all parameters except ε_o are already known, ε_o can be obtained by iterative calculation using equation (A1).

The absorption coefficient, α is obtained from the λ and *k* values by the conversion equation:

$$\alpha=4\pi k/\lambda \qquad \text{(A2)}$$

where *k* is the extinction coefficient and λ is the wave length of light. Figure 4 shows the resulting graphs of the extinction ocefficients for the different oxide films.

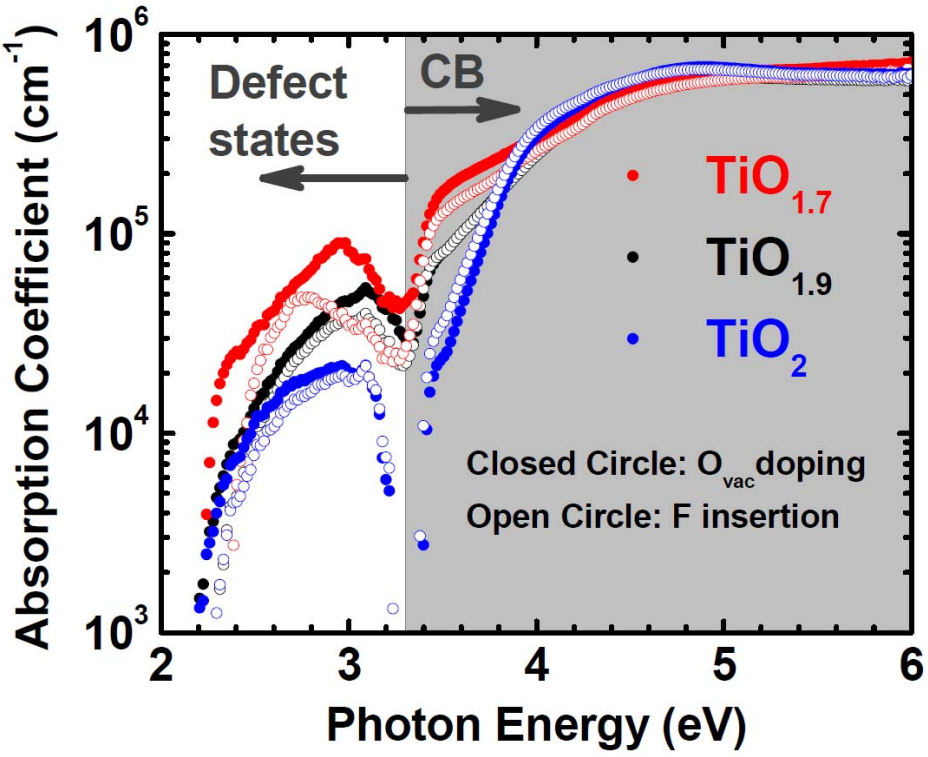

Figure 4 – *Absorption coefficient spectra for undoped and F-doped $TiO_{1.7}$, $TiO_{1.9}$, TiO_2 taken by SE measurement and three-phase analysis. Closed circles show undoped TiO_X, and open circles show F doped TiO_X.*

Figure 5A shows current-voltage (IV) curves for diodes consisting of TiO_x on highly doped p-Si. We present results for TiO_2 and $TiO_{1.7}$ before and after F insertion. Without F insertion, both TiO_2 and $TiO_{1.7}$ heterojunction devices show almost symmetrical IV curves where the reverse bias leakage current is nearly as high as the forward bias current. This is the result of two factors. First, the high density of subgap states in $TiO_{1.7}$ provide a path for carrier transport in the reverse bias direction. Second, the low n-type character (i.e., low E_F level) of O vacancy doped TiO_X closely aligns with E_F in p-Si resulting in minimal interface band bending. For TiO_2 and $TiO_{1.7}$, the reverse bias current decreases and the forward bias current increases with F insertion. This is the combined effect of defect state passivation by F and increased E_F in the F-TiO_X layer to achieve greater band bending at the p-Si interface. In figure 5B, the rectifying factor (taken as the ratio of forward to reverse bias current) increases with F insertion by a factor of 3 for both cases. A similar trend was observed for $TiO_{1.9}$ (not shown), except that the

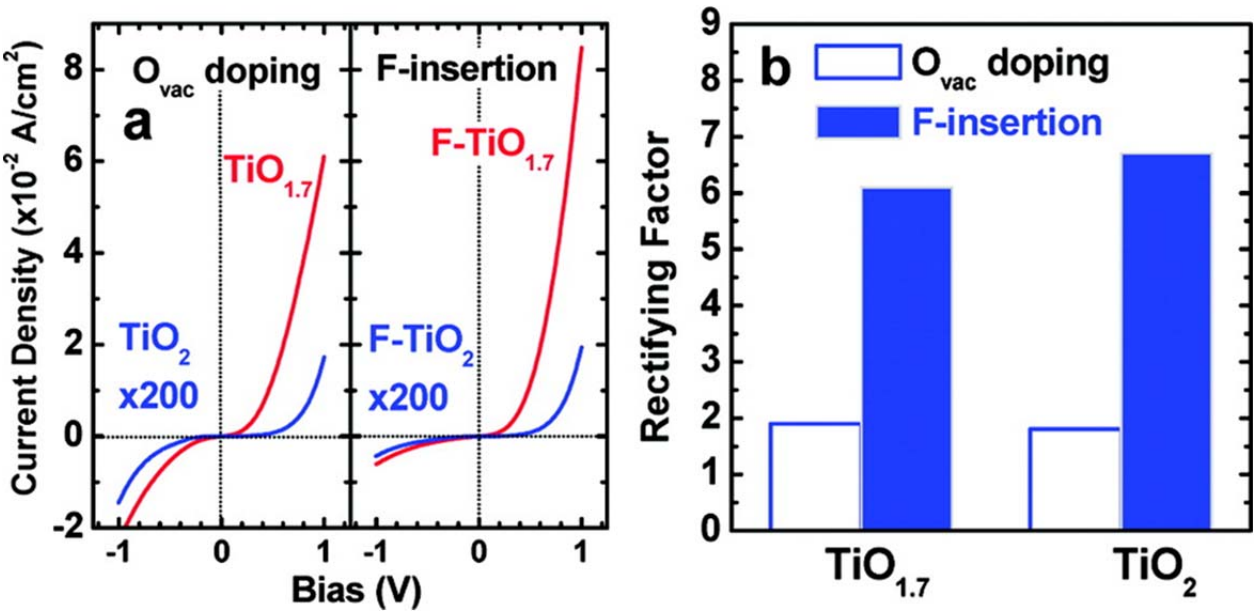

Figure 5 – ***(a)*** *Current-voltage (IV) curves for ~ 10 nm TiO_X on highly doped (0.01 Ω cm) p-Si. Red lines show $TiO_{1.7}$ samples, and blue lines show TiO_2. On the left is before F insertion, and on the right is after F insertion. The current density values of all TiO_2 diodes were multiplied by a factor of 200.* ***(b)*** *Rectifying factor for TiO_2 and $TiO_{1.7}$ before and after F doping. Rectifying factors are the ratio of forward to reverse bias current. For O vacancy doped TiO_X, low rectifying factors are the result of a high concentration of defect states and low Fermi level (E_F). By passivating defects and raising E_F, F doping increases the rectifying factor for each precondition by more than a factor of 3.*

rectifying factor before F insertion was 3.4 and increased to 22.4 after F insertion. This is much higher than for TiO_2 and $TiO_{1.7}$. We do not fully understand this anomaly but believe it is in part a result of the higher EF in $TiO_{1.9}$ before F insertion compared to either TiO_2 or $TiO_{1.7}$ as discussed below. It may seem counterintuitive that surface F doping could affect rectification at the buried Si-TiO_X interface. However, the thickness of the TiO_X layer (i.e. 10 nm) is much smaller than the depletion width. Consequently, n-type doping to the surface will still effect rectification due to the mean field across the depletion region of this p-n heterojunction.

Figure 6A shows E_F for TiO_2, $TiO_{1.9}$, and $TiO_{1.7}$ before and after F insertion. We determined E_F by fitting the valence band edge XPS spectra (see figure 7). It is insightful to first consider the effect of O vacancies on the Femi level before considering the effect of F doping. In the case of stoichiometric TiO_2, we measured E_F to be 2.4 eV. Doping by O vacancies initially introduces partially occupied Ti^{3+} states about 0.3~0.5 eV below the CB edge,[17] and these states serve to pin E_F at approximately 2.8 eV in the $TiO_{1.9}$ sample. However, if the oxide is further reduced, semi-metal states form that pin E_F at a much lower energy. This is evident in the $TiO_{1.7}$ sample that shows E_F to be 2.1 eV. We note that this value is in excellent agreement with the spectroscopic ellipsometry spectra that showed a minimum excitation at 2.2 eV (see figure 2D). Although this reduced oxide is highly conductive, transport occurs in the metallic band

structure of the suboxide, and it is not possible to use this material as a semiconductor because of the high density of mid-gap states.

Figure 6A also shows that F insertion raises E_F for each pre-condition by up to 1 eV. In the case of $TiO_{1.7}$, where E_F is initially pinned at 2.1 eV by the semi-metal states of the suboxide, F insertion increases E_F to 3.1 eV, just below the CB edge. This is partly the result of F passivation of suboxides states in the bandgap. However, the resulting E_F is 0.7 eV greater than undoped, stoichiometric TiO_2. We conclude that in addition to passivating defects, F acts as an n-type donor. These results demonstrate the ability of F insertion to tune E_F outside the limits of O vacancy doping. Comparing E_F after F insertion for each pre-condition shows that E_F scales with the atomic ratio of F to Ti determined by XPS (see figure 6B). This indicates that F binding to an O vacancy gives rise to a free CB electron in titanium oxide. We call this effect n-type doping by F insertion. Figure 6B also indicates another binding state of F which we assign as interstitial insertion. Theoretical calculations discussed below explain the origin of these two binding states and discuss their respective contributions to modifying the bulk electronic properties. We note that E_F scales with the concentration of a F binding state at 684.9 eV that we assign as O substitution (or binding to a preexisting O vacancy).

Figure 6C shows the Ti2p spectrum for O vacancy doped and F inserted $TiO_{1.7}$. The peak binding state at 458.5 eV is characteristic of the Ti^{4+} states in the stoichiometric oxide, while the shoulder at lower binding energy (BE, 456.9 eV) represents Ti^{3+} and Ti^{2+} states in the suboxides. Comparison of the Ti2p spectra of $TiO_{1.7}$ before and after F insertion shows a decrease in Ti^{3+} states from 41% to 9%. This is a dramatic reduction in the density of defect states with F insertion, and is direct evidence that F passivates O vacancies by binding Ti^{3+}. Figure 6D shows the absorption ratio of mid-gap to CB states before and after F insertion for each TiO_X pre-condition based on spectroscopic ellipsometry measurements. This provides additional evidence that F binding is primarily to O vacancies, and that F passivates defect states in non-stoichiometric oxides. Because the chemical instability of O vacancies is one of the primary factors that limit TMO device reliability, we believe that F insertion may greatly improve the chemical stability of TMO semiconductor devices. However, we have not yet investigated the effect of F insertion on chemical stability. Note that in the case of stoichiometric TiO_2, F insertion does not significantly change the O vacancy concentration because it is already so low.

We note that SF_6 can etch TiO_2 by formation of TiF_4 which has a vapor pressure at room temperature. Fracassi et al. showed that during SF_6 plasma etching a layer of TiF_3 and TiF_4 forms on the surface of the oxide.[18] TiF_4 leaves the surface by sublimation which is likely assisted by ion sputtering in the plasma. Consequently, the formation of titanium fluorides(TiF_X) and subsequent etching represents an upper limit to F doping in TiO_2. For our plasma exposures, the F concentration stayed beneath the limit for formation of TiF_4 as can be seen by atomic fractions of F to Ti below 0.6. Fracassi et al. also showed that formation of TiF_3 and TiF_4 during etching is easily visible in the Ti2p XPS spectrum by a 3–5 eV shift to higher BE.[19] We observe no significant shift (< 0.2 eV) in the Ti2p BE with plasma treatment. This suggests true chemical doping by F insertion rather than formation of a fluoride phase.

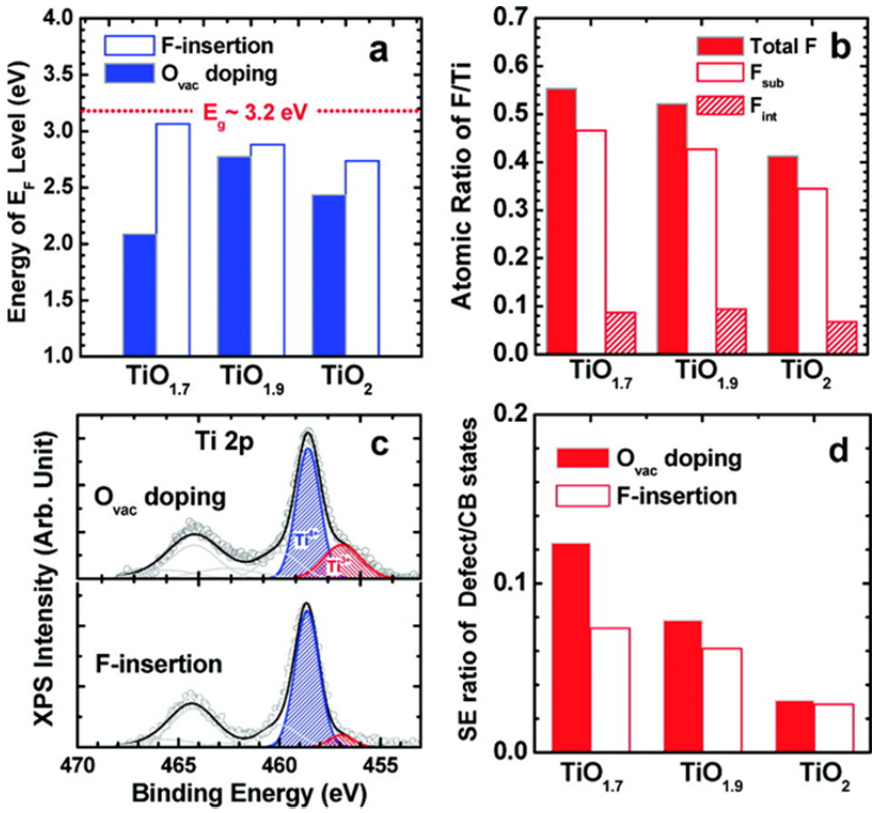

Figure 6 – ***(a)*** *Fermi level (E_F) before and after F insertion for each TiO_X precondition determined by fits to the valance band edge XPS spectra (see figure 8). For the O vacancy doped samples, E_F is determined by Fermi pinning to O vacancy defect states. By passivating O vacancy states, F removes the effects of Fermi pinning. Additionally, F acts as an extrinsic n-type donor. As a result, F insertion raises E_F higher than is possible by O vacancy doping. For the doped samples, E_F scales with F concentration.* ***(b)*** *The atomic ratio of F to Ti after 3 min. plasma treatment for each TiO_X precondition. Atomic ratios are shown for two different binding states identified by XPS (see figure 8B) and for total F. We assign these two binding states as F substituted for O and as interstitial F. Substitutional F concentration depends strongly on the initial O vacancy concentration before plasma treatment and appears to determine E_F after F insertion.* ***(c)*** *Ti2p XPS spectrum of $TiO_{1.7}$ before and after F insertion. Open circles show the raw data, and lines show the results of a Gaussian deconvolution. The peak state at 458.5 eV is the Ti^{4+} state in stoichiometric TiO_2. The lower binding energy peak at 456.9 eV is the Ti^{3+} state and is a marker for O vacancy induced defect states. The decrease in Ti^{3+} state concentration with F insertion indicates that F passivates defects by binding to Ti^{3+} at O vacancies.* ***(d)*** *Ratio of defect state to CB absorption measured by spectroscopic ellipsometry before and after F insertion for $TiO_{1.7}$, $TiO_{1.9}$, and TiO_2. Defect state/CB absorption was taken as the maximum absorption coefficient below/above 3.2 eV. The trend shows that F passivates O vacancies that give rise to defect states.*

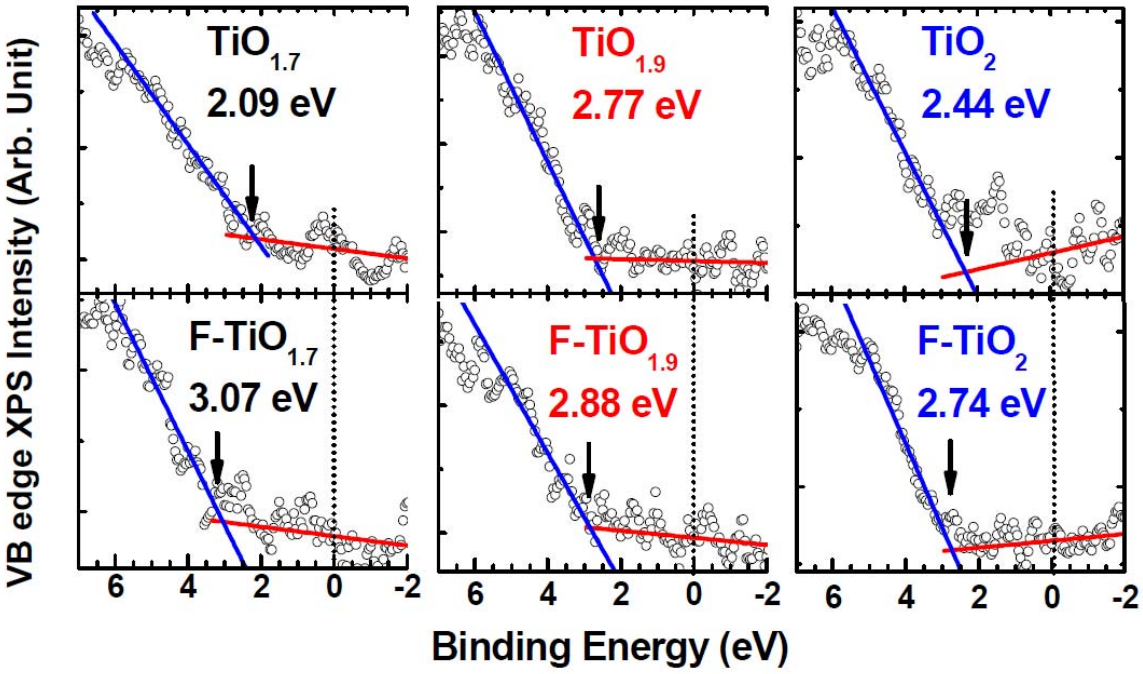

Figure 7 – *VB edge XPS spectra for undoped and F-doped $TiO_{1.7}$, $TiO_{1.9}$, TiO_2. Open circles show raw data, and lines show fitting used to determine Fermi level.*

Theoretical calculations are carried out using a high level, many-electron theory in order to investigate fundamental properties of TiO_2. This is a well-established method for investigating the electronic structure of metal oxides.[20] The theoretical model considers three different modifications to TiO_2: a) interstitial F, b) F substitution for oxygen or c) an O vacancy. Of particular interest are effects on the electronic excitation spectrum and induced spin states that accompany changes in the occupancy of Ti d orbitals. We use a geometry optimized $Ti_{18}O_{36}$ nanoparticle to investigate these effects. While the nanoparticle differs in detail from bulk TiO_2, the interior sites involve the same basic electronic structure. Figure 8A depicts $Ti_{18}O_{36}$ nanoparticle model with an interstitial F site. In other calculations, a subsurface vacancy is created by removing a neutral O atom at the interior of the particle, and a F atom is substituted for O.

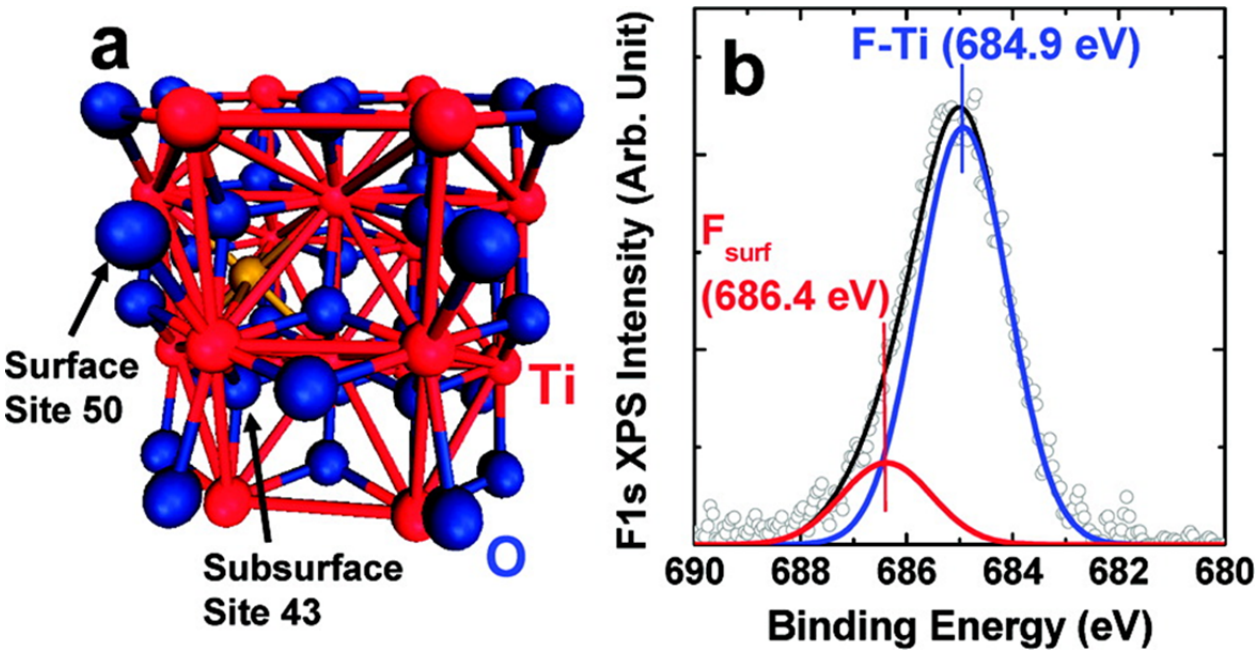

Figure 8 – ***(a)*** *$Ti_{18}O_{36}$ nanoparticle model with interstitial F (yellow ball) used for theoretical calculation. In this site, F sits in a distorted octahedral formed by six Ti atoms. In this case charge transfer to the F ion is primarily from a surface O atom (shown as site 50) because the nearest neighbor Ti atoms are already fully oxidized. The substitutional F site and O vacancy site (shown as site 43) have three Ti nearest neighbors.* ***(b)*** *F1s XPS spectrum of TiO_2 after 3 min. F insertion. Open circles show the raw data, and lines show the results of a Gaussian deconvolution. The peak state at 684.9 eV indicates Ti-F bonding as a result of O subsitution. We assign the state at 686.5 eV as interstitial F. The relative energies of the two binding states are explained by the qualitatively different charge exchange between F and either Ti or O depending on the insertion site.*

In all three systems, the lowest energy excitation is best described as exciton, with a hole that is largely localized on a single O2p and an electron that is transferred to the d-shell of a nearest neighbor Ti. In the nanoparticle, the oxygen vacancy and interstitial F alter the excitation energy or "bandgap" from the ~3eV of the unmodified $Ti_{18}O_{36}$. Substitutional F increases the excitation energy while an O vacancy decreases the excitation energy (see table 1). This explains why F insertion does not alter the minimum excitation energy observed experimentally. Although F insertion creates new states in the bandgap, the lowest excitation energy is still the difference between the unmodified valance and conduction band edges of stoichiometric TiO_2.

	O Vacancy	Substitutional F	Interstitial F
Increase in number of Ti 3d electrons*	1.58	0.89	0.00
Increase in number of unpaired O 2p electrons*	0.00	0.00	0.93
F population	—	9.55	9.62
Change in O2p-Ti3d excitation energy (eV)*	−0.3	+0.8	+0.2

Table 1 – *Changes in electronic properties on modification of a $Ti_{18}O_{36}$ nanoparticle by formation of a) O vacancy, b) substitutional F, and c) interstitial F. *Changes are relative to unmodified $Ti_{18}O_{36}$.*

The calculations also reveal major differences in the concentration of free carrriers: an O vacancy and substitutional F induce unpaired electron spin in the d-shell of a nearest neighbor Ti, while interstitial F induces unpaired spin on nearby oxygen. One of the key findings that relates to the present investigation is the difference in behavior of subsurface species in the creation of surface electronic states involving oxygen atoms that are substantially undercoordinated, e.g., 2-fold coordinated, on the surface of TiO_2. O atoms on the surface can serve as receptors of unpaired spins generated internally and are strongly affected by nearby subsurface modifications. To summarize, substitutional F is responsible for the increase of electron density in CB of TiO_2 in contrast to the increase in mid-gap states by O vacancy doping. Furthermore, interstitial F leads to an unpaired spin in the O2p orbital of surface O that draws free carriers to the surface and acts as a surface conduction.

To emphasize the high level of correlation between the experimental results and the theoretical study, we briefly discuss the nature of F binding states in TiO_2 as identified by XPS spectra. Figure 8B shows the F1s XPS spectrum for TiO_2 after F insertion. The peak is composed of two binding states centered at 684.9 and 686.4 eV. This spectrum is identical to previous reports for F insertion of TiO_2 by solution phase methods.[19] The peak state at 684.9 eV indicates Ti-F bonds by substitutional F doping. The shoulder at higher BE is a F surface state, and previous reports have hypothesized as to its exact origin.[19] We propose that the higher BE state represents interstitial F insertion (i.e. F insertion without removal of an O atom). In the case of O substitution, F coordinates to a partially oxidized Ti atom, electron density is transferred from the Ti to the F, and the Ti atom assumes a 4+ oxidation state. However, if F is inserted or bound

to the surface without the removal of O, F could not draw electron density from a Ti nearest neighbor because all nearest neighbor Ti atoms are fully oxidized. In this case, the calculation suggests that F attracts electron density from a nearby O atom creating a partially unoccupied O2p state. This is what we term interstitial insertion. The relative energies of the two binding states are explained by the qualitatively different charge exchange between F and either Ti or O depending on the insertion site.

In figure 1B, two F binding states are resolved at 684.9 eV and 686.4 eV. Based on Ti2p XPS data in figure 1A, Ti^{3+} species is reduced by F passivation forming Ti-F bonds. At this bond, F attracts about one electron from the neighboring Ti because the electronegativity of F is higher than Ti. This F-induced charge exchange causes the shift of binding energy of Ti higher than Ti^{3+} and that of F lower than neutral F. This Ti-F formation is equivalent to the substitutional F doping either replacing the lattice oxygen (O) site or passivating O-vacancy sites. The theoretical calculation (to be discussed later) predicts the origin of this kind of Ti-F bond as the substitutional F-doping by replacing (i) the top-surface O site having two near-neighboring Ti atoms and (ii) the sub-surface O or O-vacancy site having three near-neighboring O sites with F. For all cases, F attracts electron from Ti, causing the singly occupied 3d electron in Ti. Thus, the F1s biding state at 684.9 eV is assigned as the substitutional F doping to Ti. On the other hand, the F 1s bonding state at 686.4 eV is assigned as the surface F ($F_{surface}$) because it has a higher concentration at the more surface region. The theoretical calculation considers the interstitial F at subsurface. The interstitial F occupies the octahedral sites formed by Ti ions. F attracts electron density because of its electronegativity but since Ti is already depleted by its normal bonding with O, the electron attracted to F comes from O2p electron density of top-surface undercoordinated O, which leads to the unpaired electron in O2p orbital. However, the electronegativity of O is far higher than Ti, the electron density that F attracted from O is a partial electron density smaller than that for Ti-F case. This partial charge exchange causes the higher binding energy of interstitial F than that of substitutional F. Therefore, the density of surface-segregated $F_{surface}$ binding state in XPS data and theoretical result strongly suggest that F1s bonding state at 686.4 eV is due to the interstitial F.

Considering the two binding states to be equivalent to substiutional and interstitial F insertion considered by the theoretical calculations, we find excellent agreement between the theoretical conclusions and the experimental findings. First, we observe that substitutional F (i.e. binding state at 684.9 eV) scales with the O vacancy concentration before doping while interstitial F (i.e. binding state at 686.4 eV) shows little dependence on the precondition to plasma treatment. Second, we find that E_F scales closely with the concentration of substitutional F which theory predicts to generate a free electron in the Ti d shell, unlike interstitial F. Finally, the role of interstitial F to increase surface conductivity by drawing free charge carriers to the surface can explain the enhancement of surface conductivity in stoichiometric TiO_2 after F insertion. We refer the reader back to figures 2A and 6A/B for this data.

Conclusion

This study demonstrates that F passivates O vacancy defects and acts as an extrinsic n-type donor for titanium oxide, resulting in greatly enhanced CB transport. This effect is stable at ambient temperature with no measureable loss of surface conductivity over several months. It is likely that F will have the same effect on other TMO semiconductors. The ability to remove mid-gap states and tune E_F while stabilizing the intrinsic TiO_2 band structure can result in a highly conductivity oxide suitable for device architecture and overcomes the limitations of current O vacancy doping technology for oxide semiconductors. The highly conductive surface electronic structure of n-type titanium oxide with F insertion, free of E_F level pining, is promising for many metal-oxide applications including solar cells, resistive switching memory, transparent oxide transistors, sensors, and catalysts.

References

(1) Wager, J. F. *Science* **2003**, *300*, 1245 -1246.
(2) Xie, X.; Li, Y.; Liu, Z.-Q.; Haruta, M.; Shen, W. *Nature* **2009**, *458*, 746-749.
(3) Park, J. Y.; Lee, H.; Renzas, J. R.; Zhang, Y.; Somorjai, G. A. *Nano Lett.* **2008**, *8*, 2388-2392.
(4) Fujishima, A.; Honda, K. *Nature* **1972**, *238*, 37-38.
(5) Bach, U.; Lupo, D.; Comte, P.; Moser, J. E.; Weissortel, F.; Salbeck, J.; Spreitzer, H.; Gratzel, M. *Nature* **1998**, *395*, 583-585.
(6) Kwon, D.-H.; Kim, K. M.; Jang, J. H.; Jeon, J. M.; Lee, M. H.; Kim, G. H.; Li, X.-S.; Park, G.-S.; Lee, B.; Han, S.; Kim, M.; Hwang, C. S. *Nat Nano* **2010**, *5*, 148-153.
(7) Peng, X.; Chen, A. *J. Mater. Chem.* **2004**, *14*, 2542-2548.
(8) Di Valentin, C.; Pacchioni, G.; Selloni, A. *J. Phys. Chem. C* **2009**, *113*, 20543-20552.
(9) Zhang, Y.; Kolmakov, A.; Chretien, S.; Metiu, H.; Moskovits, M. *Nano Lett.* **2004**, *4*, 403-407.
(10) Frederikse, H. P. R. *Journal of Applied Physics* **1961**, *32*, 2211-2215.
(11) Cao, F.; Oskam, G.; Searson, P. C.; Stipkala, J. M.; Heimer, T. A.; Farzad, F.; Meyer, G. J. *J. Phys. Chem.* **1995**, *99*, 11974-11980.
(12) Asahi, R.; Morikawa, T.; Ohwaki, T.; Aoki, K.; Taga, Y. *Science* **2001**, *293*, 269 -271.
(13) Chen, X.; Burda, C. *J. Am. Chem. Soc.* **2008**, *130*, 5018-5019.
(14) Choi, W.; Termin, A.; Hoffmann, M. R. *J. Phys. Chem.* **1994**, *98*, 13669-13679.
(15) Janisch, R.; Gopal, P.; Spaldin, N. A. *Journal of Physics: Condensed Matter* **2005**, *17*, R657-R689.
(16) Cox, P. A. *Transition Metal Oxides: An Introduction to Their Electronic Structure and Properties*; Oxford University Press, 2010.
(17) Lucovsky, G.; Seo, H.; Lee, S.; Fleming, L. B.; Ulrich, M. D.; Lüning, J.; Lysaght, P.; Bersuker, G. *Japanese Journal of Applied Physics* **2007**, *46*, 1899-1909.
(18) Fracassi, F.; d' Agostino, R. *Pure and Applied Chemistry* **1992**, *64*, 703-707.
(19) Czoska, A. M.; Livraghi, S.; Chiesa, M.; Giamello, E.; Agnoli, S.; Granozzi, G.; Finazzi, E.; Valentin, C. D.; Pacchioni, G. *J. Phys. Chem. C* **2008**, *112*, 8951-8956.
(20) Lucovsky, G.; Whitten, J. L. *Surface Science* **2007**, *601*, 4138-4143.

Chapter 9

Highly *n*-Type Titanium Oxide as an Electronically Active Support for Platinum in the Catalytic Oxidation of Carbon Monoxide

The role of the oxide-metal interface in determining the activity and selectivity of chemical reactions catalyzed by metal particles on an oxide support is an important topic in science and industry. A proposed mechanism for this strong metal-support interaction is electronic activation of surface adsorbates by charge carriers. Motivated by the goal of using electronic activation to drive non-thermal chemistry, we investigated the ability of the oxide support to mediate charge transfer. We report approximately twofold increase in the turnover rate of catalytic carbon monoxide oxidation on platinum nanoparticles supported on stoichiometric titanium dioxide (TiO_2) when the TiO_2 is made highly n-type by fluorine (F) doping. However, for non-stoichiometric titanium oxide ($TiO_{X<2}$) the effect of F on the turnover rate is negligible. Studies of the titanium oxide electronic structure show that the energy of free electrons in the oxide determines the rate of reaction. These results suggest that highly n-type TiO_2 electronically activates adsorbed oxygen (O) by electron spillover to form an active O^- intermediate.

Introduction

Although metals alone are often catalytically active, most industrial catalysts consist of metal particles supported on a porous oxide. This not only provides a high surface area for the heterogeneous catalyst, but as shown by many studies, the oxide support plays an important role in determining the activity and selectivity of the catalyst.[1–4] This phenomenon, known as the strong metal-support interaction (SMSI), has been widely studied and is an important topic in both science and industry.[5]

SMSI affects a wide range of catalytic reactions, including carbon monoxide (CO) and carbon dioxide (CO_2) hydrogenation[4–6], selective hydrogenation,[7–9] and CO oxidation.[10–13] Although not traditionally termed SMSI, the catalyst support also plays an important role in activating molecular oxygen for selective partial oxidation reactions. Industrially relevant examples include the synthesis of aldehydes from primary alcohols[14], the production of hydrogen peroxide from hydrogen,[15–19] and the conversion of methane to synthesis gas.[20–22] In all of these cases, molecular oxygen is preferred over other oxygen donors due to cost, energy efficiency, and environmental concerns.[14,22]

Titanium oxide is perhaps the best known example of an SMSI support.[2,4] Additionally, titanium oxide is a common support for catalysts demonstrating high selectivity toward partial

oxidation.[14,18,22] The majority of proposed mechanisms for the role of titanium oxide fall into one of the following categories: (1) formation of active sites when the support wets (or "decorates") the metal particle[23,24], (2) oxygen (O) activation and/or spillover from chemically active defects in the support[25], and (3) electronic mediation through various forms of charge transfer[12,26]. Although each of these mechanisms can play an important role, this study focuses on the role of charge transfer and electronic mediation due to its importance in energy conversion reactions.

Previous studies have indicated that, at least in certain instances, catalytic oxidation reactions proceed by an electronically activated pathway.[27–32] Bonn *et al.*[27] showed that for CO oxidation on Ru, the activation of chemisorbed O occurs by charge transfer from the metal. Because the active O species cannot form thermally until well above the desorption temperature of CO, a temperature ramp of a CO/O_2 co-adsorbed Ru surface produces CO and O_2, but not CO_2. However, a femtosecond laser pulse can produce very high electronic temperatures on the short time scale without significant lattice heating. This serves to activate the O without CO desorption resulting in CO_2 formation.

Although fundamentally insightful, this type of experiment employing a femtosecond laser cannot be scaled for high turnover applications. Another approach to achieve electronic activation is to use an electronically modified catalyst. Several variables can tune the electronic structure of a catalyst including size,[31] support,[32] and doping.[30] The objective of this study was to identify the role of the support in electronic activation of surface chemistry. Here we demonstrate the ability to modify the electron transport properties of titanium oxide by controlling the O stoichiometry and by fluorine (F) doping. We find that stoichiometric titanium dioxide (TiO_2) modified by F doping is an electronically active support for CO oxidation on platinum (Pt) under conditions of high pressure and temperature (760 Torr and 443 K). However, the highly conductive reduced oxide shows little or no electronic activity toward CO oxidation, with or without F.

We have previously reported the production of hot electron flow during catalytic CO oxidation using the Pt/TiO_2 nanodiode system.[33] In that work we demonstrated that there is an electron flow from the Pt to the TiO_2 in proportion to the catalytic turnover. We now find that the opposite effect occurs by F doping TiO_2. In this case, an electron flow from the titanium oxide to the surface adsorbates significantly increases the catalytic reaction rate by activating surface O for reaction with CO.

Experimental

Catalyst Preparation

Thin films of titanium oxide with variable oxygen (O) vacancy concentrations served as supports for the platinum (Pt) catalyst. First, titanium oxide films (100 nm) were deposited on Si(100) wafers with a 500-nm-thick thermal oxide by direct-current magnetron sputtering. Sputtering conditions were 400 W plasma power, 450 V bias voltage, 50 sccm Ar flow, and 3 sccm O_2 flow. As deposited, the titanium oxide films were highly O deficient. Rapid thermal annealing in O_2 at temperatures between 623 and 773 K was used to vary the O concentration

in the films. To avoid grain size variations due to annealing at different temperatures, all samples were annealed in nitrogen (N_2) at 773 K. The titanium oxide films with three stoichiometries were prepared: TiO_2, $TiO_{1.9}$, and $TiO_{1.7}$, as determined from the ratio of Ti^{3+} and Ti^{4+} in the Ti 2p X-ray photoelectron spectra (XPS) (see previous chapter).

Fluorine (F) insertion was achieved by plasma treatment in N_2 gas with trace sulfur hexafluoride (SF_6). Trace SF_6 was introduced into the chamber by flowing a 9:1 mixture of SF_6 and O_2 followed by pumping to chamber base pressure (5 mTorr). After pumping, a small background pressure of SF_6 remained in the chamber. N_2 gas was then introduced at 80 sccm for plasma treatment. Plasma power was 20 W and DC substrate bias was 130 V. F concentration was tunable with the length of the plasma treatment. Two samples of each TiO_X stoichiometry were fabricated, and one of each type was plasma treated. This produced six supports for subsequent Pt deposition: TiO_2, $TiO_{1.9}$, and $TiO_{1.7}$, each with and without F. All samples were stored under a dry N_2 atmosphere until the reaction rate measurements.

Pt nanoparticles were deposited onto the samples by electron beam evaporation. Vapor deposited, rather than colloidally synthesized, nanoparticles were used to avoid the presence of an insulating polymer capping layer between the metal nanoparticles and the support. For electron beam evaporation the chamber base pressure was less than 10^{-5} Torr, and the deposition rate was 0.02 Å/s. The average film thickness monitored by quartz crystal microbalance was 1 nm. SEM showed that at this average thickness the Pt nanoparticles left ~50% of the support exposed as shown in figure 1.

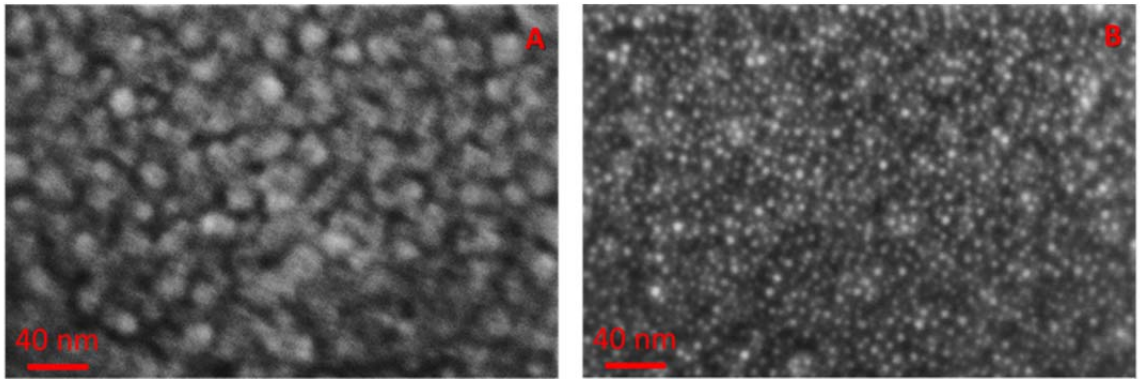

Figure 1 – *SEM image of the catalyst (1 nm Pt vapor deposited on TiO_2) before (**A**) and after (**B**) reaction at 543 K. Although the morphology of the Pt particles undergoes some change at high temperature, the particles do not agglomerate, and the Pt coverage does not significantly change.*

Catalyst Characterization

The electronic structure of the titanium oxide supports was characterized by XPS, spectroscopic ellipsometry, and measurements of surface conductivity and activation energy for charge transport.

XPS was used to analyze the chemical binding states of the titanium oxide films and the supported Pt catalysts both before and after reaction (Physical Electronics, PHI 5400 ESCA/XPS system with an Al anode source at 1486.6 eV). The energy resolution for each point is 0.05 eV. The analyzer was positioned at 50° relative to sample normal. All binding energies were calibrated to the Ti 2p peak state.

The real and imaginary parts of the complex dielectric constant, $\varepsilon c = \varepsilon_1 + i\varepsilon_2$, and absorption coefficients for titanium oxide samples were determined by visible-ultra violet spectroscopic ellipsometry in a rotating compensator enhanced spectrometer. The monochromatic light source from a Xenon lamp at photon energies of 1.5–6 eV was used with spectral resolution of 15 meV.

To measure surface conductivity of the titanium oxide films, ohmic contact was made to the titanium oxide using thin film electrodes consisting of 10 nm Ti and 100 nm Au. All metals were deposited by electron beam evaporation. Measurements were made with a Keithley 2400 sourcemeter.

Reaction Rate Measurements

A batch mode reactor with a boron nitride substrate heater was used to determine the reaction rates of CO oxidation on each of the above described catalysts. A metal bellows circulation pump provided gas mixing. Gas pressures were 40 Torr CO and 100 Torr O_2 in a background of He. The catalyst temperature was 443 K. Each catalyst was tested for 112 min and CO_2 production was monitored as a function of time using a gas chromatograph with a thermal conductivity detector.

Reaction rates are reported in turnover frequency (TOF) as CO_2 molecules produced per Pt site per minute. All error bars represent the 95% confidence interval based on the rate of CO_2 production normalized to the estimated number of Pt sites. The number of Pt sites, was estimated by assuming a uniform (111) surface structure over the entire catalyst area. Although this calculation is approximate, it provides a consistent normalization to the catalyst area and yields a reasonable estimate of the absolute TOF.

Results and Discussion

Figure 2 shows the effect of F on the reaction rate and on the surface conductivity of each stoichiometry. In the case of stoichiometric TiO_2, F doping increased the reaction rate by 61%, while F doping to $TiO_{1.7}$ and $TiO_{1.9}$ decreased the reaction rate by 21 and 8%, respectively. There is a surprising similarity between the effect of F on the turnover rate, and the effect of F on the surface conductivity of the titanium oxide support. As in the turnover rate measurements, F doping to TiO_2 dramatically increased (40-fold) the surface conductivity, while F doping to $TiO_{1.7}$ and to $TiO_{1.9}$ resulted in only a slight decrease (approximately twofold) in surface conduction. We can explain these results by considering the electronic structure of stoichiometric and reduced titanium oxide. We characterized the electronic structure using two measurements: the activation energy of surface conduction and the optical absorption spectrum.

To understand how the activation energy of transport relates to the electronic structure, it is necessary to consider the role of grain boundary defects in polycrystalline TiO_2. Grain boundaries produce defects in the band structure of titanium oxide with a localized defect state ~0.3 eV below the conduction band edge. Consequently, this is the activation energy for conduction in polycrystalline TiO_2 because electrons thermally trap and de-trap at grain boundaries during transport. In contrast, O vacancies at high concentrations form a sub-oxide band structure at a reduced energy. This sub-oxide band shows semi-metal, or nearly unactivated, electron transport.[34]

Figure 3A shows the activation energies for electron transport in $TiO_{1.7}$ and TiO_2. As expected, the highly reduced oxide shows low activation energy for conduction (0.07 eV) consistent with semi-metal transport in a low energy sub-band, while F-doped TiO_2 shows activation energy of 0.29 eV, consistent with conduction band transport across grain boundaries. TiO_2 without F was too insulating to accurately measure the activation energy of transport. However, F insertion to $TiO_{1.7}$ did not change the transport mechanism.

Figure 3B compares the optical absorption of $TiO_{1.7}$ and TiO_2. To illustrate the differences between these samples, we show the minimum excitation energy having a fixed absorption coefficient of 2×10^4 cm^{-1}. We find that $TiO_{1.7}$ has a strong absorption located ~0.7 eV below the conduction band edge that arises from excitation of electron-hole pairs in the sub-oxide band. This measurement reflects the decrease in bandgap energy for the reduced oxide and shows the difference in the energy of free electrons in the two supports.

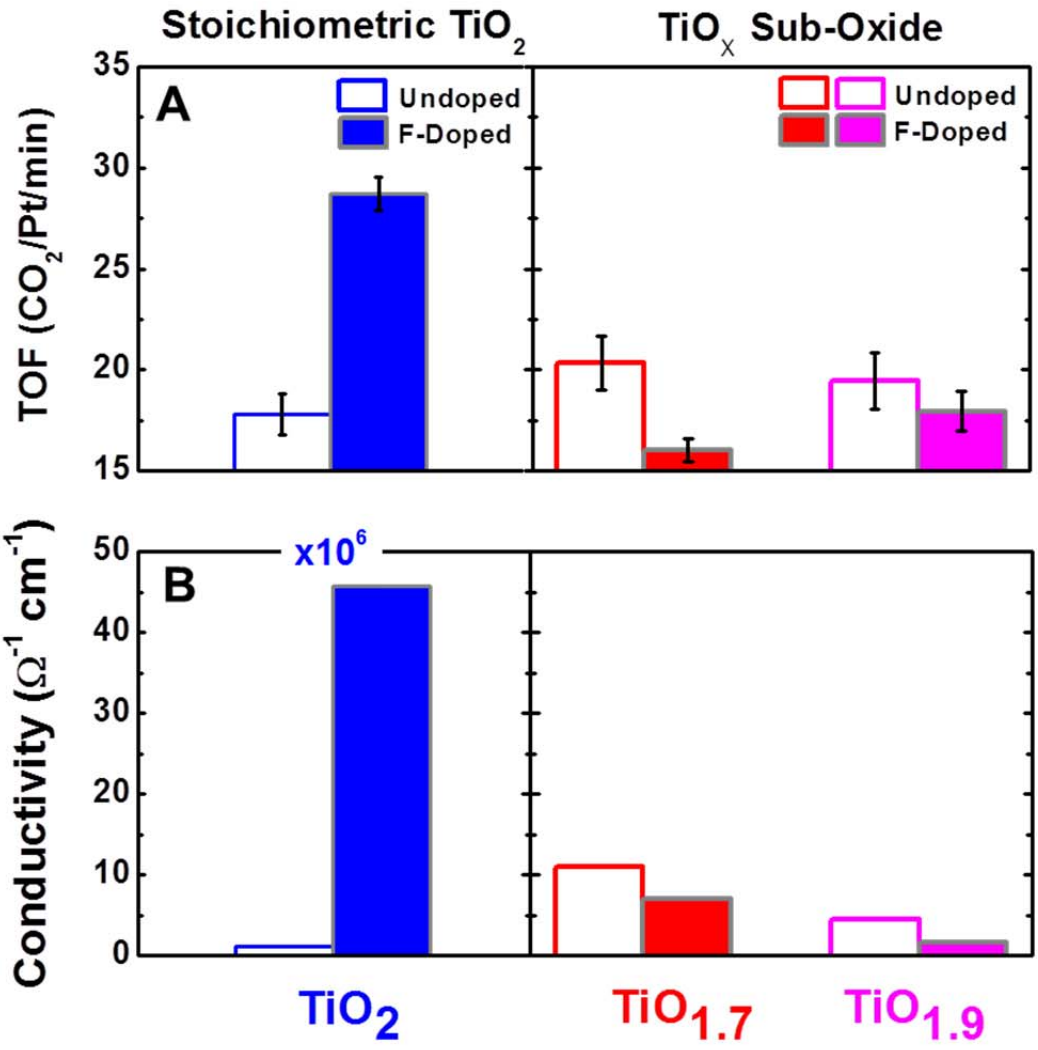

Figure 2 A – *Turnover frequencies (TOF) for CO oxidation on Pt nanoparticles supported on the six titanium oxide supports: TiO_2, $TiO_{1.9}$, and $TiO_{1.7}$, each with and without F insertion. Reaction occurred in 40 Torr CO, 100 Torr O_2, and 620 Torr He at 443 K. TOF data reflect the stable rate after ~30 min. of deactivation. Error bars represent 95% confidence intervals.* ***B*** *Surface conductivity measurements for all six titanium oxide supports before Pt nanoparticle deposition. In the case of TiO_2, F insertion increased surface conductivity by a factor of 40 by acting as an extrinsic n-type donor. However, in the case of $TiO_{1.7}$ and $TiO_{1.9}$, F insertion slightly decreased the conductivity because F binds to Ti at O vacancy sites resulting in the removal of sub-gap states that act as a transport channel in these samples. Note that TiO_2 with and without F is magnified by 10^6. This reflects the insulating nature of TiO_2 without the presence of a sub-band conduction channel. Comparison of* ***A*** *and* ***B*** *shows a surprising similarity between the effect of F on the TOF and on the surface conductivity.*

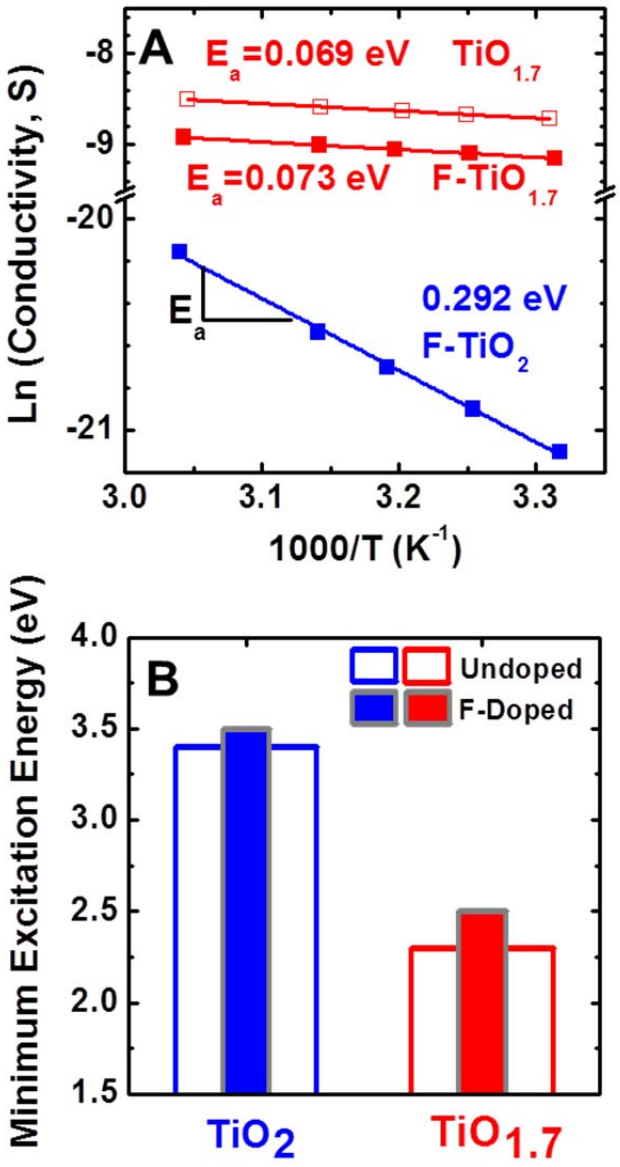

Figure 3 A – *Arrhenius plots showing the activation energy for charge transport in $TiO_{1.7}$ and TiO_2. Because TiO_2 without F is highly insulating, the Arrhenius curve could not be accurately measured for this sample. The different activation energies for conduction in $TiO_{1.7}$ and TiO_2 confirm different transport channels as depicted in figure 4A.* ***B*** *Minimum excitation energy having a fixed absorption coefficient of 2×10^4 cm^{-1}. This measurement reflects the decrease in bandgap energy for the reduced oxide and shows the difference in the energy of free electrons in the two supports.*

Figure 4A is a diagram of the two band structures of stoichiometric and reduced titanium oxide based on the above measurements. In the cases of both $TiO_{1.7}$ and $TiO_{1.9}$, F doping decreased the surface conductivity. The reason for this is that F binds to Ti at the sites of O vacancies resulting in passivation of defect states. Conduction in these samples occurs primarily in the sub-oxide band structure induced by the high concentration of O vacancies. Consequently, a decrease in the O vacancy concentration partially removes the conduction channel in these two samples. However, F insertion in the TiO_2 sample increased conductivity by a factor of 40. This is because F acts as an extrinsic n-type donor in metal oxide semiconductors increasing the concentration of free electrons in the conduction band of TiO_2.[35]

Assuming a reaction mechanism where a rate limiting step is activated by a conduction band electron from the titanium oxide support, the electronic structure of the titanium oxide explains the observed trend in reactivity. In the case of $TiO_{1.7}$ and $TiO_{1.9}$, the presence of F decreased the surface electron density in the oxide support resulting in a slightly reduced reaction rate. However, because the majority of electrons in these supports reside in the sub-oxide band at an energy that is presumably too low to induce chemistry, changes in electron density have a minimal effect on surface chemistry. In the case of TiO_2 where free carriers reside in the conduction band from which they can spillover to adsorbates, an increase of surface electron density induced by F correlates with a significant increase in catalytic activity by electronic activation.

We propose that the mechanism for electronic activation is electron spillover from TiO_2 to adsorbed O to form an activated O^- intermediate that readily reacts with CO. This is depicted schematically in figure 4B. In the case of O vacancy doping, the energy of the sub-oxide band is 0.5–1.0 eV below the conduction band edge. This energy is much higher than kT (≥13 kT at a reaction temperature of 443 K). Consequently, a reaction pathway that is electronically activated by free carriers in the conduction band of TiO_2 would not be thermally accessible until a temperature of ~6,000 K. However, because F insertion to TiO_2 increases the surface concentration of free electrons without formation of any mid-gap states, free electrons reside in the actual conduction band making this material an electronically active support for CO oxidation.

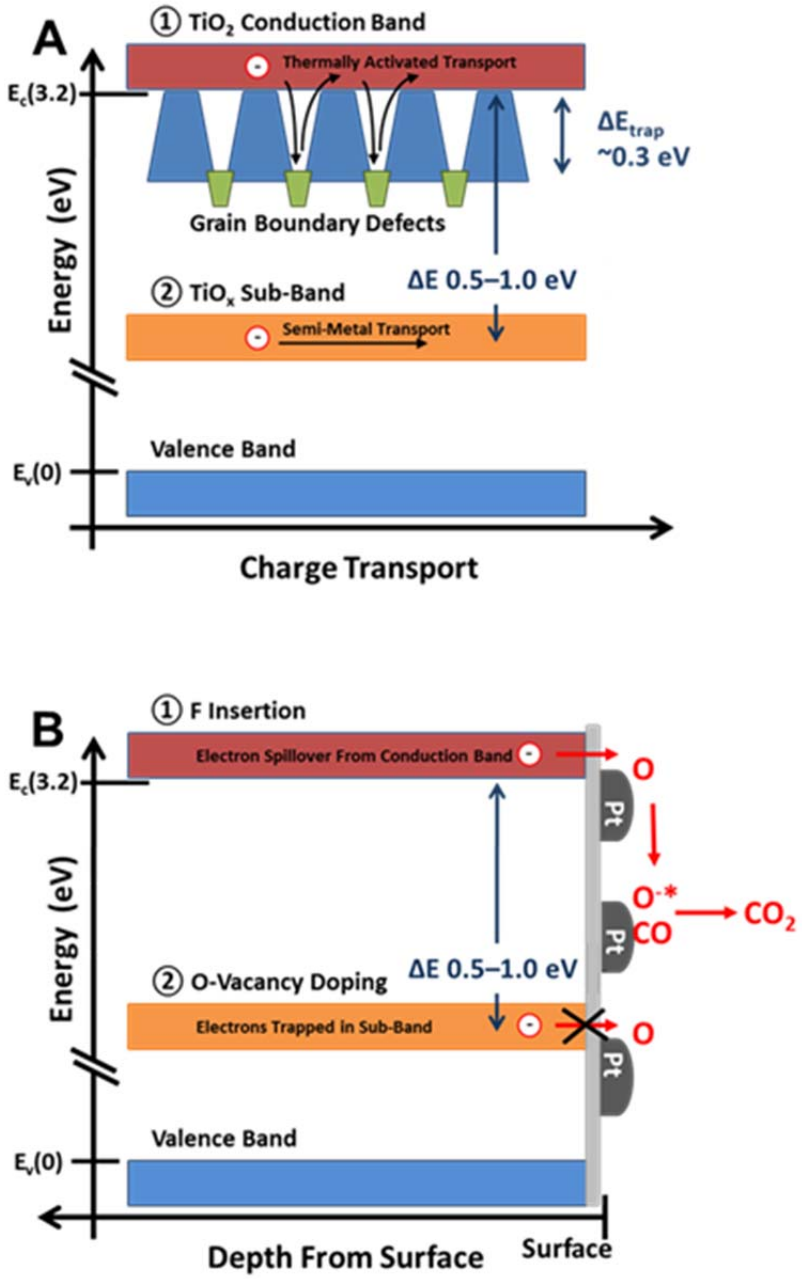

Figure 4 A – *Band diagram depicting two types of transport in titanium oxide. Sub-band defect states in the reduced oxide provide a semi-metal transport channel. In stoichiometric TiO_2, transport occurs in the actual conduction band. Due to grain boundary defects, conduction band transport is thermally activated as charges trap and de-trap at grain boundaries. Although semi-metal transport in the sub-band states is several orders higher than true conduction band transport, the carrier energy is 0.5–1.0 eV higher in the case of conduction band transport.*

***B** Schematic depicting why electronic activation is possible by F doping and not by O-vacancy doping. Although a high density of free charge carriers exist in the reduced oxide, these carriers reside in the sub-band located ~0.5–1.0 eV below the conduction band edge. At this low energy, the electrons cannot activate surface O for reaction with CO. However, in stoichiometric TiO_2, electrons reside in the true conduction band. Charge transfer from the conduction band results in electronic activation of surface O for CO_2 formation.*

XPS and reaction kinetics provide evidence that electronic activation by the F-doped support occurs by electron spillover to surface O. Fresh catalysts prepared and treated under reaction conditions for 1 h at 373, 473, or 573 K showed significant changes in the O 1s spectrum that correlate with deactivation of the undoped catalyst. Figure 5A shows the O 1s

XPS spectrum for the Pt/TiO_2 catalyst following reaction at various temperatures. The surface O peak at high binding energy (~532.5 eV) increased with reaction temperature. The XPS spectra for the F-doped analog of this catalyst (not shown here) were identical to those shown in figure 5A. Figure 5B shows how the formation of surface O affects the activity of the undoped catalyst. Initially we observe a TOF of ~25 min^{-1} at 443 K; however, following reaction at high temperature (543 K), the catalyst deactivated by a factor of four. The initial activity was restored by removing surface O in CO. Treatment in O_2 again resulted in catalyst deactivation by the formation of surface O.

Figure 5C shows time dependent reaction rate measurements for Pt on each TiO_X stoichiometry and on F-doped TiO_2. Each undoped catalyst showed between 20–36% deactivation during 1 h under reaction conditions. However, Pt supported on F-doped TiO_2 showed a 49% rate increase. We propose that these kinetics correspond to the formation of surface O during the reaction and the ability or inability of electrons from the oxide support to activate it for CO_2 formation. The high energy of the electrons in the F-doped stoichiometric support is responsible for enhancing the catalytic activity by electron spillover. However, this effect cannot occur with catalysts containing high concentrations of O vacancies. Although there is a high density of free carriers in these supports, they are trapped in the sub-oxide band structure and do not have enough energy to transfer to surface O.

We also investigated the stability of F in reaction conditions at 373, 473, and 573 K. XPS showed that F concentration decreased with increasing reaction temperature and was undetectable after 1 h at 573 K. Figure 6 shows the F to Ti atomic ratio for F-doped TiO_2 as fabricated and after 1 h in reaction conditions at each of the three treatment temperatures. Although the surface F concentration began to decreases even at 473 K, it was still present at significant levels. Consequently, we safely assume that F remained in the support throughout the duration of the reaction rate measurements shown above which took place at 443 K. Figure 7 shows the C1s, Ti2p and Pt4f spectra of the same samples.

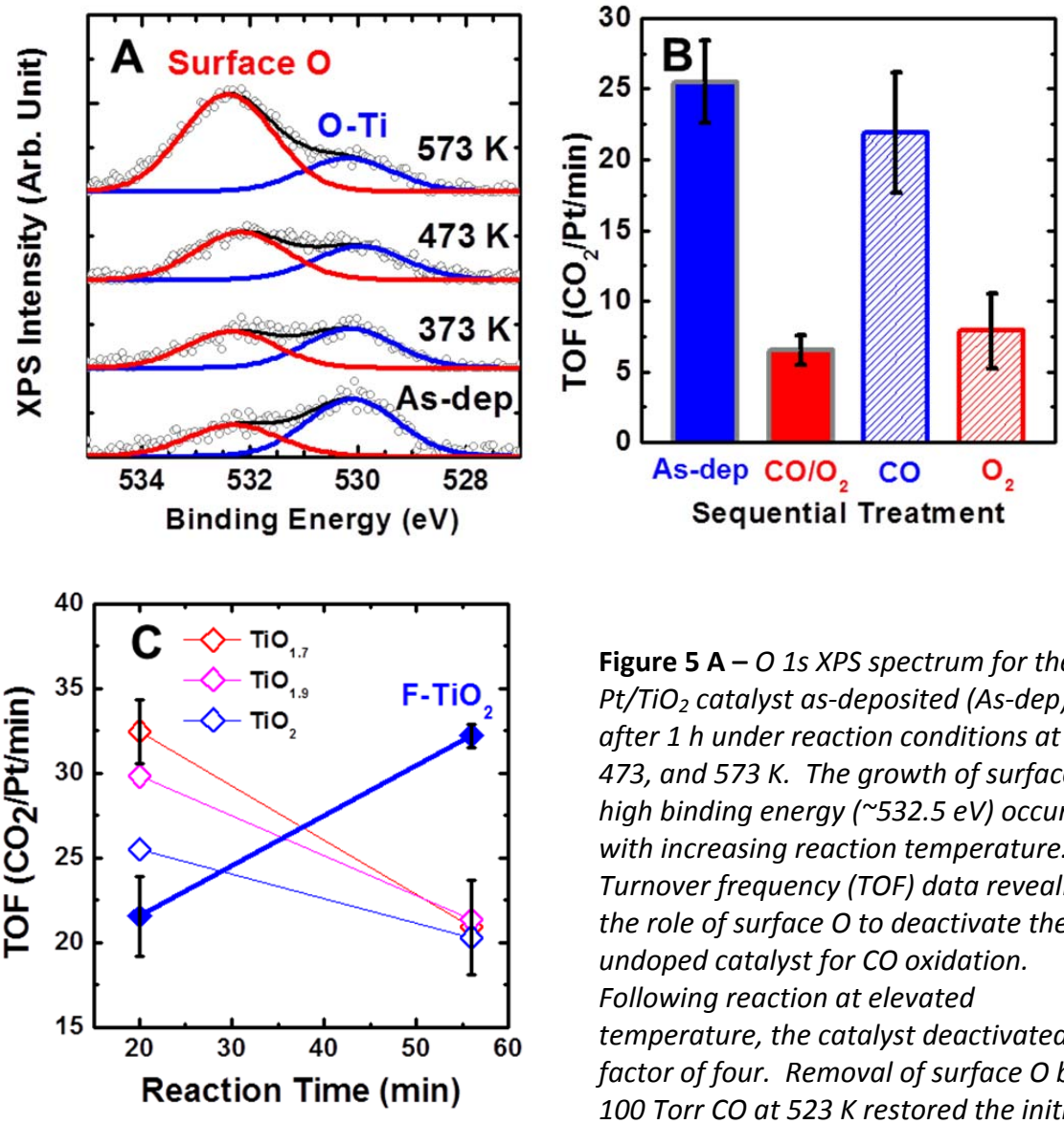

Figure 5 A – *O 1s XPS spectrum for the Pt/TiO_2 catalyst as-deposited (As-dep) and after 1 h under reaction conditions at 373, 473, and 573 K. The growth of surface O at high binding energy (~532.5 eV) occurs with increasing reaction temperature.* ***B*** *Turnover frequency (TOF) data revealing the role of surface O to deactivate the undoped catalyst for CO oxidation. Following reaction at elevated temperature, the catalyst deactivated by a factor of four. Removal of surface O by 100 Torr CO at 523 K restored the initial activity. Treatment in 100 Torr O_2 at 523 K again produced surface O resulting in deactivation.* ***C*** *Turnover frequency (TOF) data showing a change in catalyst activity at 443 K over 1 h. In all cases except for the Pt/TiO_2-F, the catalyst deactivated over this time. This is attributed to the build-up surface O. However, in the case of Pt supported on F-doped TiO_2, the activity increased by 49% during the reaction, indicating that the highly n-type support can electronically activate surface O as it forms for reaction with CO. Although not shown, F doping to the $TiO_{1.7}$ and $TiO_{1.9}$ catalysts did not result in a rate increase with time, suggesting the inability of electrons in the sub-oxide band to activate surface O.*

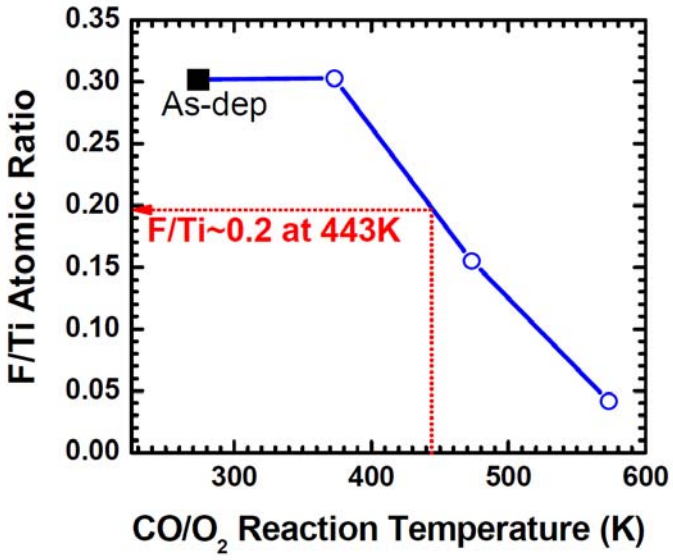

Figure 6 – *F to Ti atomic ratio in F-doped TiO_2 as-deposited (As-dep) and after 1 h in reaction conditions at 373, 473, and 573 K. The atomic ratio is based on the integrated intensity of the F 1s and the Ti 2p XPS spectra and corrected for sensitivity factors. The F concentration decreases at increasing temperature, but F is still present up to 473 K.*

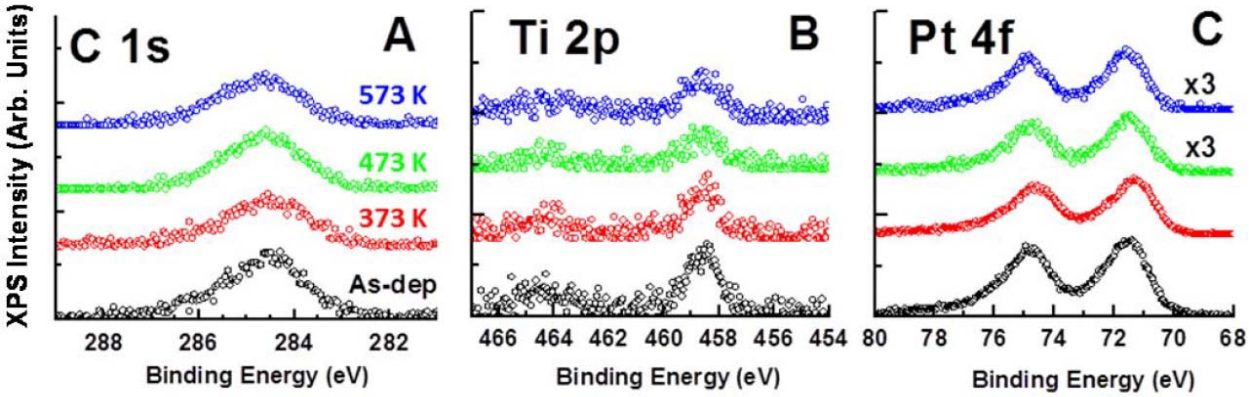

Figure 7 – *XPS spectra for C 1s (**A**), Ti 2p (**B**), and Pt 4f (**C**) states for the Pt/TiO_2 catalyst as-deposited (As-dep) and after 1 h in reaction conditions at 373, 473, and 573 K.*

Conclusion

We achieved approximately twofold increase in the reaction rate of CO oxidation on a Pt/TiO_2 catalyst when the TiO_2 is made n-type by F doping. A correlation of this effect with the

electronic structure of titanium oxide indicates that the mechanism responsible for increased catalytic activity is activation of surface O by electron spillover from the oxide support.

Noting that certain catalytic reactions proceed via charged intermediates, it seems intuitive that hot carriers can activate non-thermal reaction pathways by spillover to surface intermediates. Hot carriers are difficult to generate in a metal catalyst because of their fast relaxation times. However, n-type doping of oxide semiconductors is a feasible method for supplying charges of controlled energy to a catalytic interface. This unique utility of oxides also enlightens the widely studied strong metal-support interaction (SMSI), in which the properties of an oxide used to support metal clusters strongly influences the activity and selectivity of the catalyst system.

This result demonstrates that tuning the electronic structure of metal-oxide semiconductors used as catalyst supports can provide access to reaction pathways that on other catalysts would not be thermally accessible. This ability implicates applications in many other charge mediated processes, including energy conversion reactions, electrochemical processes, solid acid/base catalysis, and selective partial oxidation chemistry.

References

(1) Schwab, G.-M. *Trans. Faraday Soc.* **1946**, *42*, 689-697.
(2) Tauster, S. J.; Fung, S. C.; Garten, R. L. *J. Am. Chem. Soc.* **1978**, *100*, 170-175.
(3) Tauster, S. J.; Fung, S. C.; Baker, R. T. K.; Horsley, J. A. *Science* **1981**, *211*, 1121 -1125.
(4) Tauster, S. J. *Acc. Chem. Res.* **1987**, *20*, 389-394.
(5) Somorjai, G. A.; Li, Y. *Introduction to Surface Chemistry and Catalysis*; John Wiley and Sons, 2010.
(6) Boffa, A.; Lin, C.; Bell, A. T.; Somorjai, G. A. *Journal of Catalysis* **1994**, *149*, 149-158.
(7) Vannice, M. A.; Sen, B. *Journal of Catalysis* **1989**, *115*, 65-78.
(8) Lin, S. D.; Sanders, D. K.; Albert Vannice, M. *Applied Catalysis A: General* **1994**, *113*, 59-73.
(9) Malathi, R.; Viswanath, R. P. *Applied Catalysis A: General* **2001**, *208*, 323-327.
(10) Oh, S. H.; Eickel, C. C. *Journal of Catalysis* **1988**, *112*, 543-555.
(11) Zhu, H.; Qin, Z.; Shan, W.; Shen, W.; Wang, J. *Journal of Catalysis* **2004**, *225*, 267-277.
(12) Chen, M. S.; Goodman, D. W. *Science* **2004**, *306*, 252 -255.
(13) Goodman, D. W. *Catalysis Letters* **2005**, *99*, 1-4.
(14) Enache, D. I.; Edwards, J. K.; Landon, P.; Solsona-Espriu, B.; Carley, A. F.; Herzing, A. A.; Watanabe, M.; Kiely, C. J.; Knight, D. W.; Hutchings, G. J. *Science* **2006**, *311*, 362 -365.
(15) Landon, P.; Collier, P. J.; Papworth, A. J.; Kiely, C. J.; Hutchings, G. J. *Chem. Commun.* **2002**, 2058-2059.
(16) Landon, P.; Collier, P. J.; Carley, A. F.; Chadwick, D.; Papworth, A. J.; Burrows, A.; Kiely, C. J.; Hutchings, G. J. *Phys. Chem. Chem. Phys.* **2003**, *5*, 1917-1923.
(17) Fu, Q.; Saltsburg, H.; Flytzani-Stephanopoulos, M. *Science* **2003**, *301*, 935 -938.
(18) Edwards, J. K.; Solsona, B. E.; Landon, P.; Carley, A. F.; Herzing, A.; Kiely, C. J.; Hutchings, G. J. *Journal of Catalysis* **2005**, *236*, 69-79.
(19) Fan, S.; Yi, J.; Wang, L.; Mi, Z. *Reaction Kinetics and Catalysis Letters* **2007**, *92*, 175-182.

(20) Vernon, P.; Green, M.; Cheetham, A.; Ashcroft, A. *CATALYSIS LETTERS* **1990**, *6*, 181-186.
(21) Ashcroft, A. T.; Cheetham, A. K.; Green, M. L. H.; Vernon, P. D. F. *Nature* **1991**, *352*, 225-226.
(22) Nakagawa, K.; Ikenaga, N.; Suzuki, T.; Kobayashi, T.; Haruta, M. *Applied Catalysis A: General* **1998**, *169*, 281-290.
(23) Haruta, M. *CATTECH* **2002**, *6*, 102-115.
(24) Pietron, J. J.; Stroud, R. M.; Rolison, D. R. *Nano Lett.* **2002**, *2*, 545-549.
(25) Molina, L. M.; Rasmussen, M. D.; Hammer, B. *The Journal of Chemical Physics* **2004**, *120*, 7673.
(26) Akubuiro, E. C.; Verykios, X. E. *Journal of Catalysis* **1988**, *113*, 106-119.
(27) Bonn, M.; Funk, S.; Hess, C.; Denzler, D. N.; Stampfl, C.; Scheffler, M.; Wolf, M.; Ertl, G. *Science* **1999**, *285*, 1042 -1045.
(28) Lambert, R. M.; Cropley, R. L.; Husain, A.; Tikhov, M. S. *Chem. Commun.* **2003**, 1184-1185.
(29) Zhang, Y.; Kolmakov, A.; Chretien, S.; Metiu, H.; Moskovits, M. *Nano Lett.* **2004**, *4*, 403-407.
(30) Zhang, J.; Liu, X.; Blume, R.; Zhang, A.; Schlögl, R.; Su, D. S. *Science* **2008**, *322*, 73 -77.
(31) Kaden, W. E.; Wu, T.; Kunkel, W. A.; Anderson, S. L. *Science* **2009**, *326*, 826 -829.
(32) Zhang, Z.; Yates, J. T. *J. Am. Chem. Soc.* **2010**, *132*, 12804-12807.
(33) Park, J. Y.; Somorjai, G. A. *ChemPhysChem* **2006**, *7*, 1409-1413.
(34) Cox, P. A. *Transition metal oxides : an introduction to their electronic structure and properties*; Clarendon Press ; Oxford University Press: Oxford New York, 1992.
(35) Seo, H.; Baker, L. R.; Hervier, A.; Kim, J.; Whitten, J. L.; Somorjai, G. A. *Nano Lett.* **2011**, *11*, 751-756.

Chapter 10

Titanium Oxide/Platinum Catalysis: Charge Transfer from Titanium Oxide Support Controls Activity and Selectivity in Methanol Oxidation on Platinum

Platinum films of thickness 1 nm were deposited by electron beam evaporation onto 100-nm-thick titanium oxide films (TiO_x) with variable oxygen vacancy concentrations and fluorine (F) doping. Methanol oxidation on the platinum films produced formaldehyde, methyl formate, and carbon dioxide. F-doped samples demonstrated significantly higher activity for methanol oxidation when the TiO_x was stoichiometric (TiO_2), but lower activity when it was non-stoichiometric ($TiO_{1.7}$ and $TiO_{1.9}$). These results correlate with the chemical behavior of the same types of catalysts in CO oxidation. Fluorine doping of stoichiometric TiO_2 also increased selectivity toward partial oxidation of methanol to formaldehyde and methyl formate, but had an opposite effect in the case of non-stoichiometric TiO_x. Introduction of oxygen vacancies and fluorine doping both increased the conductivity of the TiO_x film. For oxygen vacancies, this occurred by the formation of a conduction channel in the bandgap, whereas in the case of fluorine doping, F acted as an n-type donor, forming a conduction channel at the bottom of the conduction band, about 0.5-1.0 eV higher in energy. The higher energy electrons in F-doped stoichiometric TiO_x led to higher turnover rates and increased selectivity toward partial oxidation of methanol. This correlation between electronic structure and turnover rate and selectivity indicates that the ability of the support to transfer charges to surface species controls in part the activity and selectivity of the reaction.

Introduction

Heterogeneous catalysts often consist of metal nanoparticles dispersed over an oxide support. While the oxide is usually inert by itself, it may affect the catalyst's behavior in significant ways, a phenomenon known as strong metal support interaction.[1,2] This phenomenon is in part attributed to charge transfer involving the oxide support.[3] For example, it has been observed that partially covering Rh foil with an oxide enhanced the reaction rates for hydrogenation of CO and CO_2,[4] despite the fact that the oxide was not active by itself and blocked the active Rh sites. The enhancement factor was found to correlate with the Lewis acidities of the oxides used, i.e., their ability to accept a charge. These results suggest that modifying the conditions for charge transfer from the oxide support may yield significant changes in catalytic behavior.

In the present study, methanol oxidation was carried out over Pt/TiO_2 catalysts for which the oxide was modified by introducing oxygen vacancies and fluorine dopant. It is reported that

fluorine doping of stoichiometric TiO_2 allows the oxide to transfer an electron to an adsorbate. This activates one or multiple steps in the reaction, leading to a significant increase both in turnover frequency and selectivity toward the partial oxidation products, formaldehyde and methyl formate. The present study is the first to correlate a change in selectivity due to doping of the oxide support with the charge transfer properties of the oxide. Results indicate that reaction selectivity is controlled, to a significant extent, by charge transfer from the oxide.

The aforementioned results are consistent with a previous study of CO oxidation on Pt/TiO_x catalysts.[5] In that study, TiO_x films were annealed under different conditions to obtain various stoichiometries, i.e., $TiO_{1.7}$, $TiO_{1.9}$, and TiO_2, as determined by X-Ray photoelectron spectroscopy (XPS). Introducing oxygen vacancies into TiO_2 leads to the formation of electronic states in the bandgap about 0.5-1.0 eV below the bottom of the conduction band.[6,7] These midgap states act as a conduction channel, and the conductivity of the film increases by orders of magnitude.[8,9]

One titanium oxide film of each sample was also doped in SF_6 plasma, yielding six types of oxide support: $TiO_{1.7}$, $TiO_{1.9}$, and TiO_2, both doped and undoped. Fluorine was found to bind to Ti by filling oxygen vacancies, slightly offsetting the increased conductivity.[9] However, F also acts as an n-type donor, forming donor levels just below the conduction band. For TiO_2, this increases conductivity by forty-fold (figure 1B). In the presence of oxygen vacancies, the vacant midgap states 0.5-1.0 eV below the bottom of the conduction band capture any donor electrons, and F doping slightly decreases the conductivity of the $TiO_{1.7}$ and $TiO_{1.9}$ films.[9]

While both oxygen vacancies and fluorine doping can increase the film conductivity, the resulting conduction channels are about 1.0 eV apart in energy. This difference correlates with the surface chemistry of the Pt/TiO_x catalysts. Although the turnover frequency (TOF) increases by nearly two-fold when stoichiometric TiO_2 is F-doped, no such increase is observed with the non-stoichiometric $TiO_{1.7}$ and $TiO_{1.9}$ films (figure 1A).

Kinetic measurements of this particular system indicated that O poisons the reaction in this range of temperature and pressure. As a result, the increase in turnover may be attributed to electron transfer from the oxide to surface O, activating it for reaction with CO. Non-stoichiometric TiO_x does not show this effect because the conduction channel formed by midgap states is much lower in energy. Electrons in those states have insufficient energy to transfer to surface O.

The above information suggests that the turnover rates of a catalyst can be tuned by modifying the electronic structure of the support. An important contribution of the present investigation is the proof that the same method can be used to tune selectivity, a metric of great importance in industrial catalysis. Methanol oxidation (Scheme 1) was chosen for this purpose because it is relatively simple (only three different products are produced under the conditions of this study) and turnover can easily be measured at 333 K. At this temperature, the fluorine concentration in the TiO_2 lattice is stable.[5] The reaction begins with the adsorption of methanol that leads to the formation of methoxy, which then dehydrogenates to form formaldehyde that can either bind with O to form CO_2, or with methoxy to form methyl

formate.[10] Methyl formate conversion to CO_2 was not observed at 333 K. This reaction is of major industrial relevance, because it is the primary method of producing formaldehyde,[11] also forming the basis of operation of the direct methanol fuel cell.[12] In the former, methanol must only be partially oxidized, whereas in the latter, the energy efficiency is maximized if the oxidation is carried out to form only CO_2; hence the need for selectivity control.

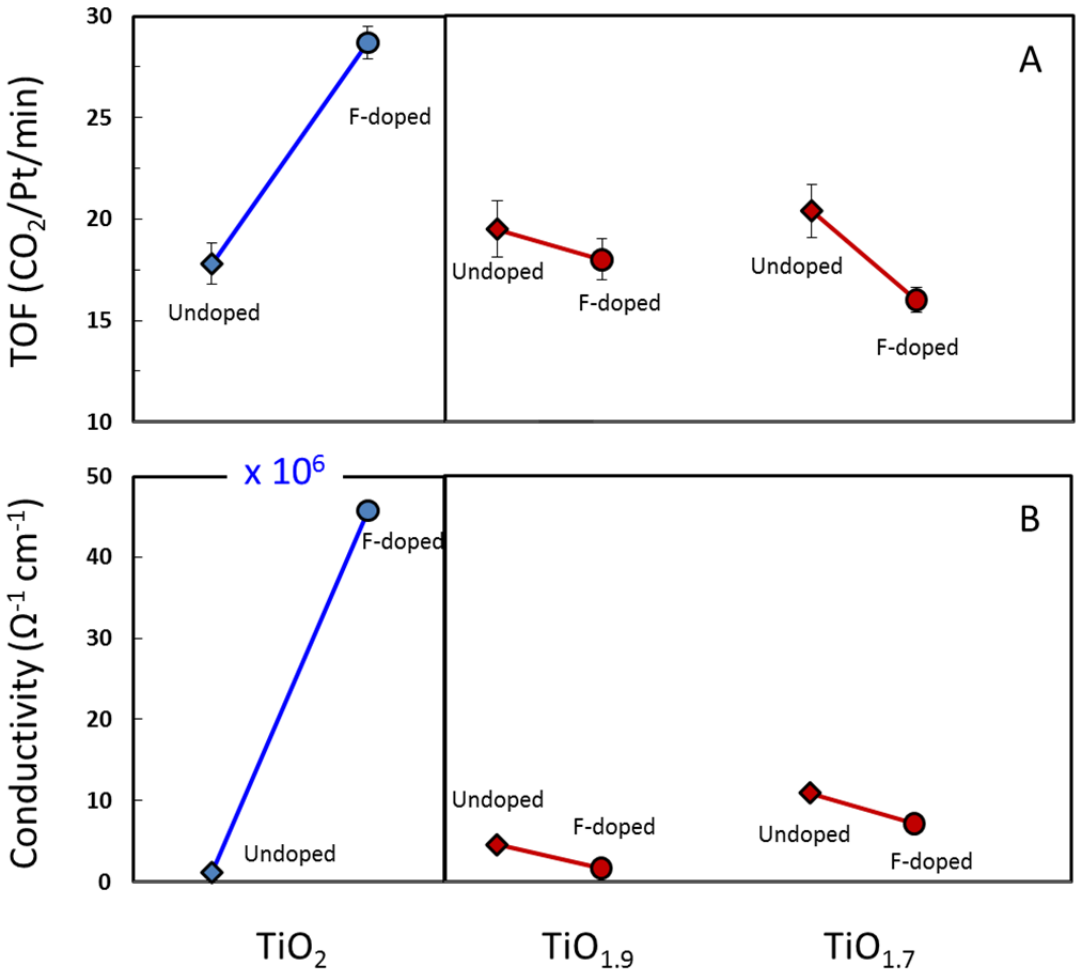

Figure 1 – *(A)* *Turnover frequencies (TOF) for Pt/TiO_x catalysts identical to those of the present study reported for CO oxidation.[5] Fluorine doping only shows a significant effect for stoichiometric TiO_2. Reaction occurred at 443 K under conditions of 40 Torr CO, 100 Torr O_2, and 620 Torr He. TOF data represent stable rates obtained after 30 min in reaction conditions, when deactivation had stopped.* ***(B)*** *Surface conductivity measurements for the same set of TiO_x supports prior to Pt deposition.[5] The numbers for TiO_2 and F-doped TiO_2 have been magnified by a factor of 10^6 for clarity.*

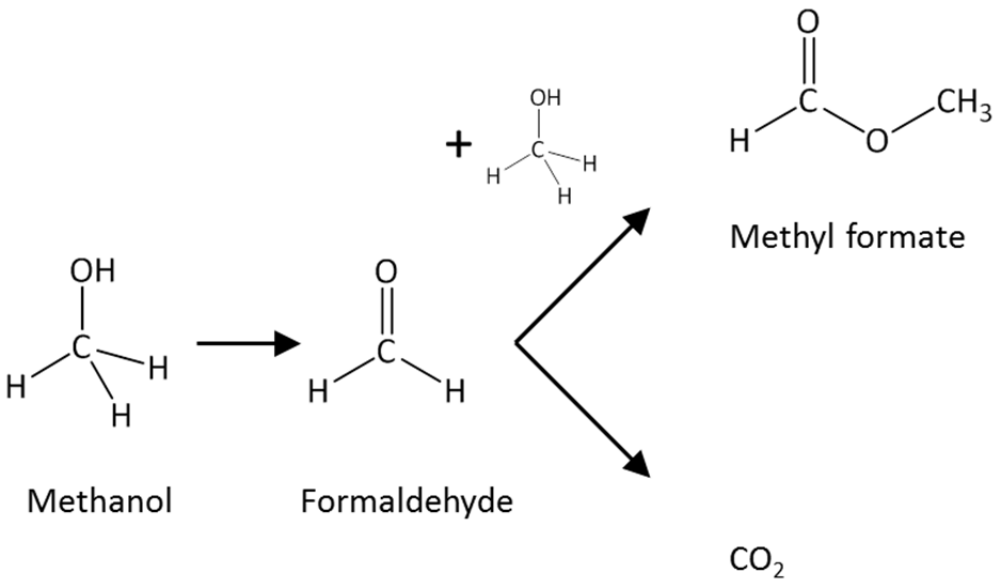

Scheme 1

Experimental Procedures

Catalyst Preparation

Thin films of TiO_x with variable O vacancy concentrations were used as supports of the Pt catalyst. These films were deposited on Si(100) wafers by direct current (DC) magnetron sputtering under conditions of 400 W plasma power, 450 V bias voltage, and Ar and O_2 gas flow rates of 50 and 3 sccm, respectively.

The Si(100) wafers had a 500-nm-thick thermally grown SiO_2 film, while the thickness of the TiO_2 films was equal to 100 nm. As-deposited titanium oxide films were highly O deficient. The O concentration in the films was controlled by rapid thermal annealing in O_2 at temperatures between 623 and 773 K. To avoid variations in grain size due to the different annealing temperatures, all samples were first annealed in N_2 at 773 K. TiO_x films of three different stoichiometries were prepared for this study, i.e., TiO_2, $TiO_{1.9}$, and $TiO_{1.7}$. These stoichiometries were determined from the ratio of Ti^{3+} and Ti^{4+} in the Ti 2p XPS spectra.[9]

Fluorine doping was accomplished by plasma treatment in N_2 gas and trace amounts of sulfur hexafluoride (SF_6), introduced into the chamber by flowing a 9:1 mixture of SF_6 and O_2, followed by pumping to a chamber base pressure of 5 mTorr. A low background pressure of SF_6 remained in the chamber after pumping. N_2 gas was then introduced at a flow rate of 80 sccm for plasma treatment under conditions of 20 W power and 130 V DC substrate bias. XPS analysis of the F-doped samples did not reveal any S traces.[9] One of the two samples of each TiO_X stoichiometry was plasma treated, resulting in six supports for subsequent Pt deposition, i.e., TiO_2, $TiO_{1.9}$, and $TiO_{1.7}$, each with and without F doping. All substrates were stored in dry N_2 between the time of fabrication and the reaction rate measurements.

Pt nanoparticles were deposited onto TiO_x/Si(100) substrates by electron-beam evaporation. This deposition method was selected instead of colloidal synthesis to avoid the presence of an insulating polymer capping agent between the Pt nanoparticles and the oxide support. During electron beam evaporation, the chamber base pressure was less than 10^{-5} Torr. The average Pt film thickness, monitored by a quartz crystal microbalance, was equal to about 1 nm.

Reaction Rate Measurements

Reaction rates of methanol oxidation on each of the six catalysts described above were measured with a batch mode reactor equipped with a boron nitride substrate heater and a metal bellows circulation pump for gas mixing. In reaction, gas pressures were set at 10 Torr CH_3OH and 50 Torr O_2 in He background, while the temperature was fixed at 333 K. All of the samples showed significant deactivation (up to two orders of magnitude) in the first 60 min of reaction, thereafter producing stable rates for several hours. Rates reported here refer to the steady-state rates obtained after initial deactivation.

Turnover rates were measured by a gas chromatograph (GC) with a thermal conductivity detector. Selectivities were estimated after calibrating the detector's response by injecting known amounts of CO_2 and methyl formate. Because it was difficult to obtain formaldehyde in pure form, the same calibration could not be performed. Therefore, the thermal conductivity of formaldehyde was assumed to be the same as that of methyl formate.

Formaldehyde and methyl formate are treated together and referred to as partial oxidation products. For some samples, the production rate of formaldehyde was less than its consumption rate, leading to a negative turnover number. That rate was counted as contributing negatively to selectivity for partial oxidation. Selectivities reported here should not be compared directly to other results in the literature, and are only used for relative comparisons between samples of this study.

Reaction rates are presented in the form of turnover frequencies (i.e., number of CO_2 molecules per Pt site per minute). Error bars represent a 95% confidence interval based on the rate of production normalized by the estimated number of Pt sites. Assuming a Pt(111) surface of uniform structure, the number of Pt sites was determined as the number of Pt atoms over the catalyst area. Although this is an approximate calculation, it provides consistent normalization to catalyst area and a reasonable estimate of the absolute turnover rate.

Results and Discussion

Methanol oxidation was carried out on Pt/TiO_x catalysts that differed only in the preparation of the oxide support. As mentioned earlier, the oxide support was modified by oxygen vacancy doping and fluorine doping. Figure 2 shows the effect of these treatments on the turnover frequencies of the three products, CO_2, formaldehyde, and methyl formate. The graph shows the difference between turnover frequencies of F-doped and undoped samples, □(TOF). In the case of stoichiometric TiO_2, fluorine doping increased activity – TOF increased by 71% for CO_2, two-fold for formaldehyde, and four-fold methyl formate. An opposite trend was

observed for non-stoichiometric TiO_2, i.e., $TiO_{1.9}$ and $TiO_{1.7}$. Variation in oxygen vacancy concentration also exhibited a significant effect on activity, although a clear trend cannot be established.

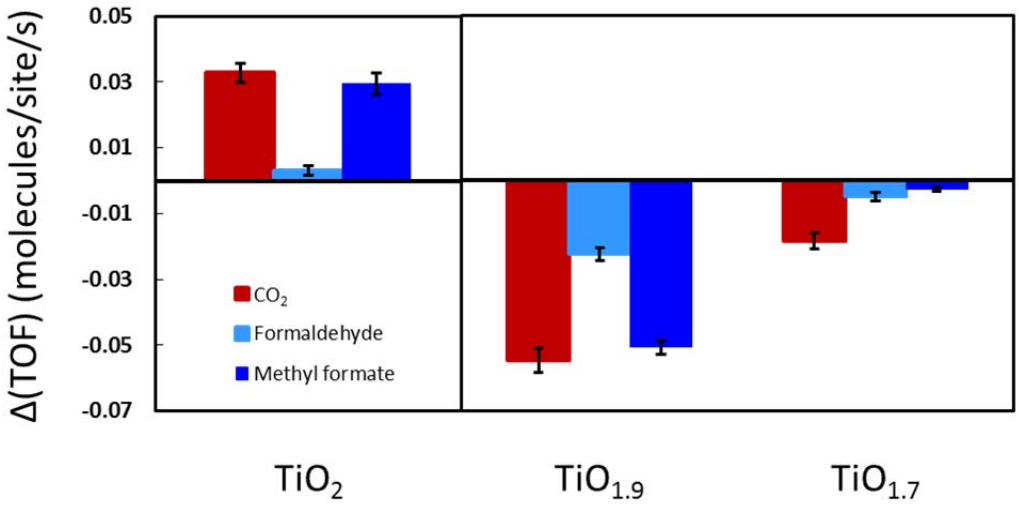

Figure 2 – *Change in turnover frequency Δ(TOF) of CO_2, formaldehyde, and methyl formate products of methanol oxidation over Pt catalysts on six different TiO_x supports: $TiO_{1.7}$, $TiO_{1.9}$, and TiO_2, both doped and undoped. Δ(TOF) denotes the difference in turnover frequency between F-doped and undoped TiO_x supports. Error bars represent 95% confidence intervals. Measurements were obtained at 333 K under reaction conditions of 10 Torr CH_3OH, 50 Torr O_2, and 720 Torr He.*

A similar fluorine effect was observed when measuring the selectivity of the reaction. Figure 3 shows the percentage of partial oxidation products (combining formaldehyde and methyl formate) obtained in reaction, as opposed to the total oxidation product, CO_2. For stoichiometric TiO_2, fluorine doping increased the selectivity toward partial oxidation from 17 to 35%, whereas for non-stoichiometric TiO_2, selectivity toward partial oxidation decreased as a result of fluorine doping.

The effects of fluorine doping observed here are consistent with a previous study dealing with CO oxidation.[5] In that study, the same catalysts produced turnover frequencies for CO oxidation that correlated strongly with the conductivities of the TiO_x films prior to Pt deposition (figure 1). Selectivities and turnover frequencies reported here for methanol oxidation also correlate with conductivity measurements (figure 1B), suggesting that the same phenomenon governs the effect of fluorine in both reactions.

Differences in activities observed in this study can be explained by considering the charge transfer mechanism in non-stoichiometric and F-doped stoichiometric TiO_2, shown schematically in figure 4. TiO_2 has a bandgap of 3.2 eV, and the density of electronic states in the bandgap, by definition, is very low for stoichiometric TiO_2. Oxygen vacancies introduced into the lattice give rise to energy levels in the bandgap (midgap states) between 0.5 and 1.0 eV

below the bottom of the conduction band,[6] increasing dramatically the conductivity of the material (figure 1B). Fluorine binding to Ti at O vacancy sites partially passivates these midgap states, resulting in lower conductivity.[9] However, in the case of stoichiometric TiO_2, where there are no midgap states, fluorine acts as an n-type dopant, creating donor states just below the conduction band. This increases conductivity by a factor of 40 (figure 1B).

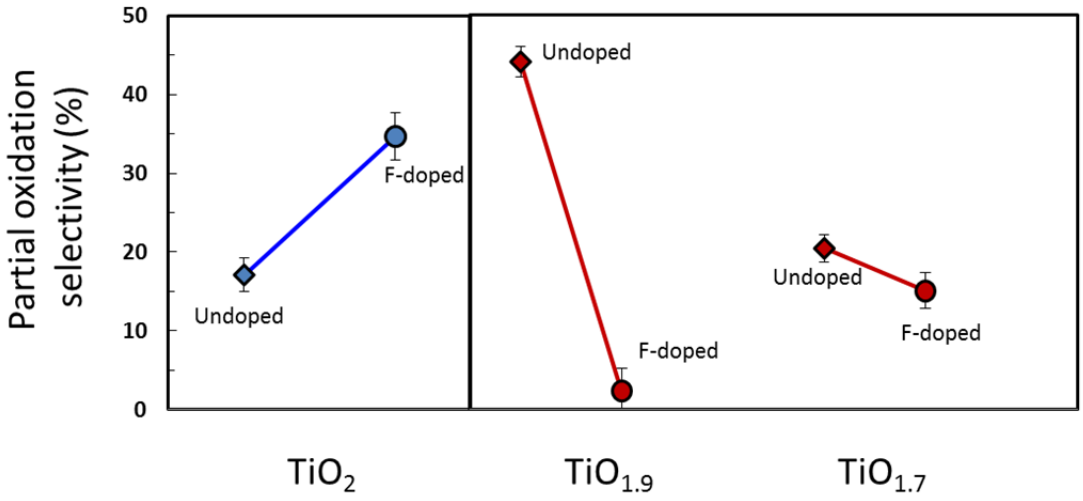

Figure 3 – *Selectivity toward partial methanol oxidation of F-doped and undoped Pt/TiO_x catalysts. Partial oxidation products refer to formaldehyde and methyl formate, as opposed to total oxidation that produces CO_2.*

Both oxygen vacancy doping and fluorine doping produce a population of surface electrons available for conduction. These electrons may also transfer to nearby adsorbate orbitals, provided they are close in energy. For CO oxidation, this charge transfer occurs in F-doped stoichiometric TiO_2 from the oxide to surface O, which activates the O to react with CO, leading to increased turnover rate.[5] For oxygen-vacancy doped TiO_2, midgap electrons produced from oxygen doping are lower in energy by 0.5-1.0 eV. Because these electrons cannot transfer to surface O, an increase in turnover is not observed. The effect of fluorine is observed under steady-state conditions, excluding the possibility of charge accumulation. Therefore, the charged intermediate must return its additional electron to the oxide support before desorbing as a CO_2 molecule. Such a scheme of CO oxidation on platinum has been described in a previous theoretical study.[13] In the last step of the reaction, a charged CO_2^- intermediate simultaneously undergoes desorption and loss of an electron to yield CO_2.

In the case of methanol oxidation, it is likely that the same activation of a surface species is responsible for the increased turnover and the shift in selectivity toward formaldehyde and methyl formate. Further experiments must be carried out to identify which species on the surface is activated by the support.

A sharp decrease in turnover rate (up to two orders of magnitude) was observed after approximately 60 min in reaction with each sample, regardless of oxidation state or doping, due to CO poisoning of the Pt layer. Initial rates obtained before the deactivation did not show a

dependence on the TiO_2 substrate, and the turnover frequencies reported here refer to the steady-state rates obtained after initial deactivation.

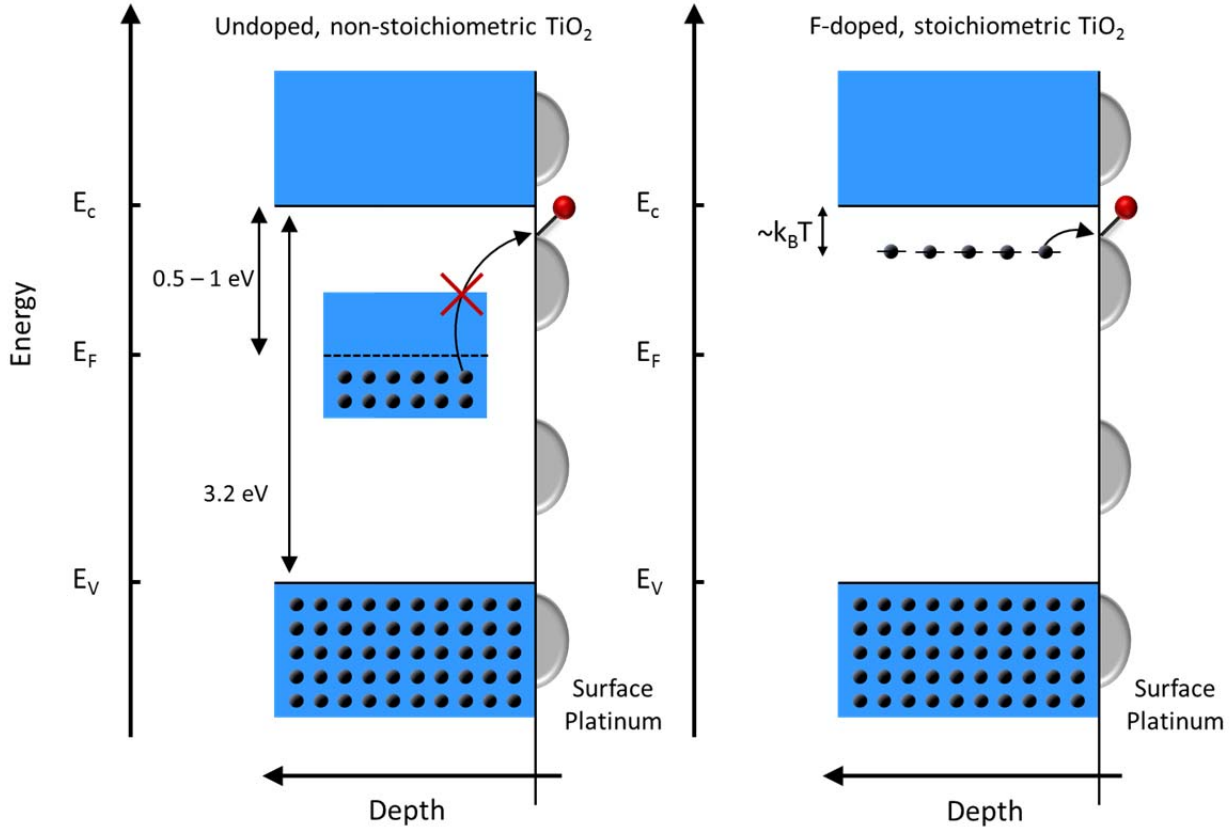

Figure 4 – *Schematic of charge transfer mechanism in non-stoichiometric TiO_x and F-doped stoichiometric TiO_2. In the presence of midgap states, electron transfer from the oxide to an adsorbate species involves an electron with energy between 0.5 and 1.0 eV below the bottom of the conduction band. In the case of F-doped TiO_2, donor electrons occupy states at the bottom of the conduction band that were previously not thermally accessible. These higher energy electrons may transfer to an adsorbate species, resulting in higher turnover frequency and enhanced selectivity toward partial oxidation. (E_c, E_F, and E_v denote conduction, Fermi, and valence energy levels, respectively.)*

Deactivation was found to be reversible. When the sample was cooled down to room temperature, the gases pumped out, and the reaction restarted, original rates were restored, and the same deactivation occurred after about 60 min, without any significant change in turnover rates. CO produced from methanol oxidation is known to poison Pt.[14] When 0.5 Torr of CO was added to the reaction mixture, turnover rates at 333 K decreased below the detection limit. After the surface was cooled down to room temperature, the reactor evacuated, and a new reaction was initiated on the same sample without any CO, the turnover rate was restored to its previous value. This suggests that, although CO was not produced in amounts detectable by GC, it resulted in Pt poisoning. The reversibility of poisoning indicates

that, even at room temperature, a monolayer of CO is easily removed when the reaction is stopped, in agreement with earlier observations.[15]

Conclusion

Methanol oxidation over Pt/TiO_x catalysts showed that fluorine doping of stoichiometric TiO_2 increases the selectivity toward the formation of formaldehyde and methyl formate from 17 to 35%. The activities and selectivities of the fabricated Pt/TiO_x samples closely followed the conductivities of F-doped TiO_x films, similar to CO oxidation. This effect is likely due to an increased electron population in the conduction band of the oxide, allowing for charge transfer that activated a surface species. The present study is the first to show that the electronic structure of the oxide support can be tuned to control the oxidation pathways on catalyst surfaces.

References

(1) Schwab, G.-M. *Discussions of the Faraday Society* **1950**, *8*, 166.
(2) Tauster, S. J.; Fung, S. C.; Garten, R. L. *J. Am. Chem. Soc.* **1978**, *100*, 170-175.
(3) Jochum, W.; Eder, D.; Kaltenhauser, G.; Kramer, R. *Topics in Catalysis* **2007**, *46*, 49-55.
(4) Boffa, A. B.; Lin, C.; Bell, A. T.; Somorjai, G. A. *Catalysis Letters* **1994**, *27*, 243-249.
(5) Baker, L. R.; Hervier, A.; Seo, H.; Kennedy, G.; Komvopoulos, K.; Somorjai, G. A. *J. Phys. Chem. C* **2011**, *115*, 16006-16011.
(6) Cronemeyer, D. C. *Phys. Rev.* **1959**, *113*, 1222.
(7) Asahi, R.; Morikawa, T.; Ohwaki, T.; Aoki, K.; Taga, Y. *Science* **2001**, *293*, 269-271.
(8) Bilmes, S. A.; Mandelbaum, P.; Alvarez, F.; Victoria, N. M. *J. Phys. Chem. B* **2011**, *104*, 9851-9858.
(9) Seo, H.; Baker, L. R.; Hervier, A.; Kim, J.; Whitten, J. L.; Somorjai, G. A. *Nano Lett.* **2011**, *11*, 751-756.
(10) Outka, D. A.; Madix, R. J. *J. Am. Chem. Soc.* **2011**, *109*, 1708-1714.
(11) Weissermel, K.; Arpe, H.-J. *Industrial organic chemistry*; Wiley-VCH, 2003.
(12) Surampudi, S.; Narayanan, S. R.; Vamos, E.; Frank, H.; Halpert, G.; LaConti, A.; Kosek, J.; Prakash, G. K. S.; Olah, G. A. *Journal of Power Sources* **1994**, *47*, 377-385.
(13) Maximoff, S. N.; Head-Gordon, M. P. *Proceedings of the National Academy of Sciences* **2009**, *106*, 11460 -11465.
(14) Beden, B.; Hahn, F.; Leger, J.-M.; Lamy, C.; Lopes, M. I. dos S. *Journal of Electroanalytical Chemistry and Interfacial Electrochemistry* **1989**, *258*, 463-467.
(15) Zhang, C.; He, H. *Catalysis Today* **2007**, *126*, 345-350.

Chapter 11

In situ Spectroscopic Study of CO Oxidation on F-doped TiO_2 Supported Pt catalysts

Ambient Pressure X-Ray Photoelectron Spectroscopy was used to characterize the state of surface oxygen on Pt/TiO_2 catalysts in CO oxidation conditions, up to pressures of 140 mTorr of O_2 and 50 mTorr CO, between 333 and 573 K. Specifically, the effect of O vacancy doping and F doping of the TiO_2 support was investigated. In a previous study, F-doping was shown to increase turnover for CO oxidation in stoichiometric TiO_2, but to decrease it in non-stoichiometric TiO_2. The O1s spectra shown here are taken in reaction conditions, and show two main peaks. The intensity of the lower binding energy peak varies little relative to the signal from Pt. The intensity of the higher binding energy peak decreases with F-doping in stoichiometric TiO_2, but increases with F-doping in non-stoichiometric TiO_2. The intensity of this peak is therefore inversely correlated with the reactivity of the Pt/TiO_2 catalysts.

Introduction

One of the main challenges of studying catalysis is the so-called pressure gap.[1] Many of the classic techniques used for studying surfaces, such as X-Ray Photoelectron Spectroscopy (XPS), Auger electron spectroscopy (AES) or Low Energy Electron Diffraction (LEED), operate at pressures in the range of 10^{-9} Torr, while most industrial catalysis is done well above atmospheric pressure. This has led to the development of surface characterization techniques that can operate at much higher pressures.[2–7] These techniques rely on differential pumping: the catalyst is placed in a chamber at high pressure, as close as possible to an aperture which leads to a separate chamber, where the vacuum is low enough for electrons to ballistically reach the detector. Even with this design, the pressure around the catalyst is limited to about 1 Torr, since the corresponding electron mean free path is on the order of 1 mm.[3] This nonetheless bridges 9 out of the 12 or 13 orders of magnitude between UHV and working conditions.

There have already been studies showing that some spectroscopic features are only visible in reaction conditions, and can disappear simply by removing the gas mixture.[8,9] Thus even a setup where spectroscopic measurements can be carried out before and after a reaction, without exposing the sample to ambient conditions, will miss key elements of the spectrum. In one study in particular, two different oxygen containing species were identified on a silver catalyst under ethylene epoxidation.[9] One is nucleophilic and presents when the catalyst is inactive, while the other is more nucleophilic, and correlated with the formation of ethylene oxide.

The Ambient Pressure XPS (AP-XPS) setup at the Advanced Light Source beamline 9.3.2 combines differentially pumped chambers with a synchrotron X-Ray source, providing intense and tunable light for probing surfaces.[6,10] This facility was used to examine the nature of the oxygen species present on the surface of Pt/TiO_2 catalysts under CO oxidation conditions, and in particular the effect of doping the oxide with oxygen vacancies and F atoms.

As shown in the previous chapters, F doping of stoichiometric TiO_2 creates new, electronically activated pathways for catalytic reactions, namely CO oxidation and methanol oxidation.[11–13] In the case of CO oxidation, kinetic and conventional XPS measurements have provided evidence that oxygen activation is the limiting step of the reaction, and that the modified electronic structure of F-doped stoichiometric TiO_2 allows high energy electrons present in the oxide to transfer to an adsorbed oxygen species, activating it for reaction with CO.

We show here spectra taken in AP-XPS of the surface of Pt/TiO_2 in CO oxidation conditions similar to those used in our previous studies. These spectra indicate the presence of a surface oxygen species with high binding energy, whose abundance on the surface correlates strongly with activity observed previously. The complexity of the O1s spectrum did not allow us to reach a conclusion as to the nature of this species.

Experimental section

- Sample preparation

Thin films of TiO_x with variable O vacancy concentrations were used as supports for the Pt catalyst. These films were deposited by direct current (DC) magnetron sputtering under 300 W plasma power, an Ar flow rate of 20 sccm, and no substrate heating other than from the plasma. The substrates used were 0.2 mm thick strips of gold and Si(100) wafers with a 500 nm layer of thermal oxide. The silicon wafer substrates were used for conductivity measurements, while the gold substrates were used for the AP-XPS measurements. The TiO_x film thickness is in excess of 100 nm.

The films were then subjected to rapid thermal annealing at 773 K, under a flow of N_2 or O_2, to obtain non-stoichiometric or stoichiometric oxides, respectively, and to improve their crystallinity. The base pressure of the deposition chamber was 10^{-5} Torr, two orders of magnitude higher than the 10^{-7} Torr in the chamber used in our previous studies.[11–13] This higher base pressure was enough to produce highly oxidized films. As a result, no Ti^{3+} peak was detected by conventional XPS spectra of the films, whether N_2 or O_2 annealed, or even before annealing.

The difference in gas environment during the annealing procedure did produce markedly different films, however, such that the N_2 and O_2 annealed can be referred to as non-stoichiometric and stoichiometric, respectively. The former was bright yellow on the silicon wafer, while the latter was blue. Additionally, the conductivity of the N_2 annealed film was much greater than that of the O_2 annealed film, a strong indication of the presence of oxygen vacancies.[11,14] The conductivities for both films are shown in figure 1. They were measured

using a Keithley 2400 Sourcemeter, after depositing Au ohmic pads onto the oxide films by electron beam evaporation.

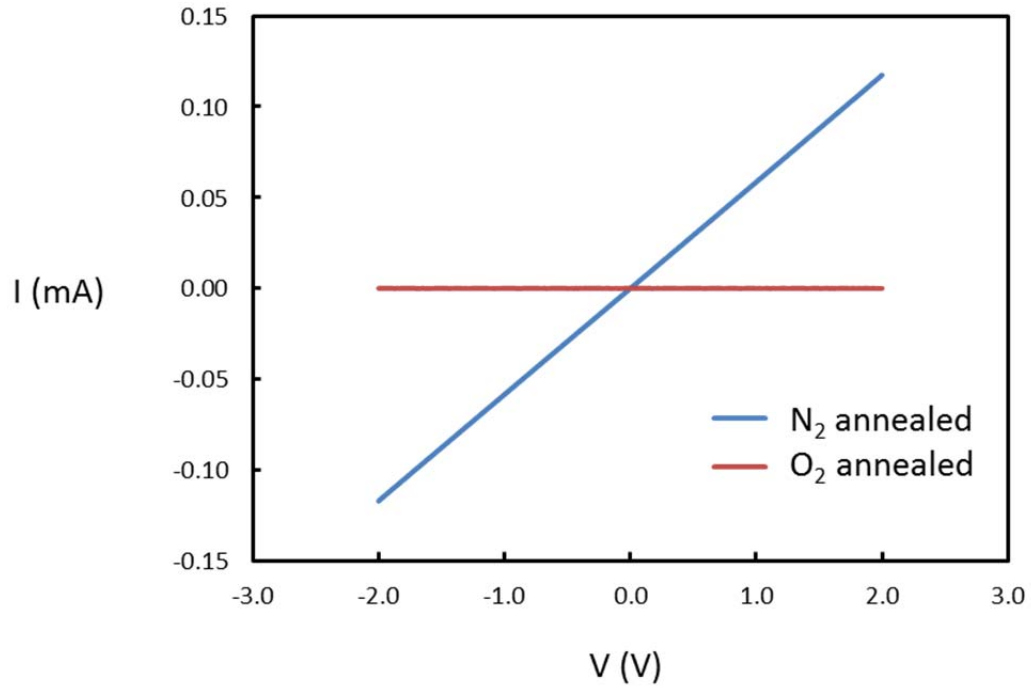

Figure 1 – *I-V graphs for the N_2 annealed and the O_2 annealed TiO_2 films, showing a much higher conductivity for the N_2 annealed films. This is due to the presence oxygen vacancies, which give rise to midgap states.*

Fluorine doping was achieved by exposing the oxide films to a plasma of N_2 gas and trace amounts of sulfur hexafluoride (SF_6), introduced into the chamber by flowing a 9:1 mixture of SF_6 and O_2, followed by pumping to a chamber base pressure of 5 mTorr. A low background pressure of SF_6 remained in the chamber after pumping. N_2 gas was then introduced at a flow rate of 80 sccm for plasma treatment under conditions of 20 W power and 130 V DC substrate bias. XPS analysis of the F-doped samples did not reveal any S traces.[9] One of the two samples of each TiO_X stoichiometry was plasma treated, resulting in four supports for subsequent Pt deposition, i.e., TiO_2 and TiO_x, each with and without F doping. All substrates were stored in dry N_2 between the time of fabrication and the XPS measurements.

Pt nanoparticles were deposited onto the TiO_x/Au substrates by electron-beam evaporation. This deposition method was selected instead of colloidal synthesis to avoid the presence of an insulating polymer capping agent between the Pt nanoparticles and the oxide support. During electron beam evaporation, the chamber base pressure was less than 10^{-5} Torr. The average Pt film thickness, monitored by a quartz crystal microbalance, was equal to about 1 nm.

- AP-XPS

XPS spectra were taken at beamline 9.3.2 at the Advanced Light Source. The experimental setup has been described elsewhere.[15] Briefly, the sample is mounted on a heater placed inside an ultra-high vacuum chamber equipped with leak valves. The sample can be positioned less than 1 mm away from an aperture leading to a set of differentially pumped chambers, where the ionized electrons are focused onto a hemispherical PHI-360 SCA electron energy analyzer.

For each gas and temperature condition, and for each beam energy used, a spectrum of the valence band edge is recorded in order to establish an absolute energy scale. O1s spectra were recorded at 650 and 800 eV, Pt4f spectra at 340, 405, 650, 725 and 800 eV, and C1s spectra at 405 eV. Shirley background subtraction was applied to all of the spectra shown here.

Spectra were taken in four successive conditions: at 333 K in vacuum, at 333 K in 140 mTorr O_2, at 443 K in 140 mTorr O_2, at 443 K in 140 mTorr O_2 and 50 mTorr CO, and at 573 K in 140 mTorr O_2 and 50 mTorr CO. Since the history of the catalyst may affect the nature of the chemical species on the surface, gas species were not removed once they had been introduced, and the catalyst was not cooled over the course of the experiment.

Results and Discussion

Four catalysts were fabricated, which we will refer to as TiO_2, F-TiO_2, TiO_x and F-TiO_x, with $x<2$. Figure 2 shows the O1s spectra for all four samples, at 443 K in 140 mTorr O_2, taken with a beam energy of 650 eV. All of them show two major peaks. The spectra are adjusted for differences in the valence band edge energy, and normalized in intensity so that the peaks at lower binding energies overlap for the two stoichiometric samples and the two non-stoichiometric samples. This provides a rough estimate of the abundance of the peak at higher binding energy relative to the lower binding energy peak. The lower binding energy O peak can be taken as a reference this way since it varies little relative to signal from Pt, contrary to the higher energy O peak.

The height of the higher energy peak correlates with the activity of the samples. F-doping stoichiometric TiO_2 increases turnover for CO oxidation and methanol oxidation, and decreases the height of the peak. Likewise, F-doping non-stoichiometric TiO_2 decreases turnover for the two reactions, and increases the height of the peak.

Figure 3 shows the same spectra taken at a beam energy of 800 eV. The higher beam energy increases the mean free path of the photo-ionized electrons through the sample, making the measurement more sensitive to the bulk of the material. The difference between the fluorinated and non-fluorinated samples is decreased, indicating that the species responsible for the higher energy peak in the O1s spectrum is located near the surface. Figure 4 shows the same spectra with CO present, to mimic the reaction conditions from the previous CO oxidation study, albeit at lower pressure. The same effect is observed, only enhanced, and with the high binding energy peak shifted roughly 1 eV higher.

The interpretation of the O1s spectrum is notoriously difficult,[16,17] and identification of this species proved challenging. In a previous AP-XPS study of CO oxidation on Pt in the same experimental setup, several peaks in the O1s spectrum were assigned to specific species, namely CO on atop and bridge sites, and chemisorbed O, but on a single crystal catalyst, not a polycrystalline film. The samples used here comprise many different O components, adsorbed on different platinum sites, different oxide sites and perhaps interface sites. Gas phase oxygen was identified by comparing spectra in vacuum with spectra where gas phase O was present, and produces a peak outside of the energy range shown here.

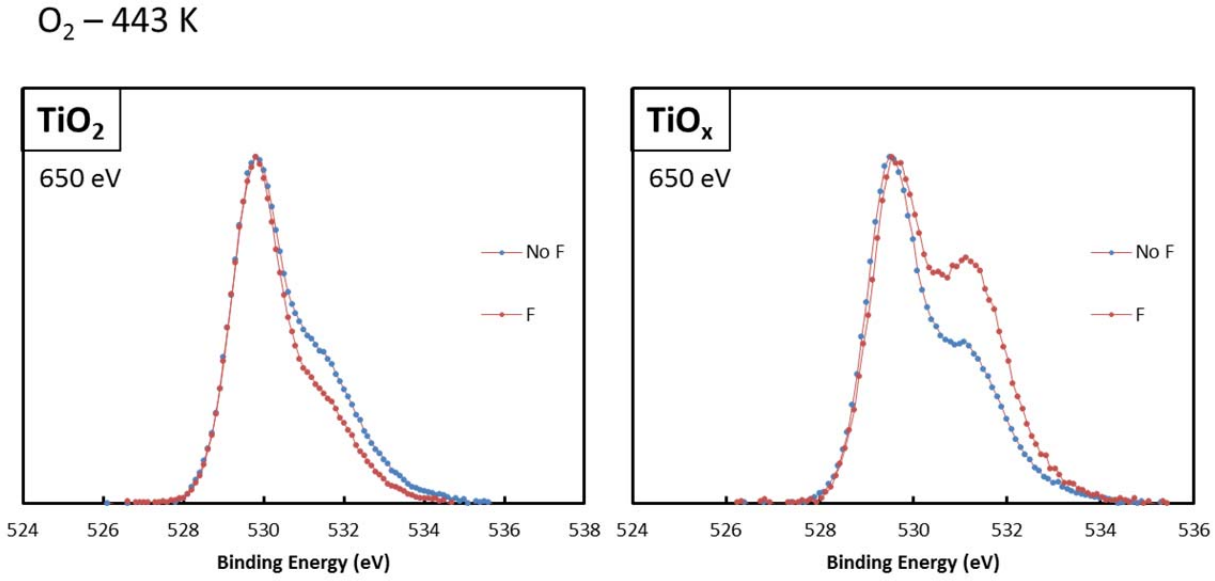

Figure 2 – *O1s spectrum of Pt/TiO_2 and Pt/TiO_x catalysts in 140 mTorr O_2 at 443 K. F-doping decreases the height of the high binding energy peak in stoichiometric TiO_2, and increases it in non-stoichiometric TiO_2. The intensity of this peak therefore scales inversely with the activity of the catalysts for CO oxidation on these Pt/TiO_2 catalysts. Spectra are normalized to the maximum of the low binding energy peak, which shows little variation with respect to Pt signal. Beam energy is 650 eV.*

By identifying the position of the peaks at each step in the sequence, then including these peaks in the subsequent step, it should be possible to identify all of the peaks that produce the spectra shown in O_2 at 443 K and in O_2 and CO at 443 K. However, no combination of peaks was found that produced a compelling fit of the data. More conclusions could be drawn from taking similar measurements on TiO_2 films without any platinum, and on continuous platinum films. It may also be that polycrystalline oxide-supported catalysts are too complex for this type of experiment.

The high energy peak observed in the spectra in figures 2 and 3 follows the reactivity of the samples, and could be assigned several different ways. The species in question may be a poison for the reaction, based on the post-reaction XPS spectra in the CO oxidation study.[12] In that

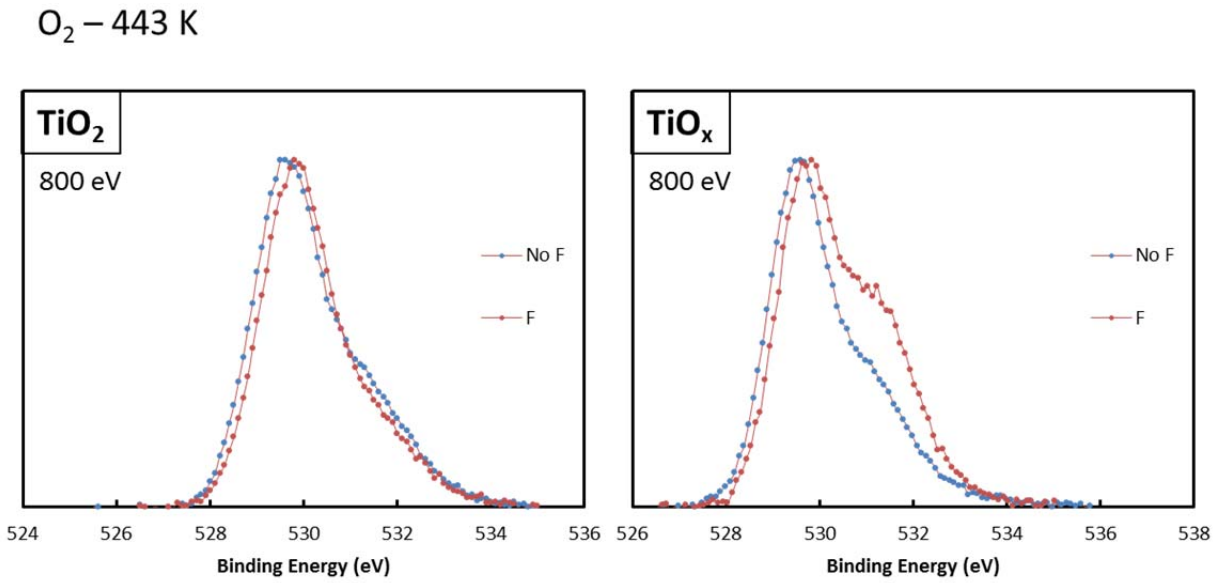

Figure 3 – *O1s spectrum of Pt/TiO_2 and Pt/TiO_x catalysts in 140 mTorr O_2 at 443 K. Beam energy is 800 eV, meaning that the probing depth is higher than for the spectra in Figure 2. The effect of F is more subtle, indicating that the species responsible for the high binding energy peak is located near the surface of the catalyst.*

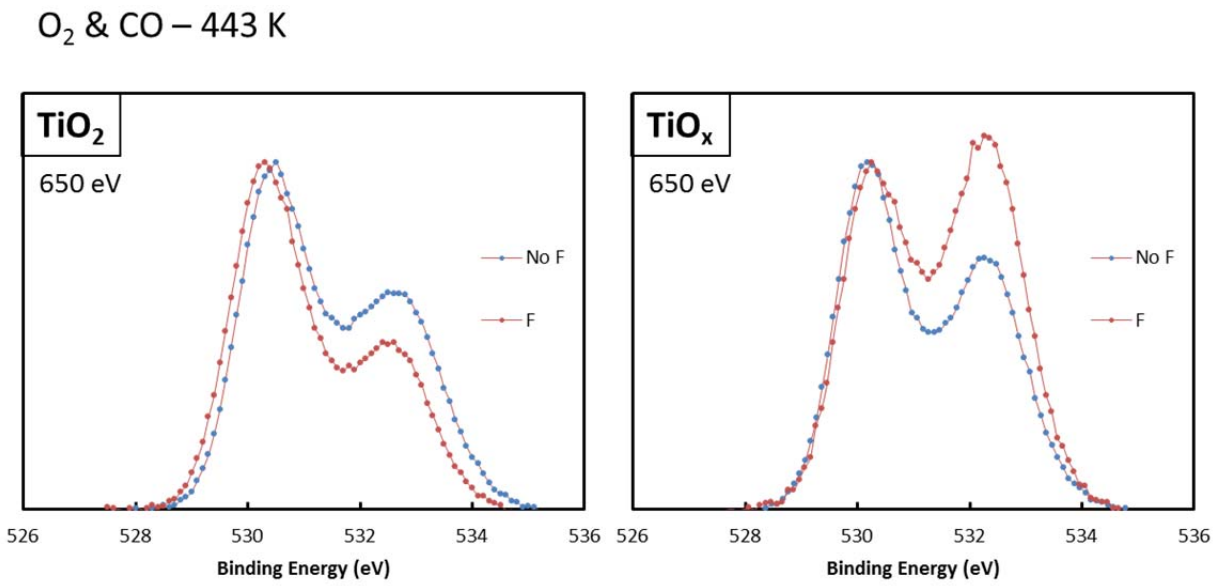

Figure 4 – *O1s spectrum of Pt/TiO_2 and Pt/TiO_x catalysts in 140 mTorr O_2 and 50 mTorr CO at 443 K. The F-doping trend is the same as in O_2 alone.*

case, the formation of this poison may be slower on F-TiO_2. It may also be that this species is a poison for every catalyst, except for F-TiO_2, where it can be electronically activated. Finally, this species could be a reaction intermediate on all of the samples, the activation being the limiting step for reaction with CO, but to a lesser extent on F-TiO_2 than on the other samples.

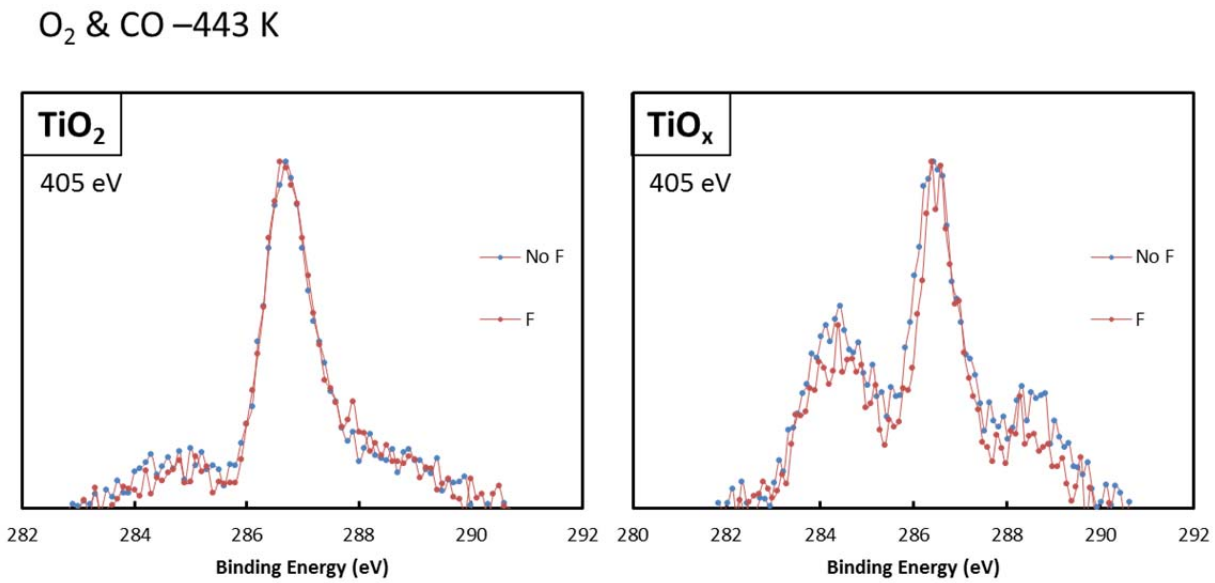

Figure 5 – *C1s spectrum of Pt/TiO_2 and Pt/TiO_x catalysts in 140 mTorr O_2 at 443 K. No significant change is visible with the addition of F.*

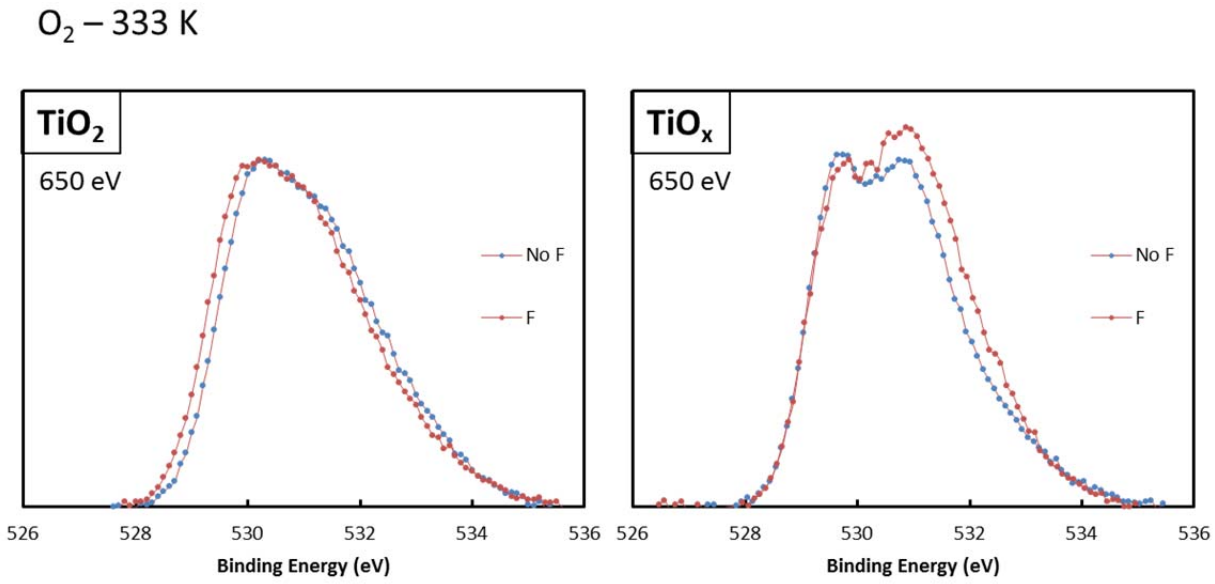

Figure 6 – *O1s spectrum of Pt / TiO_2 and Pt/TiO_x catalysts in 140 mTorr O_2 at 333 K.*

This data strengthens the evidence that the electronically activated species on F-doped stoichiometric TiO_2 is an oxygen species. Electronic activation of oxygen has been found to be the limiting step for CO oxidation in several other studies.[18,19]

Figure 5 shows the C1s spectra for all four samples taken at 443 K in 140 mTorr O_2 and 50 mTorr CO, at a beam energy of 405 eV. No major differences are visible with F doping. Figures 6 and 7 show the O1s spectra at 333K for all four samples, in vacuum and in 140 mTorr O_2, respectively. The high binding energy oxygen peak is either not visible, or does not trend with the reactivity. This suggests that the electronic activation mechanism observed for methanol oxidation is distinct from CO oxidation.[13] This may explain why, in that study, no features in the O1s spectrum could be correlated to the reactivity by conventional XPS.

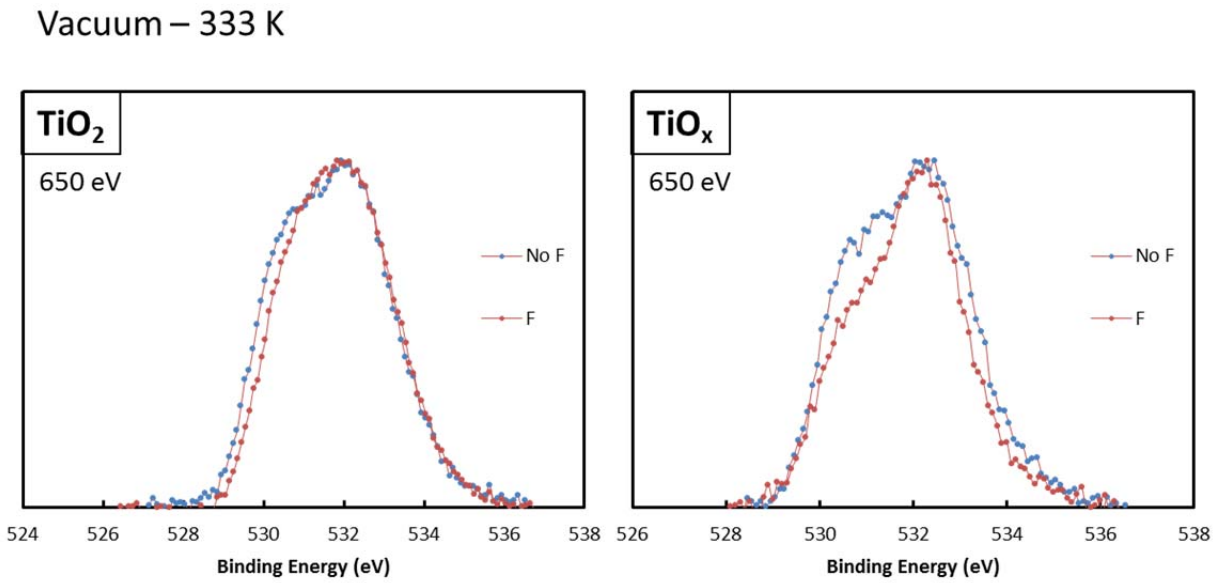

Figure 7 – *O1s spectrum of Pt/TiO_2 and Pt/TiO_x catalysts in vacuum at 333 K.*

F inserted in the TiO_2 lattice is not stable above 473 K, as inferred from XPS spectra of F-doped samples after different temperature treatments lasting one hour.[11] This may be through evaporation of a fluorine containing compound, or by diffusion of the fluorine into the bulk, since the fluorine is only present in the first few nanometers of the oxide.

In order to observe how this affects the O1s spectrum during reaction, all samples were heated to 573 K, and two subsequent spectra of the F-doped spectra were taken approximately one hour apart, as well as a spectrum of the undoped samples at the same temperature as a reference.

Figure 8 shows these spectra for both the stoichiometric and non-stoichiometric samples. In the stoichiometric samples, the trend is consistent with our conclusions: the high binding energy peak is smaller in the F-doped sample, and increases as F leaves the surface, bringing it closer to the peak in the undoped sample. In the non-stoichiometric sample, however, the

trend is opposite. The peak is higher in the F-doped sample, and only grows as the sample is heated. We could find no explanation for this trend.

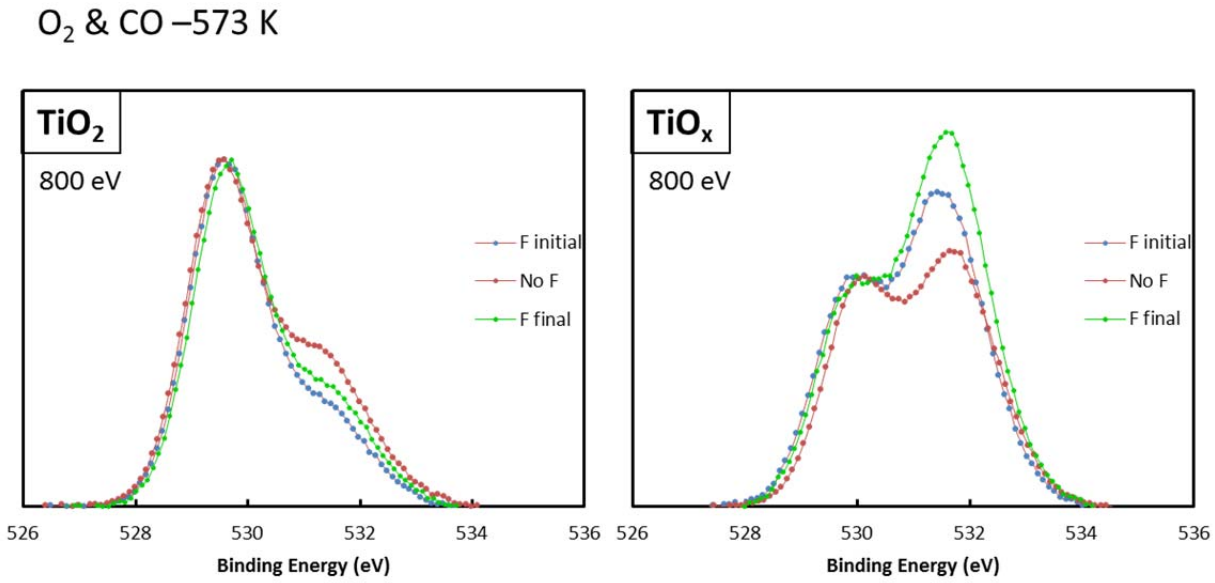

Figure 8 – *O1s spectrum of Pt/TiO_2 and Pt/TiO_x catalysts in 140 mTorr O_2 and 50 mTorr CO at 573 K. The spectrum of the F-doped catalyst is measured first (initial F), followed by the undoped (no F), and finally a second spectrum of the F-doped catalyst is measured (final F). At this temperature F is not stable, and the effect of F-doping should disappear. This is the case with the Pt/TiO_2 catalyst, but not with Pt/TiO_x.*

Conclusion

Previous studies have shown that F-doping of stoichiometric TiO_2 leads to the electronic activation of surface O for CO oxidation and of some unknown species for methanol oxidation. The spectroscopic measurements presented here show an excellent correlation of the intensity of a high binding energy peak in the O1s spectrum with the activity of these catalysts and the conductivities of the oxide supports. The C1s spectrum shows no such correlation.

This high-binding energy peak could not be assigned to any particular species on the surface catalyst. More detailed experiments are required to understand what this species is, as well as the mechanism for the electronic activation in F-TiO_2.

References

(1) Somorjai, G. A.; York, R. L.; Butcher, D.; Park, J. Y. *Phys. Chem. Chem. Phys.* **2007**, *9*, 3500-3513.
(2) Siegbahn, H.; Siegbahn, K. *Journal of Electron Spectroscopy and Related Phenomena* **1973**, *2*, 319-325.
(3) Joyner, R. W.; Roberts, M. W.; Yates, K. *Surface Science* **1979**, *87*, 501-509.

(4) Ruppender, H. J.; Grunze, M.; Kong, C. W.; Wilmers, M. *Surface and Interface Analysis* **1990**, *15*, 245-253.
(5) Kelly, M. A.; Shek, M. L.; Pianetta, P.; Gür, T. M.; Beasley, M. R. *Journal of Vacuum Science & Technology A: Vacuum, Surfaces, and Films* **2001**, *19*, 2127.
(6) Ogletree, D. F.; Bluhm, H.; Lebedev, G.; Fadley, C. S.; Hussain, Z.; Salmeron, M. *Review of Scientific Instruments* **2002**, *73*, 3872.
(7) Yamamoto, S.; Bluhm, H.; Andersson, K.; Ketteler, G.; Ogasawara, H.; Salmeron, M.; Nilsson, A. *Journal of Physics: Condensed Matter* **2008**, *20*, 184025.
(8) Bluhm, H.; Hävecker, M.; Knop-Gericke, A.; Kleimenov, E.; Schlögl, R.; Teschner, D.; Bukhtiyarov, V. I.; Ogletree, D. F.; Salmeron, M. *J. Phys. Chem. B* **2004**, *108*, 14340-14347.
(9) Bukhtiyarov, V. I.; Nizovskii, A. I.; Bluhm, H.; Hävecker, M.; Kleimenov, E.; Knop-Gericke, A.; Schlögl, R. *Journal of Catalysis* **2006**, *238*, 260-269.
(10) Grass, M. E.; Karlsson, P. G.; Aksoy, F.; Lundqvist, M.; Wannberg, B.; Mun, B. S.; Hussain, Z.; Liu, Z. *Review of Scientific Instruments* **2010**, *81*, 053106.
(11) Seo, H.; Baker, L. R.; Hervier, A.; Kim, J.; Whitten, J. L.; Somorjai, G. A. *Nano Lett.* **2011**, *11*, 751-756.
(12) Baker, L. R.; Hervier, A.; Seo, H.; Kennedy, G.; Komvopoulos, K.; Somorjai, G. A. *J. Phys. Chem. C* **2011**, *115*, 16006-16011.
(13) Hervier, A.; Baker, L. R.; Komvopoulos, K.; Somorjai, G. A. *J. Phys. Chem. C* **2011**.
(14) Bilmes, S. A.; Mandelbaum, P.; Alvarez, F.; Victoria, N. M. *J. Phys. Chem. B* **2011**, *104*, 9851-9858.
(15) Chung, J.-Y.; Aksoy, F.; Grass, M. E.; Kondoh, H.; Ross Jr., P.; Liu, Z.; Mun, B. S. *Surface Science* **2009**, *603*, L35-L38.
(16) Stoch, J.; Gablankowska-Kukucz, J. *Surface and Interface Analysis* **1991**, *17*, 165-167.
(17) Liu, J. H.; Blanpain, B.; Wollants, P. *Key Engineering Materials* **2008**, *368-372*, 1347-1350.
(18) Bonn, M.; Funk, S.; Hess, C.; Denzler, D. N.; Stampfl, C.; Scheffler, M.; Wolf, M.; Ertl, G. *Science* **1999**, *285*, 1042 -1045.
(19) Zhang, Z.; Yates, J. T. *J. Am. Chem. Soc.* **2010**, *132*, 12804-12807.

Conclusion

The objective of this work was to show evidence of charge transfer in reactions on metal surfaces, to identify the role of charge transfer in shaping reactivity, and to attempt to tune reactivity by controlling charges.

Pt/TiO_2 nanodiodes were used to demonstrate that hydrogen oxidation leads to the non-adiabatic excitation of electrons within the metal, in the form of a current through the diode, referred to as chemicurrent. The number of electrons collected per reaction event is on the order of 10^{-4}, which is consistent with previous results from the literature on other reactions. It is unknown, however, whether this low yield is due to a low probability of electronic excitation, or rather is the result of low collection efficiency. If it is the latter, these diodes may one day serve as a novel type of fuel cell.

The same type of chemicurrent measurements had also been shown for CO oxidation and the adsorption of many different molecules on diodes fabricated from different materials, confirming the notion that breakdown of the Born-Oppenheimer approximation is a general phenomenon for reactions on metal surfaces.

The generalized application of nanodiodes to surface chemistry is complicated by the fact that they are generally unstable in reaction conditions. In the case of Pt/TiO_2 for example, H_2 dissociatively adsorbs on the surface and spills over onto the TiO_2. Without a high excess of O_2 to mitigate this effect, the device quickly loses rectification and can no longer function.

This is unfortunate, given the exquisite sensitivity these diodes exhibit to chemical conditions. While ordinary gas sensors are sensitive to concentration, these diodes are sensitive to turnover events. A stable, reproducibly fabricated diode would allow us to measure turnover on a metal film within seconds, as opposed to hours with a gas chromatograph.

These experiments confirm the important role that charges play in surface chemistry, and suggest the possibility of tuning reactivity by controlling the charges.

This was achieved by exposing a Pt/Si diode to visible light in H_2 oxidation conditions. The light creates a steady state population of electron-hole pairs in the Si. The band bending at the interface gives rise to a steady-state flow of hot holes to the surface, which was correlated with a decrease in the turnover frequency for the reaction. Photodesorption of H_2 from the sample heater interfered with the experiment, and prevented a quantitative measurement.

Similar experiments for CO oxidation on Pt/Si diodes were more conclusive. A strong reverse bias, which forms a negative charge on the Pt, was shown to increase turnover. This effect could be diminished by exposing the diode to visible light, in which case a flow of positive charges is created from the metal to the semiconductor.

The other approach for controlling charge transfer was to dope TiO_2 with fluorine, and use it as the support for a platinum catalyst. In the case of stoichiometric TiO_2, fluorine acts as an *n*-type dopant, creating a population of occupied electronic states below the conduction band. By correlating reactivity and electronic measurements, it was determined that the electrons in those states could activate certain reaction pathways for CO oxidation and methanol oxidation, leading to increased activity and a change in selectivity for methanol oxidation. Oxygen vacancy doping also leads to the formation of bandgap states, but at energies lower by 0.5 to 1 eV, and did not enhance the electronic activation pathways observed for fluorine.

Ambient pressure X-ray photoelectron spectroscopy measurements seemed to confirm that the increased activity for CO oxidation on Pt supported on F-doped stoichiometric was due to electronic activation of surface O atoms.

Future work

The diode experiments show that reactivity can be affected in two ways. In the current mode, the diode is exposed to visible light or subjected to a forward bias, giving rise to a flow of hot charge carriers from the semiconductor to the metal. In the field mode, a reverse bias is applied which creates an electric field at the interface.

A device better suited for the field mode experiments would be a field effect transistor, where catalytic nanoparticles are deposited onto an oxide thin film, which serves both as a catalyst support and as the gate oxide for the transistor. By varying the gate bias, it would be possible to change the conductivity of the oxide film by many orders of magnitude, which may lead to dramatic changes in reactivity. The main challenge of such an experiment is to fabricate a transistor with an active surface area large enough that a turnover frequency could be measured, but small enough that an entire device could be fabricated with no defects, which would leak current.

The fluorine doping experiments point to the possibility of creating new reaction pathways by modifying the electronic structure of the support. Just as with many of the investigations of Strong Metal Support Interactions, these experiments could be reproduced across a range of different oxides. The resulting trends may provide further clues on the mechanism by which reactivity is changed.

Finally, these experiments were carried out on 2D catalysts. Many synthetic strategies have been developed for mesoporous structures of TiO_2 and many other oxides. Once combined with catalytic metal nanoparticles, these structures routinely serve as model catalysts in the laboratory. It should be possible to modify the electronic properties of these 3D supports, just as with thin films, and to obtain similar changes in activity and selectivity, which would be of great relevance to industrial catalysis.